Characterization and age determination of Quaternary volcanism in the southern Ankaratra region (central Madagascar) through novel approaches in luminescence dating

Inauguraldissertation
der Philosophisch-naturwissenschaftlichen Fakultät
der Universität Bern

vorgelegt von

Daniel Rufer
von Ittigen / BE

Leiter der Arbeit:

PD Dr. G. Schreurs
Institut für Geologie, Universität Bern

PD Dr. A. Berger
Department of Geography and Geology, University of Copenhagen

PD Dr. E. Gnos
Muséum d'Histoire naturelle de Genève

PD Dr. F. Preusser
Institut für Geologie, Universität Bern

Characterization and age determination of Quaternary volcanism in the southern Ankaratra region (central Madagascar) through novel approaches in luminescence dating

Inauguraldissertation
der Philosophisch-naturwissenschaftlichen Fakultät
der Universität Bern

vorgelegt von

Daniel Rufer
von Ittigen / BE

Leiter der Arbeit:

PD Dr. G. Schreurs
Institut für Geologie, Universität Bern

PD Dr. A. Berger
Department of Geography and Geology, University of Copenhagen

PD Dr. E. Gnos
Muséum d'Histoire naturelle de Genève

PD Dr. F. Preusser
Institut für Geologie, Universität Bern

Von der Philosophisch-naturwissenschaftlichen Fakultät angenommen.

Der Dekan:

Bern, 23. Oktober 2009 Prof. Dr. Urs Feller

Characterization and age determination of Quaternary volcanism in the southern Ankaratra region (central Madagascar) through novel approaches in luminescence dating

Dissertation
submitted to the Faculty of Science of the University of Bern
for the degree of Doctor of Science (Dr. phil. nat.)

by

Daniel Rufer
from Ittigen / BE

Supervisors:

PD Dr. G. Schreurs
Institute of Geological Sciences, University of Bern

PD Dr. A. Berger
Department of Geography and Geology, University of Copenhagen

PD Dr. E. Gnos
Museum of Natural History, Geneva

PD Dr. F. Preusser
Institute of Geological Sciences, University of Bern

No man should escape our universities without knowing how little he knows.

J. Robert Oppenheimer (1904 – 1967), Physicist

CONTENTS

ABSTRACT

This work introduces two novel approaches for the application of luminescence dating techniques to Quaternary volcanic eruptions: crystalline xenoliths from lava flows are demonstrated to be basically suitable for luminescence dating, and a set of phreatic explosion deposits from the Late Quaternary Vakinankaratra volcanic field in central Madagascar is successfully dated with infrared stimulated luminescence (IRSL).

Using a numerical model approach and experimental verification, the potential for thermal resetting of luminescence signals of xenoliths in lava flows is demonstrated. As microdosimetry is an important aspect when using sample material extracted from crystalline whole rocks, autoradiography using image plates is introduced to the field of luminescence dating as a method for detection and assessment of spatially resolved radiation inhomogeneities.

Determinations of fading rates of feldspar samples have been observed to result in aberrant g-values if the pause between preheat and measurement in the delayed measurements was kept short. A systematic investigation reveals that the phenomenon is caused by the presence of three signal components with differing individual fading behaviour. As this is restricted to short pauses, it is possible to determine a minimal required delay between preheating and measurement after which the aberrant behaviour disappears.

This is applied in the measuring of 12 samples from phreatic explosion deposits from the Antsirabe – Betafo region in the Late Quaternary Vakinankaratra volcanic field. The samples were taken from stratigraphically correlatable sections and appear to represent at least three phreatic events, one of which created the Lac Andraikiba maar near Antsirabe. The obtained ages indicate that the eruptive activity in the region started in the Late Pleistocene between 113.9 and 99.6 ka. A second layer in the Betafo area is dated at approximately 73 ka and the Lac Andraikiba deposits give an age between 63.9 and 50.7 ka. The youngest phreatic layer is dated between 33.7 and 20.7 ka.

These ages are the first recorded direct ages of such volcanic deposits, as well as the first and only direct ages for the Late Quaternary volcanism in the Vakinankaratra volcanic field.

This illustrates the huge potential of this new method for volcanology and geochronology, as it enables direct numerical dating of a type of volcanic deposit which has not been successfully directly dated by any other method so far.

MISAOTRA BETSAKA! - THANKS!

"Aza mandalo tana-misy havana." – "Don't pass by the house of a friend without paying him a visit." (Malagasy proverb)

Over the past years, these 'houses' have become more and more numerous, and I would not like to simply pass them by on my way to submit this thesis…

Thank you, Guido, for giving me the opportunity to work on this project and for introducing me to (not only the geology of) Madagascar. I enjoyed the time in the field, the discussions and the THB. Even though the project turned out to be similar to driving along the back ways of the Hauts Plateaux, you kept your confidence in me. Thank you!

Alfons, thank you for all the discussions in the field, your efforts in the final drawing of the geologic map and your help with the microprobe.

Edwin, your enthusiasm in getting samples from the top of all those volcanoes made for arduous fieldwork, but this was more than balanced by the wealth of keen observations, fruitful discussions and generally the good time we spent in the field or over dinner "Chez Jacky". Thanks a lot!

I want to express a particularly big 'Thank you!' to Frank, who very kindly agreed to scientifically 'adopt' me when the entire project was on the verge of going south. Thank you for introducing me into the 'circle of bright grains' and to venture on an undertaking in which the sentence *"Hey, nobody has done this before, but lets try it!"* became something like a mission statement for a series of very interesting projects. I am grateful for your boundless optimism and enthusiasm, thank you - it was sorely needed.

I am also very grateful to Markus Fiebig, who kindly agreed to evaluate this thesis as an external referee.

I would also like to thank all other people who were, in one way or another, involved in this project: Michel Rakotondrazafy for helping with the exportation of rock samples from Madagascar, Lydia Zehnder for the XRF measurements, Marco Herweg for the introduction to the SEM and Igor Villa for providing me with the opportunity to learn so much about "Zen and the Art of Noble Gas Mass Spectrometer Maintenance".

Further thanks go to Betty Lauber for always making me feel welcome in the only 'Frutiger Chalet' in Madagascar, as well as to Honoré, Michel, Fama and particularly William, our drivers in Madagascar, for their companionship and excellent driving.

A big thank you also goes to all the colleagues and good friends at 'The Institute', you know who you are. I will fondly remember my long-term officemates Marek, Martin and of course "Dr. Dea" (thanks for all the help, laughs, fights, discussions and all other nonsense!).

Damian, and Sally deserve big thanks for providing me with a crash course introduction into the luminescence lab and into the mystical workings of certain pieces of software. Thomas and Mareike are thanked for many helpful discussions, or for simply listening to my explanations, waiting patiently until I realized my mistake and happily went away again…

I would also like to apologize (and at the same time express my gratitude!) to the people I must have annoyed to death with my incessant questions about error propagation, or when they had to "adumbrate" some vocabulary related deficiencies in my texts… Thanks ND and Sally (also for keeping my Excel and Endnote happy with a steady influx of worksheets and PDF's…)!

Jörg and Inga: even though your company didn't make the coffee taste any better or the Betty Bossy more nutritious, you did make a difference! I will always gladly remember all the scientific as well as all the nonsensical discussions we shared in the office or over yet another "after-midnight-lunch". Thank you for all your help, good advice and above all your friendship!

My special thanks go my parents who always believed in me and supported me on my way to this point.

I want to express my deepest gratitude to Michèle for always supporting me in any way imaginable, even though she lost me to the lab on far too many Friday evenings and weekends. It was your belief in me that kept me going whenever I had more or less abandoned the cause. You made this happen… Thank you!

This work was financed by the Swiss National Science Foundation (grants 200020-105453/1, 200020-118023/1, 206021-117374, 200020-121671 and 200020-121680)

CHAPTER 1

Introduction and outline of the thesis

"Every new beginning comes from some other beginning's end"
Seneca (ca. 4 BC – AD 64), Roman philosopher and statesman

INTRODUCTION AND OUTLINE OF THE THESIS

1.1 INTRODUCTION

Situated in an intraplate context in the south-western Indian Ocean, Madagascar is a continental island (de Wit, 2003) that stretches 1600 km north-south and at its widest point measures nearly 600 km across. It features an east-west asymmetric topography, with a broad axial zone where the mean elevation is about 1200 m.a.s.l. This High Plateau is flanked to the east by a steep escarpment, whereas to the west it gradually slopes towards the Phanerozoic Morondava and Mahajanga basins. The elevated interior of the island consists almost exclusively of high-grade metamorphic Precambrian basement (e.g. Collins *et al.*, 2001). Extensive erosional remnants of Upper Cretaceous flood basalts associated with the breakup between Madagascar and India can be traced across large sections of the coast (e.g. Storey *et al.*, 1995, Rasamimanana *et al.*, 1998).

As a result of the south-eastward extension of the East African Rift system (Mougenot *et al.*, 1986; Kusky *et al.*, 2007), Madagascar has come under an E-W extensional regime since the mid Miocene (Bertil and Regnoult, 1998). This is not only indicated by asthenospheric bulging (Rakotondraompiana *et al.*, 1999) and a rising of the Moho under the central plateau (Fourno and Roussel, 1994), but also by the reactivation of mainly N-S trending basement faults (Piqué *et al.*, 1999) and the formation of several N-S trending basins, the most prominent of which is the Ankay-Alaotra graben system (Laville *et al.*, 1998), which bears similarities to the East African Rift (Rakotondraompiana *et al.*, 1999, Piqué *et al.*, 1999). Associated with the lithospheric thinning and the extensional reactivation of Precambrian and old Phanerozoic tectonic structures and lineaments (Bertil and Regnoult, 1998), the occurrence of the Neogene to Quaternary intraplate volcanism of the Ankaratra, Lac Itasy and Vakinakaratra volcanic fields is a consequence of this widespread intracontinental rifting.

Ongoing tectonic activity is indicated by recent subsidence in the Ankay-Alaotra graben (Kusky *et al.*, 2007), a high seismic activity, particularly in the central highlands (e.g. Rambolamanana *et al.*, 1997) and by neotectonic displacement of the Quaternary volcanic deposits.

In order to better understand the young geological history of this dynamic system, a chronological framework is required, which would allow linking the observed extensional tectonic features with the accompanying volcanic activity.

With this goal, an initial field campaign was conducted in summer 2005, during which an extensive sample set for $^{39}Ar/^{40}Ar$ dating and geochemistry was collected in two Late

Quaternary volcanic fields, Lac Itasy and Vakinankaratra. Furthermore, an initial draft was made for a geological map of the Antsirabe – Betafo region, which was intended to be published and forwarded to local authorities in Antsirabe for educational use and tourism promotion.

Over the next 18 months, multiple attempts were made to conduct $^{39}Ar/^{40}Ar$ dating, but due to the young age of the material, overall low potassium concentrations in the whole rock samples and a distinct lack of measurable K-feldspars as well as a series of technical problems, no ages could be obtained.

Unfortunately, alternative methods for directly dating alkaline volcanic rocks of Late Pleistocene to Holocene age are rather scarce and possess some inherent pitfalls (c.f. Fattahi and Stokes, 2003). Lacking alternatives, first tests were conducted in 2007 to establish the applicability of thermoluminescence for dating basement xenoliths sampled from lava flows of the Vakinankaratra field. As these tests showed promise, a second field campaign to the Vakinankaratra field was undertaken in summer 2007, in order to sample xenoliths as well as phreatic explosion deposits for luminescence dating and to finalize the geological map.

The main focus of the project was then shifted to luminescence dating methods on these alternative materials, both, in order to obtain numerical ages for the Vakinankaratra volcanic field as well as to establish a dating method which could be applied in other volcanic regions showing similarly difficult conditions for age dating.

1.2 OUTLINE OF THE THESIS

The potential for thermal resetting of the luminescence signal of crystalline xenoliths embedded in lava flows was investigated, as it is a prerequisite for successful luminescence dating *[CHAPTER 2]*. Based on numerical model calculations, it was determined that fist-sized, crystalline xenoliths will reach core temperatures exceeding 450°C in less than 30 minutes when exposed to magmatic temperatures of only 700°C, leading to complete resetting of the thermoluminescence signal. This could be confirmed by a calefaction experiment, in which feldspar grains extracted from the center of a granite cube, previously put in an 800°C preheated oven for 30 minutes, showed no detectable luminescence signal.

While xenoliths could therefore basically be considered for luminescence dating, the fact that they are crystalline rocks, instead of the more usual unconsolidated sediments sampled for luminescence, requires special consideration. Due to their generally larger grain size compared to the sedimentary samples, often coupled with inhomogeneous distribution of certain mineral phases (e.g. pegmatitic structures or concentration of accessory minerals along veins), crystalline rocks often show significant spatial variations in their radiation fields. Such microdosimetry influences are a potential pitfall for luminescence dating (e.g. Vandenberghe *et al.*, 2003, Preusser *et al.*, 2007), particularly for single grain measurements

(Murray and Roberts, 1997), or if the entire measured material is derived from one single, large grain, as is would most likely be the case when extracting samples from a hard rock.

To provide a method to detect and assess microdosimetry in a sample, the application of autoradiography using image plates was investigated *[CHAPTER 3]*. The method records and visualizes spatially resolved radiation inhomogeneities (Rowlands, 2002) in a wide range of sample types, without being destructive to luminescence signals. It does not require elaborate sample processing and allows for rapid assessment of relative β radiation levels and radiation homogeneity. This makes it ideally suited as a rapid screening technique for determining whether microdosimetry may have to be considered as a potential contributor to an overdispersion in D_E distribution, particularly as this cannot be determined by gamma-spectrometry.

The visualization of spatially resolved radiation levels can also be a useful tool for Electron Spin Resonance (ESR) dating of tooth enamel, or in the emerging field of speleothem dating by U-Pb and U-Th series, where identifying layers of high radionuclide content is indispensable for successful dating (Cole *et al.*, 2003, Pickering *et al.*, submitted.).

An investigation into quantitative calibration of the imaging plate is also presented, which allows to calculate sample activity from the greyscale value of the recorded radiographic image. Tests performed on 16 geological samples of known specific activities illustrate that the calibration method is applicable to natural samples, as long as the relative radionuclide composition between calibration- and sample material is roughly similar.

While most materials used for luminescence dating have their luminescence signal reset by exposure to light or heat, phreatic explosion deposits are assumed to be mechanically reset during the explosive fragmentation of their bedrock source *[CHAPTER 2]*.

Due to the intrinsic difficulty of testing this assumption with a representative experimental setup, the necessary information had to be deduced from literature. Reported findings concerning mechanical resetting, from static pressure experiments (Banerjee *et al.*, 1999, Zöller *et al.*, 2009) to high magnitude shock treatments of dosimeter material (Banerjee *et al.*, 1999), were linked with observed signal resetting caused by earthquake triggered injection of material into clastic dikes (Porat *et al.*, 2007) or by shocking due to meteorite impacts (Sutton, 1985, Prescott *et al.*, 2004, Stankowski, 2007). As a result, it was accepted that mechanical resetting of luminescence signals during phreatic explosion is very likely.

Determinations of fading rates (Huntley and Lamothe, 2001) is an important point for luminescence dating of feldspar samples. Prompted by the observation of aberrant g-values if the pause between preheat and measurement in the delayed measurements was kept short, a systematic investigation into this phenomenon, using well documented samples,

was undertaken *[CHAPTER 4]*. Component fitting of the decay curve revealed that the phenomenon is caused by the presence of three signal components, showing differing individual fading characteristics. While particularly pronounced for short delays, it could be shown that, at longer delays, the fading characteristics of the individual components eventually approximate a stable fading rate equal for all three components. This allows the determination of a minimal required delay to be used between preheat and IRSL measurements; this is not only relevant in the context of fading rate determinations, but should avoid problems related to aberrant signal behaviour in any IRSL measurements. For the investigated samples, spanning fluvial, glaciofluvial and aeolian sediments from sites around the globe (Preusser *et al.*, 2001, Preusser *et al.*, 2005, Steffen *et al.*, 2009a), this minimal required delay was remarkably similar at 480 seconds.

A set of 12 samples from the Antsirabe – Betafo region in the Late Quaternary Vakinankaratra volcanic field were selected for luminescence dating *[CHAPTER 5]*. With two exceptions, the samples originate either from stratigraphically linked or stratigraphically correlatable phreatic explosion deposits in the vicinity of the Lac Andraikiba maar and the Betafo basin. The isolated samples belong to an explosion deposit found at Lac Tritrivakely, the location of the only independent age control in the entire volcanic field (e.g. Gasse and Van Campo, 2001).

Initial tests indicated that the feldspar separates from the samples are suitable for infrared stimulated luminescence (IRSL) measurements, and that complete signal resetting appears to have occurred as expected. They also showed, however, that D_E determination of quartz separates using optically stimulated luminescence (OSL) result in uncontrollable scatter and irreproducible results, most likely caused by a weak or absent fast component (Steffen *et al.*, 2009b). The reason for this adverse behaviour of quartz in these samples is not yet understood.

IRSL measurements of the phreatic explosion deposits were successful and D_Es could be obtained for all samples. An average fading rate of 6.0%/decade was determined and the measured ages were successfully corrected for fading using the method of Lamothe *et al.* (2003). The resulting ages are (with one exception) in stratigraphic order, and stratigraphically correlatable layers display similar ages. The study shows that the phreatic eruptions in the Antsirabe - Betafo region, and therefore the onset of the eruptive activity in this young volcanic field, started in the Late Pleistocene. The age of the Lac Andraikiba maar explosion could be constrained to between 50.7 ka and 63.9 ka, and an older phreatic eruption deposit in the same area was similarly dated to between 99.6 ka and 113.9 ka. In the area of the Betafo basin, a phreatic explosion layer underlying the volcanic deposits of the young strombolian cones was dated to approximately 73 ka. At Lac Tritrivakely, the two allochthonous phreatic deposits yielded ages between 33.7 ka and 20.7 ka.

Supplementary information related to the thesis is given in the appendices:

[APPENDIX A] contains abstracts submitted to conferences.

[APPENDIX B] is the geological map of the Antsirabe – Betafo region, including explanatory notes (the map is inserted at the rear of the thesis).

[APPENDIX C] is a reference list of the collected samples.

[APPENDIX D] contains the raw data of the conducted XRF analyses.

[APPENDIX E] contains a short overview over M.I.D.A.S., the controlling software written for the noble gas mass-spectrometer in Bern.

1.3 REFERENCES

BANERJEE, D., SINGHVI, A.K., PANDE, K., GOGTE, V.D. & CHANDRA, B.P. (1999): Towards a direct dating of fault gouges using luminescence dating techniques - Methodological aspects. *CURRENT SCIENCE* 77 (2): 256-268.

BERTIL, D. & REGNOULT, J.M. (1998): Seismotectonics of Madagascar. *TECTONOPHYSICS* 294 (1-2): 57-74.

COLE, J.M., NIENSTEDT, J., SPATARO, G., RASBURY, E.T., LANZIROTTI, A., CELESTIAN, A.J., NILSSON, M. & HANSON, G.N. (2003): Phosphor imaging as a tool for in situ mapping of ppm levels of uranium and thorium in rocks and minerals. *CHEMICAL GEOLOGY* 193 (1-2): 127-136.

COLLINS, A.S., WINDLEY, B.F., KRÖNER, A., FITZSIMONS, I.C.W., RAZAKAMANANA, T., BREWER, T.S. & KINNY, P.D. (2001): The archean rocks of central Madagascar: their place in Gondwana. *AGSO – GEOSCIENCE*, Australia.

DE WIT, M.J. (2003): Madagascar: Heads it's a continent, tails it's an island. *ANNUAL REVIEW OF EARTH AND PLANETARY SCIENCES* 31 : 213-248.

FATTAHI, M. & STOKES, S. (2003): Dating volcanic and related sediments by luminescence methods: a review. *EARTH-SCIENCE REVIEWS* 62 (3-4): 229-264.

FOURNO, J.P. & ROUSSEL, J. (1994): Imaging Of The Moho Depth In Madagascar Through The Inversion Of Gravity-Data - Geodynamic Implications. *TERRA NOVA* 6 (5): 512-519.

GASSE, F. & VAN CAMPO, E. (2001): Late Quaternary environmental changes from a pollen and diatom record in the southern tropics (Lake Tritrivakely, Madagascar). *PALAEOGEOGRAPHY PALAEOCLIMATOLOGY PALAEOECOLOGY* 167 (3-4): 287-308.

HUNTLEY, D.J. & LAMOTHE, M. (2001): Ubiquity of anomalous fading in K-feldspars and the measurement and correction for it in optical dating. *CANADIAN JOURNAL OF EARTH SCIENCES* 38 (7): 1093-1106.

KUSKY, T.M., TORAMAN, E. & RAHARIMAHEFA, T. (2007): The Great Rift Valley of Madagascar: An extension of the Africa-Somali diffusive plate boundary? *GONDWANA RESEARCH* 11 (4): 577-579.

LAMOTHE, M., AUCLAIR, M., HAMZAOUI, C. & HUOT S. (2003): Towards a prediction of long-term anomalous fading of feldspar IRSL. *RADIATION MEASUREMENTS* 37 (4-5): 493-498.

LAVILLE, E., PIQUÉ, A., PLAZIAT, J-C., GIOAN, P., RAKOTOMALALA, R., RAVOLOLONIRINA, Y. & TIDAHY, E. (1998): Le fossé méridien d'Ankay-Alaotra, témoin d'une éxtension crustale récente et actuelle à Madagascar. *BULLETIN DE LA SOCIETÉ GÉOLOGIQUE DE FRANCE* 169 (6): 775-788.

MOUGENOT, D., RECQ, M., VIRLOGEUX, P. & LEPVRIER, C. (1986): Seaward extension of the East African Rift. *NATURE* 321 (5): 599-603.

MURRAY, A.S. & ROBERTS, R.G. (1997): Determining the burial time of single grains of quartz using optically stimulated luminescence. *EARTH AND PLANETARY SCIENCE LETTERS* 152 (1-4): 163-180.

PICKERING, R., KRAMERS, J.D., PARTRIDGE, T., KODOLANYI, J., & PETTKE, T. (Submitted) Uranium-lead dating of calcite-aragonite layers in low-uranium speleothems from South Africa by MC-ICP-MS. *QUATERNARY GEOCHRONOLOGY.*

PIQUÉ, A., LAVILLE, E., CHOTIN, P., CHOROWICZ, J., RAKOTONDRAOMPIANA, S. & THOUIN, C. (1999): Neogene and present extension in Madagascar: structural and geophysical data. *JOURNAL OF AFRICAN EARTH SCIENCES* 28 (4): 975-983.

PORAT, N., LEVI, T. & WEINBERGER, R. (2007): Possible resetting of quartz OSL signals during earthquakes-Evidence from late Pleistocene injection dikes, Dead Sea basin, Israel. *QUATERNARY GEOCHRONOLOGY* 2 (1-4): 272-277.

PRESCOTT, J.R., ROBERTSON, G.B., SHOEMAKER, C., SHOEMAKER, E.M. & WYNN, J. (2004): Luminescence dating of the Wabar meteorite craters, Saudi Arabia. *JOURNAL OF GEOPHYSICAL RESEARCH - PLANETS* 109 (E1): 1-8.

PREUSSER, F., MÜLLER, B.U. & SCHLÜCHTER, C. (2001): Luminescence dating of sediments from the Luthern Valley, central Switzerland, and implications for the chronology of the last glacial cycle. *QUATERNARY RESEARCH* 55 (2): 215-222.

PREUSSER, F., ANDERSEN, B.G., DENTON, G.H. & SCHLÜCHTER, C. (2005): Luminescence chronology of late pleistocene glacial deposits in North Westland, New Zealand. *QUATERNARY SCIENCE REVIEWS* 24 (20-21): 2207-2227.

PREUSSER, F., BLEI, A., GRAF, H. & SCHLÜCHTER, C. (2007): Luminescence dating of Wurmian (Weichselian) proglacial sediments from Switzerland: methodological aspects and stratigraphical conclusions. *BOREAS* 36 (2): 130-142.

RAKOTONDRAOMPIANA, S.A., ALBOUY, Y. & PIQUÉ, A. (1999). Lithospheric model of the Madagascar island [western Indian ocean]: a new interpretation of the gravity data. *JOURNAL OF AFRICAN EARTH SCIENCES* 28 (4): 961-973.

RAMBOLAMANANA, G., SUHADOLC, P. & PANZA, G.F. (1997): Simultaneous inversion of hypocentral parameters and structure velocity of the Central Region of Madagascar as a premise for the mitigation of seismic hazard in Antananarivo. *PURE AND APPLIED GEOPHYSICS* 149 (4): 707-730.

RASAMIMANANA, G., BARDINTZEFF, J.M., RASENDRASOA, J., BELLON, H., THOUIN, C., GIOAN, P. & PIQUÉ, A. (1998): Rifting-related magmatic episodes of south-western Malagasy (Morondava basin). *COMPTES RENDUS DE L'ACADEMIE DES SCIENCES - SERIE II FASCICULE A - SCIENCES DE LA TERRE ET DES PLANETES* 326 (10): 685-691.

ROWLANDS, J.A. (2002): The physics of computed radiography. *PHYSICS IN MEDICINE AND BIOLOGY* 47 (23): R123-R166.

STANKOWSKI, W.T.J. (2007): Luminescence dating as a diagnostic criterion for the recognition of Quaternary impact craters. *PLANETARY AND SPACE SCIENCE* 55 (7-8): 871-875.

STEFFEN, D., SCHLUNEGGER, F. & PREUSSER, F. (2009a): Drainage basin response to climate change in the Pisco valley, Peru. *GEOLOGY* 37 (6): 491-494.

STEFFEN, D., PREUSSER, F. & SCHLUNEGGER, F. (2009b): OSL quartz age underestimation due to unstable signal components. *QUATERNARY GEOCHRONOLOGY* 4 (5): 353-362.

STOREY, M., MAHONEY, J.J., SAUNDERS, A.D., DUNCAN, R.A., KELLEY, S.P. & COFFIN, M.F. (1995): Timing of Hot Spot-Related Volcanism and the Breakup of Madagascar and India. *SCIENCE* 267: 852-855.

SUTTON, S.R. (1985): Thermo-Luminescence Measurements on Shock-Metamorphosed Sandstone and Dolomite from Meteor Crater, Arizona - 1. Shock Dependence of Thermo-Luminescence Properties. *JOURNAL OF GEOPHYSICAL RESEARCH - SOLID EARTH AND PLANETS* 90 (Nb5): 3683-3689.

VANDENBERGHE, D., HOSSAIN, S.M., DE CORTE, F. & VAN DEN HAUTE, P. (2003): Investigations on the origin of the equivalent dose distribution in a Dutch coversand. *RADIATION MEASUREMENTS* 37 (4-5): 433-439.

ZÖLLER, L., BLANCHARD, H. & MCCAMMON, C. (2009): Can temperature assisted hydrostatic pressure reset the ambient TL of rocks? - A note on the TL of partially heated country rock from volcanic eruptions. *ANCIENT TL* 27 (1): 15-23.

CHAPTER 2

New approaches for dating young volcanic eruptions by luminescence methods

Daniel Rufer[a], Frank Preusser[a], Edwin Gnos[b] & Guido Schreurs[a]

[a] Institute of Geological Sciences, University of Bern, Switzerland
[b] Muséum d'histoire naturelle de Genève, Switzerland

Submitted to:
Geochronometria, 2009

"Research is the process of going up alleys to see if they are blind."
Marston Bates (1906 - 1974), Zoologist

NEW APPROACHES FOR DATING YOUNG VOLCANIC ERUPTIONS BY LUMINESCENCE METHODS

2.1 ABSTRACT

The application of luminescence dating to young volcanic sediments has been first investigated over three decades ago, but it was only with the technical innovations of the last decade that such analyses became viable. While current analytical procedures show promise in dating late Quaternary volcanic events, most efforts have been aimed at thermally reset, mainly unconsolidated volcanic tephra. Investigations into direct dating of lava flows or of non-heated volcanoclastics like phreatic explosion layers, however, remain scarce. These volcanic deposits are of common occurrence and represent important chrono- and volcanostratigraphic markers. Their age determination would therefore be of great importance in, for example, tectonic, geomorphological and climate studies. In this article, we adumbrate the potential of phreatic explosion deposits and xenolithic inclusions in lava flows for luminescence dating applications. Their facility for signal resetting is discussed and considerations concerning sampling and sample treatment aspects are outlined.

Keywords: luminescence dating; xenoliths; phreatic explosion; young Quaternary volcanism; geochronology

2.2 INTRODUCTION

Obtaining accurate absolute ages on young volcanic eruptions is an important issue in geomorphologic, tectonic and climate studies, as well as for volcanic hazard assessments. Unfortunately, methods for directly dating volcanic rocks of Late Pleistocene to Holocene age are rather scarce and possess some inherent pitfalls. Most approaches using radioactive decay systems have stringent requirements such as closed system behaviour, reasonable estimations of initial ratios (e.g. in the case of ^{238}U / ^{230}Th disequilibria), or require a prolonged time to accumulate sufficient radiogenic daughter isotopes needed for accurate and precise measurements. Other methods rely on the presence of datable components difficult to obtain in volcanic environments, for example sufficient amounts of organic material for radiocarbon dating. An overview of the most established methods is given in Fattahi and Stokes (2003).

Since the pioneering work of Wintle (1973), the application of luminescence methods to date young Quaternary volcanic deposits and eruptions has been a recurring topic of research

(see Table 1 in Fattahi and Stokes, 2003). Initial investigations were primarily plagued by the occurrence of strong anomalous fading of the blue luminescence signal in volcanic feldspars (Wintle, 1973; Tsukamoto *et al.*, 2007) and a low signal-to-noise ratio of most volcanic quartz and glass, both in thermoluminescence (TL) and in optically stimulated luminescence (OSL) (Miallier *et al.*, 1991; Berger and Huntley, 1994; Schweitzer, 1997). The development of red TL (RTL) single-aliquot regenerative dose (SAR) techniques allowed to circumvent most of these limitations. However, reservations concerning high thermal background (Zink and Visocekas, 1997), low dose sensitivity of high temperature RTL (Miallier *et al.*, 1991) and overlapping RTL spectra of volcanic glass, quartz and plagioclase (Kanemaki *et al.*, 1991) remain. Nonetheless, the cardinal applicability of RTL for dating heated quartz has been demonstrated (e.g. Pilleyre *et al.*, 1992; Miallier *et al.*, 1994a; Miallier *et al.*, 1994b) and further methodological advances in recent years have resulted in positioning this technique as a promising tool to date volcanic quartz and feldspar over a wide range of the Quaternary (e.g. Fattahi and Stokes, 2000; Fattahi and Stokes, 2003; Tsukamoto *et al.*, 2007).

Most of the conducted studies investigated grains extracted from volcanic tephra layers, either juvenile quartz and feldspar (e.g. Liritzis *et al.*, 1996; Ganzawa *et al.*, 2005; Tsukamoto *et al.*, 2007; Tsukamoto *et al.*, In Press) or non-volcanogenic quartz crystals embedded in the volcanic material during eruption (e.g. Miallier *et al.*, 1994a; Sanzelle *et al.*, 2000; Miallier *et al.*, 2004). Luminescence dating of effusive volcanic events was achieved indirectly by using suitable quartz rich sediments which were capped, heated and thermally reset by lava flows (e.g. Pilleyre *et al.*, 1992; Miallier *et al.*, 1994b; Bassinet *et al.*, 2006). Few studies, however, applied luminescence methods to directly date lava flows (using plagioclase and quartz, Guerin and Valladas, 1980; Guerin and Petit, 1983; Guerin and Gillot, 2007). With the exception of a precursor study by Zöller *et al.* (2009), no attempts have yet been made to date volcanic deposits in which signal resetting by thermal means is unlikely, as may be the case in phreatic or phreatomagmatic explosion deposits which comprise a substantial fraction of disaggregated country rock.

In spite of the formidable progress in luminescence measurement techniques of volcanic material, one of the crucial problems in most of these approaches remains the control over the composition of the measured material. This problem is manifested by the potentially different luminescence properties of juvenile volcanic minerals and sedimentary derived xenocrysts (e.g. Guerin and Gillot, 2007; Guerin and Samper, 2007) or volcanic glass (e.g. Berger, 1991; Kanemaki *et al.*, 1991). Thus, if the study material is collected as individual grains from a tephra matrix or a crushed lava, the purity of the sample's volcanic or xenocryst nature is difficult to ascertain, unless the genetic processes of the volcanic unit exclude one of the two. In most continental volcanic settings, this is not the case.

In this paper, we present two new approaches for dating young volcanic eruptions using luminescence methods. The first approach concerns the dating of geochronologically important phreatic explosion deposits. We provide arguments for a non-thermal bleaching of country rock material entrained during explosive fragmentation, and we outline sampling procedures. The second approach advocates the use of country rock xenoliths emplaced in lava flows in order to derive thermally bleached dosimeter grains. The potential for thermal bleaching of such volumetric rock bodies emplaced in lava is investigated and important aspects concerning sampling procedure, extraction of grains for analysis, and potential microdosimetry issues are addressed.

2.3 DATING OF PHREATIC EXPLOSION DEPOSITS

2.3.1 OCCURRENCE AND FORMATION PROCESSES OF PHREATIC EXPLOSION DEPOSITS

Phreatic to phreatomagmatic eruptions can be found in a wide range of volcanic settings (e.g. Laacher See, 12'900 a BP: Schmincke *et al.*, 1999; Krakatoa, 1883: Self and Rampino, 1981; Surtsey, 1963-1965: Thorarinsson, 1967; Jakobsson, 1972). Such eruptions occur through mechanical mixing of magma with water (e.g. at the contact between ascending magma and the phreatic nappe), triggering a chain of reactions resulting in almost instantaneous vaporization and volumetric expansion of large amounts of water

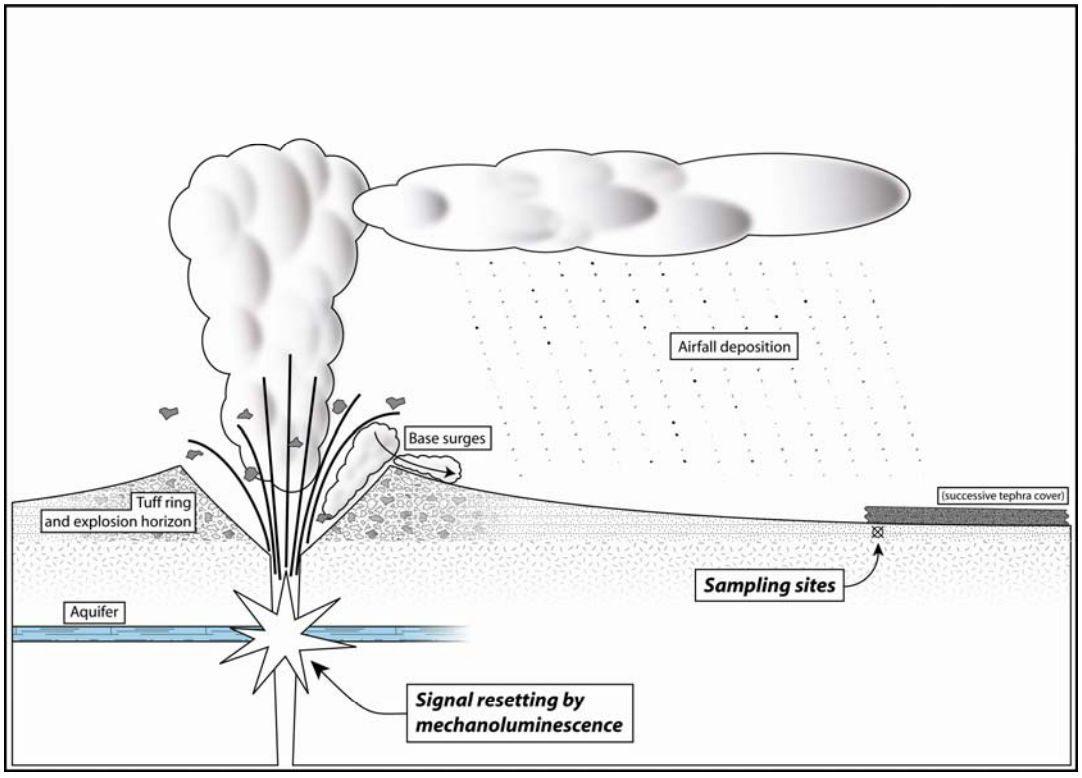

Figure 2.1: Schematic cross-section through a phreatic explosion crater with an indication of the relevant sites and processes for luminescence dating of phreatic deposits.

("Molten Fuel Coolant Interaction", e.g. Zimanowski *et al.*, 1991; White, 1996). The ensuing explosions often form distinct volcanosedimentary deposits ranging from proximal high energy surges to distal airfall deposits (Figure 2.1 & Figure 2.2). In the case of phreatic eruptions, which are defined as steam explosions primarily within the country rock above a magmatic heat source (MacDonald, 1972), the ejected mass contains only a negligible amount of juvenile material, contrary to phreato-magmatic eruptions, where new magma is disintegrated as well. The composition of phreatic explosion deposits can therefore be considered representative of the average basement rock composition. Especially in mafic volcanic provinces dominated by effusive activity, such deposits often provide clearly identifiable correlation horizons which extend far beyond the confined eruption range of cinder cones or fissure vents. As phreatic explosions often occur at the beginning or in early stages of a new eruptive stage, they may provide a means to put a maximum age constraint on a volcanic cycle. This makes them key targets for numerical dating.

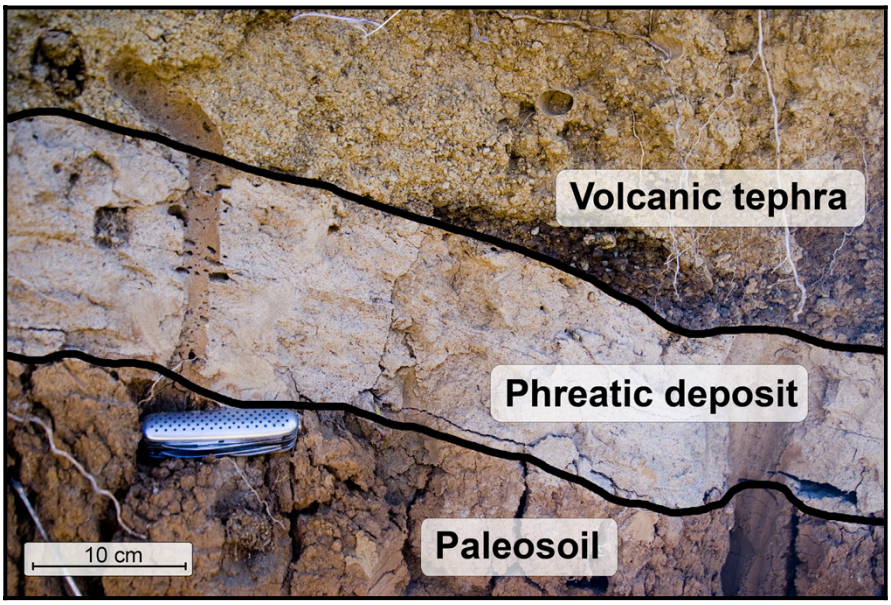

Figure 2.2: Outcrop photograph of a phreatic explosion deposit intercalated between a paleosoil from a presumably Tertiary, strongly weathered basaltic lava flow and overlying tephritic tephra. The ~15 cm thick explosion layer has a sandy grain size and is finely layered; its constituents are derived from granitic rocks. The black lines between the units are for illustrative purposes. Quaternary Ankaratra volcanic field, Central Madagascar.

2.3.2 THE PROBLEM OF SIGNAL RESETTING IN ABSENCE OF THERMAL OR OPTICAL BLEACHING

While optical bleaching of phreatic or phreatomagmatic deposits may be unlikely (due to high opacity of the eruption column and possibly rather short aerial transport times – particularly in the case of base surge deposits), there have been suggestions of luminescence and Electron Spin Resonance (ESR) signal resetting by means of (thermally assisted) hydrostatic and dynamic pressure and/or frictional shearing. Accordant experimental results given in Banerjee *et al.* (1999, and references therein) and Zöller *et al.* (2009), are mainly based on prolonged high static pressure or combinations of elevated

static pressure and mechanical shearing. As such they may not be comparable to the far more violent processes occurring during phreatic eruptions. However, Porat *et al.* (2007) report resetting of OSL signals by earthquake triggered dike-forming injection of clastic material into overlying strata under "several MPa" of hydrostatic pressure and non-elevated temperatures. Sutton (1985), Prescott *et al.* (2004) and Stankowski (2007) present evidence for resetting of TL signals in geological material shocked by meteorite impacts, though the importance of the influence of the mechanical shock vs. transient localized heating is still unclear. Finally, Banerjee *et al.* (1999) showed that short (<1ms) pressure pulses elicit mechanoluminescence from fault gouge material proportional to the applied peak pressure above 200 MPa and Sears *et al.* (1984) present a systematic study of artificially shocked chondrite material, showing both a bleaching of natural TL intensity as well as a strong reduction in TL sensitivity in plagioclase for shock waves above 27 GPa. Laboratory simulations of extremely small-scale phreatomagmatic explosions resulted in pressure pulses of 1.5 ms between 10 and 100 MPa for melt volumes of only 300 g and explosion energies of 500 J (Zimanowski *et al.*, 1991), Though extrapolating these pressure values for natural eruptions with explosion energies more than 9 orders of magnitude higher (e.g. 10^{10} to 10^{12} J, Mt. Usu, Japan, 2000; Yokoo *et al.*, 2002) may not be straightforward, it must also be taken into account, that the natural case includes several of these resetting mechanisms in combination.

Based on these observations, mechanical resetting of luminescence signals in phreatic explosion deposits is very likely.

2.3.3 SAMPLING AND SAMPLE PREPARATION

In the field, identifying potential layers for sampling includes stratigraphic correlations of the distal sandy deposits to clearly identifiable proximal explosion breccia horizons, in order to ascertain the phreatic nature of the deposit based on its characteristics (see Fischer and Schmincke, 1984), as well as pinpointing its geographical origin. Scrutinizing the mineral composition of the deposit gives a first indication whether contamination by juvenile volcanic material has to be considered or not. Sampling can be done in a similar manner to sedimentary samples (e.g. by driving steel tubes into freshly exposed outcrops). As the thickness of the sampled layer can - based on the ejected volume and the depositional distribution - fall below the minimal thickness required for assuming a homogeneous irradiation environment created by the sampled material itself, it may be necessary to take samples for dose rate determinations from the under- and overlying layers as well. This is particularly important where strong differences in radionuclide contents of paleosoils, crystalline basement material of the explosion layer and capping volcanic tephra material

occur. Sample preparation and measurement can follow standard procedures of sieving, chemical treatment and density separation.

Their chronostratigraphic importance and the rather straightforward sampling and sample preparation techniques propound phreatic explosion deposits as an important potential candidate for luminescence dating of late Quaternary volcanic sequences. Due to the non-volcanic nature of the samples, anomalous fading is expected to be a subordinate problem. However, due to the peculiar, far more violent history of the material compared to, for example, a fluvial derived sediment, it may prove prudent to conduct comprehensive fading tests.

2.4 DATING OF THERMALLY BLEACHED XENOLITHS FROM LAVA FLOWS

Lava flows are common to most volcanic systems and may form important volcanostratigraphic markers, They can be traced back to their source and are more resistant to physical weathering than unconsolidated ejecta. Particularly in mafic volcanic systems, the late stages of an eruptive cycle often are of an effusive nature (e.g. lava ponding and subsequent breakthrough through the scoriae cone rampart). Lava flows may therefore complement an initial or early stage phreatic explosion horizon in providing a minimum age to an eruptive cycle. In terms of luminescence dating they do, however, pose some particular problems, such as the predominantly volcanic origin of the natural dosimeters, the lack of quartz in the volumetrically preponderant mafic suite of volcanic rocks, and technical problems related to the extraction of individual mineral grains from an at least partially glassy matrix.

Figure 2.3: Syenogranite xenolith embedded in a proximal basanitic lava flow (Lac Tritriva, central Madagascar). The whitish appearance is due to calcination (most probably at temperatures > 1000°C).

On the other hand, lava flows often contain xenolithic material, originating from country rock at the vent or taken up during emplacement of the flow (Figure 2.3). Provided that the crustal base-

ment material contains luminescence dosimeters, such xenoliths might be used for luminescence dating. They would record the lava flow emplacement as their last heating event. As such xenoliths are cohesive entities, their identification and distinction from the petrographically different volcanic material is facilitated and any grains extracted from them certainly are of non-volcanic origin. Xenoliths may provide datable material even in situations, where the volcanic rocks themselves are devoid of quartz or feldspar. They also allow circumventing the issue of impure mixtures of volcanic and non-volcanic dosimeter grains as well as of problems specifically associated with volcanic dosimeters.

2.4.1 SAMPLING AND SAMPLE PREPARATION

As the outermost parts of the xenolith will have to be cut away in order to avoid contamination with adherent volcanic material and to remove optically bleached surface grains, selecting a specimen of at least 5 to 10 cm in diameter is recommended. Fortunately, this also allows sample collection without any special consideration regarding sunlight exposure. When extracting a xenolith from the lava, it is necessary to also take a representative sample of the volcanic material for dosimetry considerations.

Xenolith samples must be disaggregated prior to any standard sample preparation methods (which are normally applied to unconsolidated samples). A suitable generalized procedure is

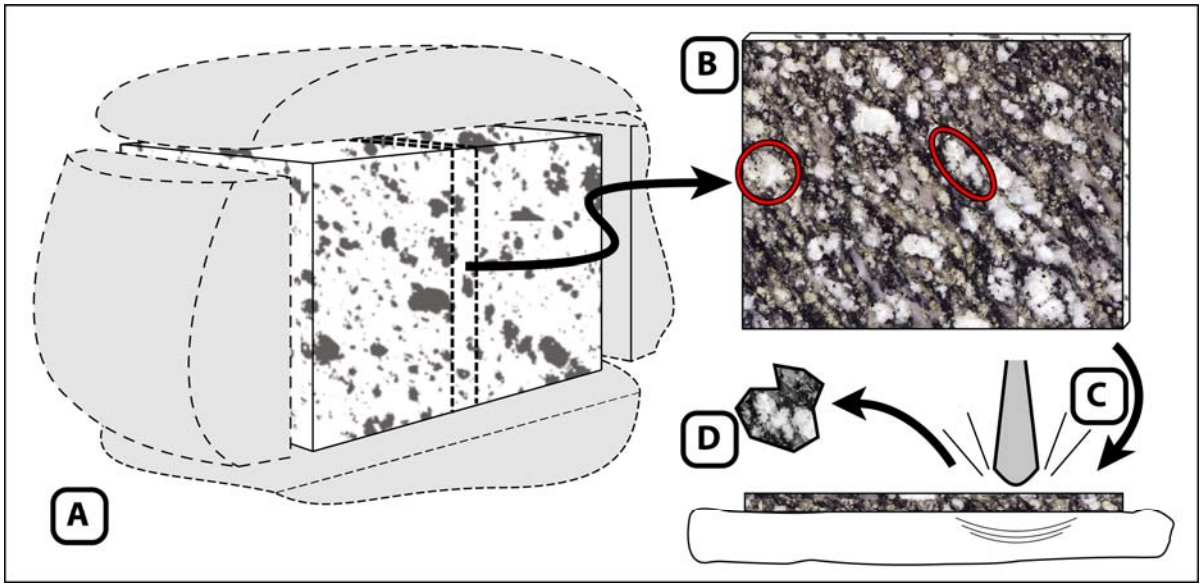

Figure 2.4: Generalized procedure for extracting mineral grains for luminescence measurements from hard rocks. A) Any exposed outer parts are removed and B) the remaining material is cut into thin slabs of a few mm thickness. After identifying and marking target mineral grains, the slab is placed on a flexible pad and manually cracked using a constant application of force (C). The pieces containing the marked grains (D) are then gently crushed in an agate mortar and sieved to the desired grainsize spectrum. If required, the obtained material can be further processed by density separation and chemical treatments, as necessitated by the intended use. If the extracted mineral phase is quartz, treatment with H_2FSi_6 is advisable to remove any contaminant feldspar (Mauz and Lang, 2004).

given in Figure 2.4. Sample disaggregation has to be non-detrimental to the type of signal that is to be measured. It must therefore be done under laboratory red light, and it is important that cutting with a diamond blade has to be done very slowly and under copious amounts of cold water in order to prevent heating of the sample. Concerning the subsequent breaking and crushing of the slabs, Zöller *et al.* (2009) report that "vigorous grinding" for 15 minutes in an agate mortar may lead to an increased natural TL signal due to triboluminescence. This might be related, however, to the concomitant intense frictional shearing, as Tsukamoto and Duller (2008) did not find any evidence for decreasing blue TL, OSL and IRSL luminescence signals due to manual crushing (S. Tsukamoto, personal communication, 2008).

2.4.2 THERMAL BLEACHING OF SAMPLES DURING EMPLACEMENT

Successful TL dating of volcanic units using embedded xenoliths prerequisites a complete thermal resetting of the luminescence signal during or shortly after the incorporation of the xenolith into the volcanic material. To achieve bulk heating of the xenolith, it has to be subjected to a sufficiently high ambient temperature (e.g. >450°C for TL).

For (non-carbonatitic) lava flows, emplacement temperatures generally range between 750 to 1200°C, as a function of chemical composition (Rittmann, 1981). Flow surface cooling rates for a 20-70 m thick rhyolitic flow of Mayor Island (NZ) are given between 0.001 and 6°C min^{-1} with the majority of the data around 0.001°C min^{-1} (Gottsmann and Dingwell, 2002). For basaltic compositions, Flynn and Mouginis-Mark (1992) report cooling of the thin surface crust of a very small volume (2 m wide, 3 m long, 30 cm thick) flow from the Pu'u O'o fissure, Kilauea, Hawaii, from 768 to 390°C over a period of 59 minutes after emplacement. During the same period, temperatures just below the cooling crust stayed between 1150 and 900°C. This indicates that most parts of a lava flow will, regardless of its composition, retain temperatures in excess of 450°C for a prolonged amount of time.

2.4.3 VOLUME HEATING MODEL AND CALEFACTION EXPERIMENTS

In order to verify the assumption that a xenolith embedded in such a lava flow will be thermally reset, a numerical model was calculated, in which a granite cube of 7 cm edge length had its surface linearly heated from 20 to 700°C over the course of 30 minutes, after which the surface temperature was kept constant at 700°C for another 30 minutes. Heat transfer towards the cube centre was controlled by a thermal conductivity of 2.25 W m^{-1} K^{-1}, which is close to the lower boundary of thermal conductivity values reported for dry granite (2.12 to 3.12 W m^{-1} K^{-1}; Cho *et al.*, 2009).

Figure 2.5 shows a central section of the modelled granite cube at various times throughout the applied heating. The depicted timesteps are A) after 24 minutes, when the core temperature exceeds 450°C, B) after 30 minutes, when the linear heating of the cube surface reaches its upper limit of 700°C and C) after 60 minutes, by keeping the surface temperature at 700°C for another 30 minutes. It can be seen that in the modelled case, a similarly sized xenolith which becomes embedded in an only 700°C hot lava flow (lower end

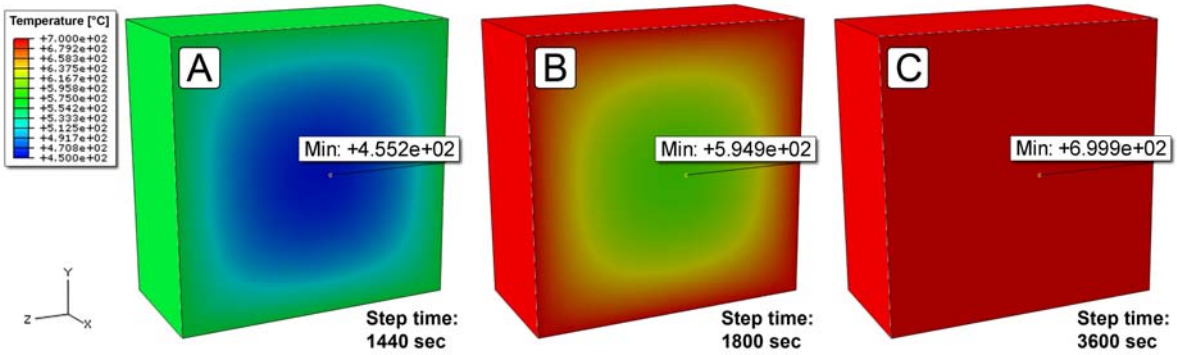

Figure 2.5: Model of conductive heat distribution in a granite cube. Even with a low heating gradient of ~23°C min^{-1} of the cube's surface, the core temperature exceeds 450°C after 24 minutes (A), while the surface is still below the "lava" temperature. For model parameters and boundary conditions, see text.

of the temperature range for lava flows, Rittmann, 1981) would be completely thermally bleached in less than half an hour. Obviously, the model differs from the natural case in it's assumption of a very low and linear heating gradient (~23°C min^{-1}) of the cube's surface. Based on Fouriers Law of thermal conduction (e.g. Cannon, 1984), the surface temperature would show a far steeper rise with initial values up to 30°C sec^{-1} (calculated for a 5 mm thick boundary layer, specific heat capacity 0.79 kJ kg^{-1} K^{-1}). This in turn would accelerate heat conduction towards the cube's centre, as this is a function of temperature gradient between core and surface of the cube. Based on these considerations and the low values used for the lava temperature and the granite's thermal conductivity, the results are encouraging in respect to the thermal resetting of a xenolith, as the model yields a very conservative temperature estimate for the cube's core after embedding into the lava flow.

A complementary laboratory calefaction test was conducted in which two granite cubes from the central Aar massif, Switzerland, were put into a oven preheated at 800°C and heated for 30 and 60 minutes respectively. Immediately afterwards, they were removed from the oven and let to cool at room temperature. The dimension of the cubes was identical to the numerical model. It must be noted that the conditions of the calefaction experiment are not the same as the conditions of the model, as inside the oven the blocks are embedded in air. Heat transfer onto the granite is therefore not primarily conductive, but is dominated by convection (heat transfer from the hot air to the granite) and radiation (heat transfer from the glowing oven walls to the granite), almost certainly resulting in a lower total heat flux

than used in the model. Irrespective of this, the cubes were glowing in the bright red to orange spectrum after 30 minutes, indicative of temperatures above 700°C. As such, this is roughly comparable to the model situation.

After cooling, feldspar separates were extracted from near the edges and from the core of the cubes (see sample preparation procedure given in this article) in order to verify the complete thermal bleaching of the sample. The TL measurements were conducted on a Risø DA-20 TL/OSL reader, fitted with an internal $^{90}Sr/^{90}Y$ beta-source and using a Schott BG39 and an interference filter. A short TL-SAR protocol with two regenerative dose points was used, similar to the one suggested by Richter and Krbetschek (2006). All tempered samples show a natural TL peak in the order of three magnitudes lower than the peak of the 200 s regenerated dose (Figure 2.6). The calculated D_E cluster close to zero (average: 0.046 ± 0.042 Gy), substantiating the thermal resetting of the luminescence signal through tempering. Recycling ratios are 1.02 ± 0.11 and the sensitivity change over the SAR sequence remained below 20 %.

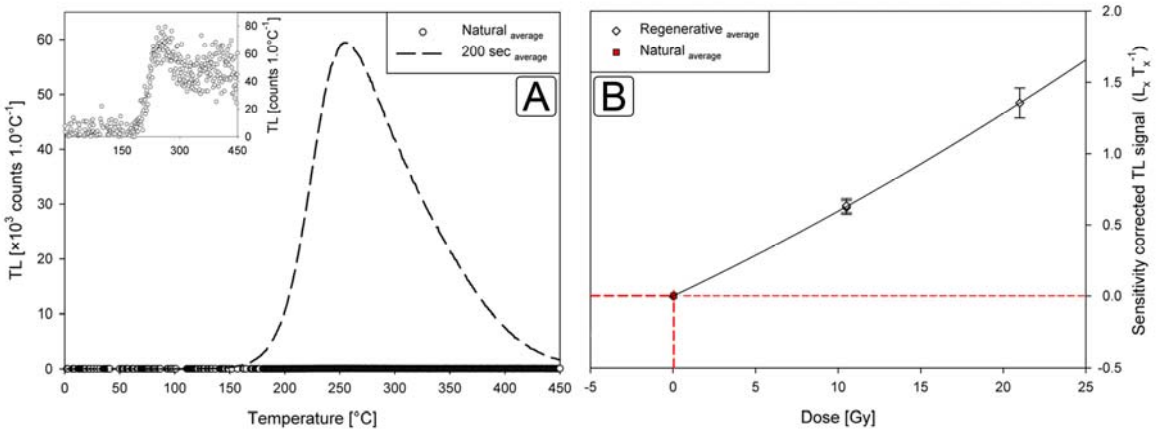

Figure 2.6: A) TL glow curve of the natural (inset) and the 200 s regenerative signal from the calefaction experiment. Shown are the average curves of 3 aliquots from a feldspar grain extracted from the core of the cube after tempering for 30 minutes at 800°C. Please note that the scaling in the inset is three magnitudes lower. B) Corresponding SAR dose response curve using a quadratic fit. D_E = 0.046 ± 0.042 Gy; recycling = 1.02 ± 0.11; measured sensitivity change during the SAR sequence is less than 20%.

Based on the results from the numerical model as well as the calefaction experiments, thermal bleaching of comparably small xenoliths during emplacement in a lava flow is to be expected. Thermal bleaching of even considerably larger xenoliths is most likely, considering 1) the very conservative values used in the numerical model, 2) the fact that lava temperatures are usually higher, and 3) that cooling rates are far lower in the natural case than in the calefaction experiment.

2.4.4 MICRODOSIMETRIC CONSIDERATIONS WHEN MEASURING COARSE GRAINED, SOLID MATERIALS

The configuration of a crystalline xenolith in a more or less homogeneous volcanic matrix material poses some profound complications in establishing effective dose rates. External dose contributions to a specific mineral grain originate both from the xenolith material itself, as well as from the volcanic matrix material surrounding the xenolith. While the latter may be reduced to mainly gamma radiation due to shielding by the rock material between the target grain and the lava, the former is dependant on the mineralogical composition of the xenolith. Being an aggregate of unequally sized mineral grains with potentially different radiation emissions (e.g. inert quartz, large radiation emitters like potassium feldspars or small, highly radiating accessory minerals like zircons or monazites), the spatial dosimetry field of a xenolith might be strongly heterogeneous. Detection of such inhomogeneities is therefore of great importance for discerning potentially problematic samples or to specifically select mineral grains from dosimetrically homogeneous regions of a xenolith. For a detailed discourse of this topic and an analytical approach see Rufer and Preusser (In Press).

2.5 SUMMARY AND OUTLOOK

We have outlined two potential candidate materials for dating young Quaternary volcanic events and discussed their cardinal usability for luminescence dating. Both, phreatic explosion deposits as well as crustal xenoliths in lava flows are common to most continental volcanic systems, making the proposed dating approaches potentially applicable to a large number of sites. While actual luminescence dating of such materials is yet outstanding, the importance of determining the age of young volcanic deposits warrants detailed investigations.

ACKNOWLEDGEMENTS

R. Mettier is gratefully thanked for helping with the calefaction model calculations and M. Suchy, S. Lowick, and I. Schindelwig are greatly acknowledged for helpful comments on the manuscript. This work was funded by the Swiss National Science Foundation (SNSF), Project No's 200020-105453/1, 200020-118023/1 and 206021-117374.

2.6 REFERENCES

BANERJEE, D., SINGHVI, A.K., PANDE, K., GOGTE, V.D. & CHANDRA, B.P. (1999): Towards a direct dating of fault gouges using luminescence dating techniques - Methodological aspects. *CURRENT SCIENCE* 77 (2): 256-268.

BASSINET, C., MERCIER, N., MIALLIER, D., PILLEYRE, T., SANZELLE, S. & VALLADAS, H. (2006): Thermoluminescence of heated quartz grains: Intercomparisons between SAR and multiple-aliquot additive dose techniques. *RADIATION MEASUREMENTS* 41 (7-8): 803-808.

BERGER, G.W. (1991): The use of glass for dating volcanic ash by thermoluminescence. *JOURNAL OF GEOPHYSICAL RESEARCH - SOLID EARTH* 96 (B12): 19705-19720.

BERGER, G.W. & HUNTLEY, D.J. (1994): Tests for optically stimulated luminescence from tephra glass. *QUATERNARY SCIENCE REVIEWS* 13 (5-7): 509-511.

CANNON, J. (1984): The one-dimensional heat equation. Addison-Wesley, Menlo Park

CHO, W.J., KWON, S. & CHOI, J.W. (2009): The thermal conductivity for granite with various water contents. *ENGINEERING GEOLOGY* 107 (3-4): 167-171.

FATTAHI, M. & STOKES, S. (2000): Extending the time range of luminescence dating using red TL (RTL) from volcanic quartz. *RADIATION MEASUREMENTS* 32 (5-6): 479-485.

FATTAHI, M. & STOKES, S. (2003): Dating volcanic and related sediments by luminescence methods: a review. *EARTH-SCIENCE REVIEWS* 62 (3-4): 229-264.

FISCHER, R.V. & SCHMINCKE, H.U. (1984): Pyroclastic rocks. Springer Verlag, Berlin

FLYNN, L.P. & MOUGINIS-MARK, P.J. (1992): Cooling rate of an active Hawaiian lava flow from nighttime spectroradiometer measurements. *GEOPHYSICAL RESEARCH LETTERS* 19 (17): 1783-1786.

GANZAWA, Y., FURUKAWA, H., HASHIMOTO, T., SANZELLE, S., MIALLIER, D. & PILLEYRE, T. (2005): Single grains dating of volcanic quartz from pyroclastic flows using red TL. *RADIATION MEASUREMENTS* 39 (5): 479-487.

GOTTSMANN, J. & DINGWELL, D.B. (2002): The thermal history of a spatter-fed lava flow: the 8-ka pantellerite flow of Mayor Island, New Zealand. *BULLETIN OF VOLCANOLOGY* 64 (6): 410-422.

GUERIN, G. & VALLADAS, G. (1980): Thermo-luminescence dating of volcanic plagioclases. *NATURE* 286 (5774): 697-699.

GUERIN, G. & PETIT, R.H. (1983): Thermo-luminescence dating of lava flows from Guadeloupe - Some Problems. *COMPTES RENDUS DE L'ACADEMIE DES SCIENCES SERIE II* 296 (23): 1791-1794.

GUERIN, G. & SAMPER, A. (2007): Aberrant thermoluminescence dates obtained from primary volcanic quartz. *RADIATION MEASUREMENTS* 42 (9): 1453-1459.

GUERIN, G. & GILLOT, P.Y. (2007): New elements of chronology of 'Bas Vivarais' Pleistocene volcanism (Ardeche, France) by thermoluminescence dating. *COMPTES RENDUS GEOSCIENCE* 339 (1): 40-49.

JAKOBSSON, S.P. (1972): On the consolidation and palagonitization of the tephra of the Surtsey volcanic island, Iceland. *SURTSEY RESEARCH PROGRESS REPORT* VI: 121-128.

KANEMAKI, M., NINAGAWA, K., YAMAMOTO, I., NAKAGAWA, M., WADA, T., YAMASHITA, Y. & ENDO, K. (1991): Red thermoluminescence of volcanic glass fractions from tephras. *NUCLEAR TRACKS AND RADIATION MEASUREMENTS* 18 (1-2): 81-88.

LIRITZIS, I., MICHAEL, C. & GALLOWAY, R.B. (1996): A significant aegean volcanic eruption during the second millennium B.C. revealed by thermoluminescence dating. *GEOARCHAEOLOGY* 11 (4): 361-371.

MACDONALD, G.A. (1972): Volcanoes. Prentice-Hall, Englewood Cliffs, N.J.

MAUZ, B. & LANG, A. (2004): Removal of the feldspar-derived luminescence component from polymineral fine silt samples for optical dating applications: evaluation of chemical treatment protocols and quality control procedures. *ANCIENT TL* 22 (1): 1-9.

MIALLIER, D., FAIN, J., MONTRET, M., PILLEYRE, T., SANZELLE, S. & SOUMANA, S. (1991): Properties of the red TL peak of quartz relevant to thermoluminescence dating. *NUCLEAR TRACKS AND RADIATION MEASUREMENTS* 18 (1-2): 89-94.

MIALLIER, D., FAIN, J., SANZELLE, S., PILLEYRE, T., MONTRET, M., SOUMANA, S. & FALGUERES, C. (1994a): Attempts at dating pumice deposits around 580-Ka by use of red TL and ESR of xenolithic quartz inclusions. *RADIATION MEASUREMENTS* 23 (2-3): 399-404.

MIALLIER, D., SANZELLE, S., FALGUERES, C., FAIN, J., MONTRET, M., PILLEYRE, T., SOUMANA, S., LAURENT, M., CAMUS, G. & DEHERVE, A.D. (1994b): Intercomparisons of red TL and ESR signals from heated quartz grains. *RADIATION MEASUREMENTS* 23 (1): 143-153.

MIALLIER, D., CONDOMINES, M., PILLEYRE, T., SANZELLE, S. & GUITTET, J. (2004): Concordant thermoluminescence and U-238-Th-230 ages for a trachytic dome (Grand Sarcoui) from the Chaine des Puys (French Massif Central). *QUATERNARY SCIENCE REVIEWS* 23 (5-6): 709-715.

PILLEYRE, T., MONTRET, M., FAIN, J., MIALLIER, D. & SANZELLE, S. (1992): Attempts at dating ancient volcanos using the red TL of quartz. *QUATERNARY SCIENCE REVIEWS* 11 (1-2): 13-17.

PORAT, N., LEVI, T. & WEINBERGER, R. (2007): Possible resetting of quartz OSL signals during earthquakes - Evidence from late Pleistocene injection dikes, Dead Sea basin, Israel. *QUATERNARY GEOCHRONOLOGY* 2 (1-4): 272-277.

PRESCOTT, J.R., ROBERTSON, G.B., SHOEMAKER, C., SHOEMAKER, E.M. & WYNN, J. (2004): Luminescence dating of the Wabar meteorite craters, Saudi Arabia. *JOURNAL OF GEOPHYSICAL RESEARCH - PLANETS* 109 (E1): 1-8.

RICHTER, D. & KRBETSCHEK, M. (2006): A new thermoluminescence dating technique for heated flint. *ARCHAEOMETRY* 48: 695-705.

RITTMANN, A. (1981): Vulkane und ihre Tätigkeit. Ferdinand Enke Verlag Stuttgart

RUFER, D. & PREUSSER, F. (In Press): Potential of autoradiography to detect spatially resolved radiation patterns in the context of trapped charge dating. *GEOCHRONOMETRIA*.

SANZELLE, S., PILLEYRE, T., MONTRET, M., FAIN, J., MIALLIER, D., CAMUS, G., DE HERVE, A.D. & DEFLEUR, A. (2000): Thermoluminescence dating: study of a possible chronological correlation between the maar of La Vestide-du-Pal and a tephra layer from La Baume-Moula-Guercy (Ardeche, France). *COMPTES RENDUS DE L'ACADEMIE DES SCIENCES, SERIE II, FASCICULE A - SCIENCES DE LA TERRE ET DES PLANETES* 330 (8): 541-546.

SCHMINCKE, H.U., PARK, C. & HARMS, E. (1999): Evolution and environmental impacts of the eruption of Laacher See Volcano (Germany) 12,900 a BP. *QUATERNARY INTERNATIONAL* 61: 61-72.

SCHWEITZER, U. (1997): Thermolumineszenz-Datierbarkeit vulkanischer Gläser des Thera-Vulkans (Santorin-Archipel, Griechenland). PhD-Thesis, University of Cologne, Cologne.

SEARS, D.W., ASHWORTH, J.R., BROADBENT, C.P. & BEVAN, A.W.R. (1984): Studies of an artificially shock-loaded H-group chondrite. *GEOCHIMICA ET COSMOCHIMICA ACTA* 48 (2): 343-360.

SELF, S. & RAMPINO, M.R. (1981): The 1883 eruption of Krakatau. *NATURE* 294(5843): 699-704.

STANKOWSKI, W.T.J. (2007): Luminescence dating as a diagnostic criterion for the recognition of Quaternary impact craters. *PLANETARY AND SPACE SCIENCE* 55 (7-8): 871-875.

SUTTON, S.R. (1985): Thermo-luminescence measurements on shock-metamorphosed sandstone and dolomite from Meteor Crater, Arizona - 1. Shock dependence of thermo-luminescence properties. *JOURNAL OF GEOPHYSICAL RESEARCH - SOLID EARTH AND PLANETS* 90 (Nb5): 3683-3689.

THORARINSSON, S. (1967): The Surtsey eruption. Course of events during the year 1966. *SURTSEY RESEARCH PROGRESS REPORT* III: 84-90.

TSUKAMOTO, S., MURRAY, A.S., HUOT, S., WATANUKI, T., DENBY, P.M. & BØTTER-JENSEN, L. (2007): Luminescence property of volcanic quartz and the use of red isothermal TL for dating tephras. *RADIATION MEASUREMENTS* 42 (2): 190-197.

TSUKAMOTO, S. & DULLER, G.A.T. (2008): Anomalous fading of various luminescence signals from terrestrial basaltic samples as Martian analogues. *RADIATION MEASUREMENTS* 43 (2-6): 721-725.

TSUKAMOTO, S., DULLER, G.A.T., WINTLE, A.G. & FRECHEN, M. (In Press): Optical dating of a Japanese marker tephra using plagioclase. *QUATERNARY GEOCHRONOLOGY*, doi:10.1016/j.quageo.2009.02.002

WHITE, J.D.L. (1996): Impure coolants and interaction dynamics of phreatomagmatic eruptions. *JOURNAL OF VOLCANOLOGY AND GEOTHERMAL RESEARCH* 74 (3-4): 155-170.

WINTLE, A.G. (1973): Anomalous fading of thermoluminescence in mineral samples. *NATURE* 245 (5421): 143-144.

YOKOO, A., TANIGUCHI, H., GOTO, A. & OSHIMA, H. (2002): Energy and depth of Usu 2000 phreatic explosions. *GEOPHYSICAL RESEARCH LETTERS* 29 (24), 2195.

ZIMANOWSKI, B., FRÖHLICH, G. & LORENZ, V. (1991): Quantitative experiments on phreatomagmatic explosions. *JOURNAL OF VOLCANOLOGY AND GEOTHERMAL RESEARCH* 48 (3-4): 341-358.

ZINK, A.J.C. & VISOCEKAS, R. (1997): Datability of sanidine feldspars using the near-infrared TL emission. *RADIATION MEASUREMENTS* 27 (2): 251-261.

ZÖLLER, L., BLANCHARD, H. & MCCAMMON, C. (2009): Can temperature assisted hydrostatic pressure reset the ambient TL of rocks? - A note on the TL of partially heated country rock from volcanic eruptions. *ANCIENT TL* 27 (1): 15-23.

CHAPTER 3

Potential of autoradiography to detect spatially resolved radiation patterns in the context of trapped charge dating

Daniel Rufer & Frank Preusser

Institute of Geological Sciences, University of Bern, Switzerland

Geochronometria, 2009, In Press

"There are two possible outcomes: if the result confirms the hypothesis, then you have made a measurement. If the result is contrary to the hypothesis, then you have made a discovery."

Enrico Fermi (1901 - 1954), Physicist

POTENTIAL OF AUTORADIOGRAPHY TO DETECT SPATIALLY RESOLVED RADIATION PATTERNS IN THE CONTEXT OF TRAPPED CHARGE DATING

3.1 ABSTRACT

Recent developments in optically stimulated luminescence (OSL) dating allow the determination of signals in increasingly smaller sample amounts. This has led to microdosimetry having a larger impact on equivalent dose (D_E) distributions and therefore, detection and assessment of spatial distribution of radionuclides has become more important. This study demonstrates the application of autoradiography using imaging plates to determine spatially resolved radiation inhomogeneities in different types of samples. Qualitative evaluations of radiation inhomogeneity are carried out on unconsolidated sediments as well as on hard rock samples. While indicating some limitations of applicability, the results demonstrate that the method is an efficient tool to detect and document spatial variations in a sample's radiation field. It therefore provides a possibility to rapidly screen samples to check whether microdosimetry might affect the D_E data.

Furthermore, an approach to calibrate autoradiographic images for quantitative use is suggested. Using pressed powder pellets of reference materials, a series of calibration images were exposed, from which a functional relation between specific sample activity and greyscale value in the autoradiographic image has been deduced. Testing the calibration on a set of 16 geological samples, of which their radionuclide content is known, shows a good correlation between specific activities calculated from the nuclide content and specific activities deduced from the autoradiographic images. These findings illustrate the potential of autoradiography with imaging plates to detect spatial distributions of radionuclides and to tackle certain aspects of the problem of microdosimetry in modern trapped charge dating.

Keywords: imaging plate; autoradiography; microdosimetry; OSL; trapped charge dating; spatially resolved radioactivity

3.2 INTRODUCTION

Over the last decades, trapped charge dating methods and their application to geological material have seen an extensive development and refinement. They are now a commonly used tool for dating samples ranging from Quaternary sediments to archaeological artefacts. In particular, the introduction of the single-aliquot regenerative-dose (SAR) protocol by

Murray and Wintle (2000) for Optically Stimulated Luminescence (OSL) dating, enables that all measurements to obtain equivalent dose (D_E) estimates can be made on single aliquots or even single grains. This allows the determination of D_E distributions as inherent properties of a sample, based on the external variance of the SAR measurements. In recent years, it has become increasingly evident that broad D_E distributions can often be attributed not only to partial bleaching or experimental scattering, but also to the effects of microdosimetry (e.g. Vandenberghe *et al.*, 2003; Lomax *et al.*, 2007; Preusser *et al.*, 2007). The main cause for such small scale local heterogeneities in dose rate are spatially discrete high radiation emitters (e.g. K-rich feldspars, zircons or monazites) which form radiation "hot-spots". This is especially important in the case of alpha and beta radiation, which are not only the major contributors to luminescence dosimetry, but also exhibit far stronger spatial variations (due to their strong intensity falloff in particulate matter) than e.g. gamma radiation. While the widely used gamma-spectrometry allows to accurately determine dose rates differentiated by radionuclides, it is an integrated measurement method that yields no information about the spatial distribution of the sources of the measured radiation. Even though this problem is of concern to all trapped charge dating methods, its ramifications are more pronounced when using small aliquot sizes. This especially holds true for single grain OSL dating, as the overall percentage of grains in a sample which are in the vicinity of radiation hotspots and therefore subject to their localized high radiation fields is linked to the hotspot concentration. An increasing number of high radiation emitters therefore cause an increasing spread in incident radiation on individual grains in the sample. If the hotspot concentration gets very high, this effect abates due to increasing overlap of the localized radiation fields, resulting in higher but more homogeneous incident radiation for these grains. On the other hand, a very low hotspot concentrations leads to statistical insignificance of high incident radiation grains. It would therefore be desirable to have a method available to visualize such hot-spots or areas of elevated radionuclide concentration, in order to verify whether the assumption of applicability of the average infinity-matrix dose rate is valid for this sample, or whether an observed scatter in D_E could also be attributable to non-uniformity in the spatial distribution of radionuclides.

In this article, we demonstrate the application of computed autoradiography using an imaging plate (IP) as a passive detection method to qualitatively document spatially resolved radioactivity in the context of trapped charge dating. The method constitutes a rapid screening and visualization procedure, which is applicable to various types of geological sample material and is non-destructive to the trapped charge signals. While an absolute calibration of the relationship between radiation energy and radiographic signal is still outstanding, we present a first investigation into using IP readout data for quantitative dosimetry.

3.3 THE PROBLEM OF DETERMINING NON-UNIFORM RADIATION FIELDS IN THE DOMAIN OF TRAPPED CHARGE DATING

Usually the possibility that microdosimetry might have an influence on measured D_E is perceived only "after the fact", i.e. by observing a large spread in D_E that cannot - or only partially - be explained by variations in luminescence sensitivity and dose saturation characteristics (Duller *et al.*, 2000), incomplete bleaching (Olley *et al.*, 1999), or post-depositional mixing (Bateman *et al.*, 2003). At that stage, determination of the nature, quantity and distribution of potential sample constituents that might have caused a heterogeneous radiation field can most often only be made on another part of that sample, as luminescence dating methods commonly require sample disaggregation and mineral separation for measurements.

This is acceptable for completely unconsolidated material, where the spatial arrangement of the different particles making up the sediment must – due to the inevitable perturbation during sampling and sample handling – be taken to be homogeneous on the scale of the sample volume. For such material, spatial dose-rate distribution is a statistical property linked to the relative concentrations of the various particle types in the sediment and their respective dose-rates. Monte-Carlo models to describe and quantify the microdosimetric effects of non-uniform dose-rate and dose-rate distributions to single grains in heterogeneous sediments have been suggested by Nathan *et al.* (2003) (β radiation), Brennan (2006) (α radiation) and Mayya *et al.* (2006) (^{40}K grains in quartz matrix).

However, in the case of hardrock samples or metaconsolidated material like sediment drill cores, variations in radiation can be structurally caused (e.g. veining or sedimentary layering) and obtaining information about its original spatial distribution allows to select parts of the sample that are either not influenced by differential radiation or where the variability is at least more uniform. Therefore, such inquiries must be made on the same material that is going to be processed for and then measured by luminescence methods, unless the measurement method does not require sample dissagregation (e.g. spatially resolved luminescence measurements using CCD imagers (Greilich *et al.*, 2002; Greilich *et al.*, 2005)). Any other case requires that these preliminary analyses must be non-detrimental to the quality of the natural luminescence signal and must keep the bulk structure of the sample intact. Moreover, they must also be feasible on larger samples, thus retaining the possibility for sufficient quartz or feldspar to be extracted (e.g. from parts of the sample that were selected due to radiation homogeneity). This forecloses most of the commonly used techniques for (radioactive) element mapping on solid samples like electron probe micro-analyzers (EPMA) or laser ablation inductively coupled plasma mass spectrometry (LA-ICP-MS) due to exposure of the sample to electromagnetic irradiation or light as well as due to stringent limitations in sample size. Optical microscopy could

accommodate larger sample sizes, but lacks the required resolution and still poses the problem of requiring light.

3.4 COMPUTED AUTORADIOGRAPHY SYSTEMS

The basic constituents of an autoradiography system are: the sample material, which emits a radioactive signal; the image sensor, in this case the IP, which temporarily stores the energy pattern from the emitted radiation; the image reader (often colloquially called a "beta-scanner"), which reads out the latent image of the IP and converts it into an analogue and subsequently digital signal, and finally the image processor, which turns that signal into a greyscale image representing the spatial distribution of the signal produced on the imaging plate by the emitted radiation from the sample.

3.4.1 THE SAMPLE MATERIAL

Samples can consist of a wide range of materials and sample types (e.g. cut stones, sand, thinsections (Hareyama *et al.*, 1998), pressed powder pellets), with sample size only limited by the size of the IP. The sample must be dry and have a flat contact surface to the IP, both to produce a sharp autoradiographic image as well as to prevent scratching and uneven load on the IP (which is susceptible to moisture and mechanical damaging). Previous studies have demonstrated the cardinal applicability of IP autoradiography to crystalline rocks (Hareyama *et al.*, 1998; Hareyama *et al.*, 2000; Tsuchiya and Hareyama, 2001) and to speleothems (Cole *et al.*, 2003; Pickering *et al.*, submitted.).

3.4.2 THE IMAGE SENSOR

Image plates are flexible, two-dimensional, integrating-type radiation sensors with a wide dynamic range in the order of five magnitudes. They consist of a backing foil coated with a layer of phosphor crystals embedded in an organic polymer binder, often sealed by a thin protective layer against humidity and mechanical wear. The photostimulable phosphor generally is barium fluorohalide activated with divalent europium ions ($BaFX:Eu^{2+}$, where X consists of Br and/or I, with modern IPs usually having a composition of $BaFBr_{0.85}I_{0.15}:Eu^{2+}$). A thorough disquisition on imaging plates and photostimulable phosphors is given in Rowlands (2002), Salis (2003), Schweizer (2001) and Spaeth (2001).

Autoradiographic exposure of an IP is achieved by placing the radioactive sample material directly onto the plate for a certain exposure time. The image plate absorbs radiation emitted from the sample, causing Eu^{2+} to oxidise to Eu^{3+} and the liberated electron can subsequently be trapped at a Br or F vacancy, introduced during the manufacturing process

of the IP (Takahashi, 2002). This results in a density pattern of filled electron traps, corresponding to the distribution of radiation intensity emitted by the sample. As the fraction of electrons that can be trapped is linked to the availability of free traps, rising irradiation leads to decreasing trapping efficiency until all available traps are charged and the IP is saturated.

3.4.3 THE IMAGE READER AND IMAGE PROCESSOR

During readout, the IP is longitudinally transported through the imager and laterally scanned by a fast-moving laser-beam in the red part of the spectrum (usually generated by solid state laser diodes [λ = 680 nm] or continuous HeNe gas lasers [λ = 633 nm]). This results in an excitation of the trapped electron and their relaxation to the ground state, thereby causing the emission of 390 nm blue light (in the case of $BaFBr_{0.85}I_{0.15}:Eu^{2+}$) in a pattern of parallel scan lines. The stimulated as well as the incident light are collected by a light guide, routed through a filter to block the red parts of the spectrum and then funnelled into a high-sensitivity photomultiplier tube. The recorded time-variant analogue signal is subsequently amplified, filtered to reduce signal noise and then digitized into a greyscale image (Miyahara, 1989; Rowlands, 2002) (Figure 3.1).

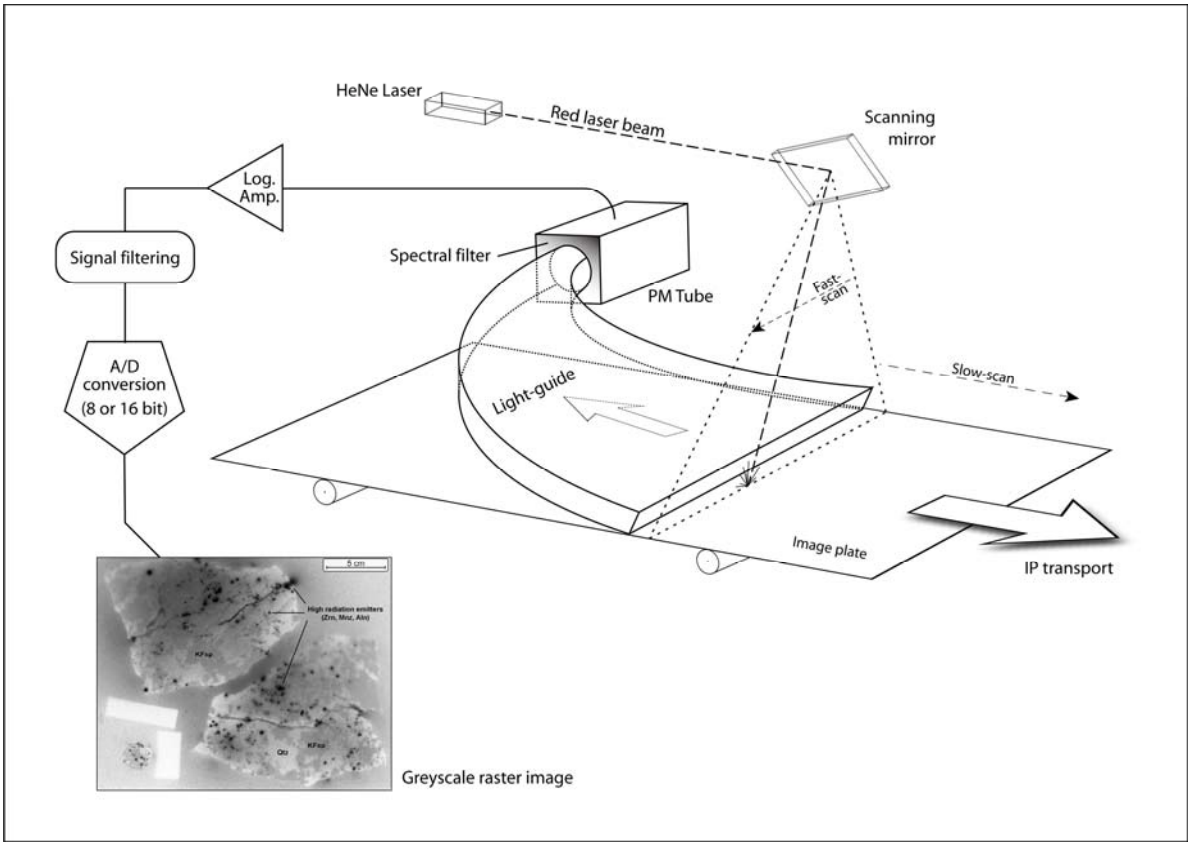

Figure 3.1: Schematic diagram illustrating the IP readout mechanism.

As not all luminescence centres release their charge during the short dwell time of the excitation laser on one spot during a normal readout, multiple scans can be obtained from the same IP. The resulting images can then be stacked to increase signal/noise ratios

In order to reuse the image plate, any residual latent charge remaining on the IP after readout must be removed by bleaching the IP with a high intensity light source (usually high-pressure sodium or fluorescent lamps (Seibert, 1997)) for several minutes.

3.5 METHODOLOGY

3.5.1 SAMPLES AND SAMPLE PREPARATION

In this study, the following types of samples were used (see also Table 3.1):

- Unconsolidated samples: a glacifluvial sand from the Swiss alpine foreland (sample "LW2") and an aeolian dune sand from central Australia (sample "MS-8"). While the Swiss sample is an immature sediment with a very heterogeneous composition, the Australian sand consists almost exclusively of quartz with very few grains of predominantly feldspar and subordinate other minerals.
- Hardrock samples: a proterozoic pegmatitic basement rock from central Madagascar of predominantly granitoid composition (sample "DR076_3") and a 3 mm thick granite slab from the Aarmassiv, Switzerland (sample "GG_slab_b"). The presence of radioactive elements in accessory minerals like monazite, zircon and allanite leads to highly inhomogeneous microdosimetric conditions in these specimens.
- Pressed powder pellets of unconsolidated sample material: comprising both geological samples (where the radionuclide content has been independently established by gamma-spectrometry) as well as IAEA standard materials with known radionuclide concentrations, these specimens were used to investigate into possible absolute or relative quantification of the radiographic signal output.

Regardless of sample type, preparation of any material which will later on be used for luminescence measurements must be done without exposing the sample to light or heat. In the case of unconsolidated sample material (e.g. sand), the main interest lies in detecting a contingent radiation inhomogeneity and obtaining information about the relative amount of radiation hotspots as a statistical property of the sample as a whole. Therefore no preparation beyond drying of the sample was required and the material was simply sprinkled in a homogeneous layer of approximately 3 mm thickness onto the IP.

The hardrock samples had to be cut in order to obtain a flat surface for the autoradiography as well as for subsequent manual breaking and extraction of selected "target grains" to be measured for luminescence. Any cutting must be done under subdued red light, while

taking utmost care not to generate heat or frictional sparking. Therefore the samples were mounted on a raisin bed and very slowly cut under cold water into slabs of 3 - 5 mm thickness. This allows the recording of autoradiographs on both sides of each slab.

The pressed powder pellets consist of a mixture of finely ground, homogenized sample material and an organic binder ("Fluxana BM-0002-1 Licowax"; $C_{38}H_{76}N_2O_2$; CAS-Nr. 00110-30-5), which is pressed into a 3.2 cm diameter disc with a hydraulic hand-press at 300 kg cm^{-2}. Blank tests have shown no signal contribution from the binder to the radiographic image and the binder / sample ratio can be chosen to accommodate enough binder to create a cohesive pill after pressing, with coarser sample material commonly requiring higher ratios. Unlike their unconsolidated source material, the pressed pellets can be used for multiple measurements without any changes in the sample geometry and composition during handling. Their size permits up to 30 pellets to be placed on an imaging plate at one time without risking irradiation from one pellet influencing the radiographic images of neighbouring pellets.

For the geological samples in this study, a weight-ratio of 2:1 with a resulting total weight of 3.00 g for the mixture was used, as this proved to be a good compromise between pill quality and not diluting the sample material overmuch. The average pellet thickness of 2.32 ± 0.05 mm and average pellet density of 1.59 ± 0.04 g cm^{-3} allow the geometry and the β-attenuation within the geological sample pellets to be taken as comparable (Table 3.1).

For the calibration pellets, a self-made mixture of IAEA reference materials RGK-1 and RGTh-1 (IAEA Report RL 148, 1987) was used with a ratio of 36 / 19 respectively. This mixture was then added to the organic binder to create a series of 3.00 g pellets with varying radionuclide concentrations. The calibration pellets have an average thickness of 3.69 ± 0.03 mm and an average density of 0.99 ± 0.01 g cm^{-3} (Table 3.1). The discrepancy between the sample and calibration pellets in terms of average thickness and density is due to the pellet pressing mechanism. As the mould did not allow constriction to a certain pellet height, all pellets were pressed at the same pressure, resulting in systematically lower densities for the calibration pellets which contain a far higher percentage of the low density organic binder.

3.5.2 EXPOSURE, READOUT AND IMAGE TREATMENT

In order to obtain comparable measurements, all exposures of the IPs were done in a temperature controlled basement lab at 21°C inside a 5 cm thick radionuclide-free lead-box, with an additional internal shielding of 1 cm of wood and 1 mm of copper in order to minimise the effects of secondary X-rays generated by particle – matter interactions in the lead shielding.

Table 3.1: Samples used in this study.

	sample name	sample description	activity [dpm]	K [wt %]	Th [µg g^{-1}]	U [µg g^{-1}]	Thickness [mm]	Density [g cm^{-3}]
Standard material for quantitative analysis	CS-0.4	calibration pressed pellet	*12.98 ± 0.11*	*0.21 ± 0.001*	*2.04 ± 0.13*	*0.02 ± 0.0004*	*3.71*	*0.98*
	CS-0.7	calibration pressed pellet	*22.82 ± 0.19*	*0.37 ± 0.003*	*3.59 ± 0.23*	*0.03 ± 0.0006*	*3.71*	*0.98*
	CS-1.0	calibration pressed pellet	*32.76 ± 0.28*	*0.53 ± 0.004*	*5.12 ± 0.33*	*0.04 ± 0.0008*	*3.71*	*0.98*
	CS-1.3	calibration pressed pellet	*42.87 ± 0.36*	*0.70 ± 0.005*	*6.70 ± 0.43*	*0.05 ± 0.0010*	*3.69*	*0.99*
	CS-1.7	calibration pressed pellet	*55.82 ± 0.47*	*0.91 ± 0.006*	*8.74 ± 0.55*	*0.07 ± 0.0014*	*3.71*	*0.98*
	CS-2.0	calibration pressed pellet	*65.31 ± 0.55*	*1.07 ± 0.007*	*10.27 ± 0.65*	*0.08 ± 0.0016*	*3.7*	*0.98*
	CS-2.5	calibration pressed pellet	*81.96 ± 0.69*	*1.33 ± 0.009*	*12.81 ± 0.81*	*0.10 ± 0.0020*	*3.68*	*0.99*
	CS-3.0	calibration pressed pellet	*98.13 ± 0.83*	*1.60 ± 0.011*	*15.41 ± 0.98*	*0.12 ± 0.0024*	*3.61*	*1.01*
						mean:	*3.69 ± 0.03*	*0.99 ± 0.01*
	RGU-1 Pill	pure, for shielding-test only	n.d.	< 20 µg g^{-1}	< 1	*400 ± 2*	--	--
	RGK-1 Pill	pure, for shielding-test only	n.d.	44.8 ± 0.3	< 0.001	*< 0.01*	--	--
Geological sample pellets for quantitative analysis	Gemmi 1	loess, Switzerland	*33.30 ± 1.07*	*0.48 ± 0.01*	*3.82 ± 0.26*	*1.81 ± 0.07*	*2.4*	*1.54*
	Gemmi 2	loess, Switzerland	*31.51 ± 0.70*	*0.45 ± 0.01*	*3.94 ± 0.23*	*1.83 ± 0.07*	*2.42*	*1.52*
	P 32	fluvial sediment, Slovenia	*60.60 ± 0.87*	*0.94 ± 0.01*	*4.74 ± 0.35*	*1.72 ± 0.10*	*2.36*	*1.6*
	P 33	fluvial sediment, Slovenia	*18.12 ± 0.61*	*0.27 ± 0.01*	*1.19 ± 0.01*	*1.14 ± 0.10*	*2.24*	*1.65*
	MSK 1	fluvial sediment, Slovenia	*79.21 ± 1.57*	*1.23 ± 0.01*	*9.93 ± 0.58*	*2.05 ± 0.18*	*2.33*	*1.58*
	MSK 2	fluvial sediment, Slovenia	*78.16 ± 1.24*	*1.21 ± 0.01*	*10.00 ± 0.51*	*2.36 ± 0.23*	*2.36*	*1.55*
	Ill 1	alluvial deposit, Switzerland	*97.83 ± 2.10*	*1.69 ± 0.02*	*3.09 ± 0.28*	*1.25 ± 0.35*	*2.28*	*1.61*
	POSL 2	aeolian sand, Peru	*63.92 ± 1.57*	*1.07 ± 0.01*	*4.30 ± 0.27*	*1.03 ± 0.28*	*2.36*	*1.56*
	POSL 11	aeolian sand, Peru	*64.41 ± 1.14*	*1.02 ± 0.01*	*4.51 ± 0.27*	*2.29 ± 0.25*	*2.28*	*1.61*
	MaJ 4	fluvial sediment, Peru	*71.53 ± 1.58*	*1.21 ± 0.01*	*4.48 ± 0.15*	*0.72 ± 0.32*	*2.24*	*1.65*
	MaJ 8	fluvial sediment, Peru	*72.39 ± 1.56*	*1.21 ± 0.01*	*5.90 ± 0.12*	*0.83 ± 0.32*	*2.28*	*1.62*
	MaJ 9	fluvial sediment, Peru	*84.52 ± 3.81*	*1.37 ± 0.01*	*7.00 ± 0.11*	*1.75 ± 1.30*	*2.36*	*1.56*
	MaJ 10	fluvial sediment, Peru	*90.88 ± 2.29*	*1.51 ± 0.01*	*6.19 ± 0.05*	*1.52 ± 0.66*	*2.3*	*1.61*
	MaJ 14	fluvial sediment, Peru	*95.99 ± 2.04*	*1.56 ± 0.01*	*7.19 ± 0.31*	*2.17 ± 0.47*	*2.31*	*1.6*
	MaJ 16	fluvial sediment, Peru	*92.09 ± 1.73*	*1.53 ± 0.01*	*6.25 ± 0.28*	*1.53 ± 0.35*	*2.3*	*1.6*
	RAT 3	fluvial sediments, Slovenia	*77.55 ± 1.31*	*1.28 ± 0.01*	*5.32 ± 0.40*	*1.54 ± 0.13*	*2.3*	*1.6*
						mean:	*2.32 ± 0.05*	*1.59 ± 0.04*
Hardrock samples	DR 076_3	Pegmatite	---------- *n.d. (qualitative analysis only)* ----------					
	GG_slab_(b)	Granite slab, Grimsel, Switzerland	---------- *n.d. (qualitative analysis only)* ----------					
Sand samples	LW2	glacifluvial sediment, Switzerland	---------- *n.d. (qualitative analysis only)* ----------					
	MS-8	aeolian sand, Australia	*21.7*	*0.54*	*2.35*	*0.53*		

In this study we used the commercially available 23 × 25 cm BAS-MS IP from Fuji Photo Film Co Ltd. A 9 µm thick protective layer out of Mylar makes it sufficiently robust for use even with geological samples. The phosphor layer has a thickness of 115 µm with the individual phosphor crystals typically having a grain size of 4 - 5 µm (Matsuda *et al.*, 1993).

The image reader used is a BAS-1800 Bio-imaging Analyzer System from Fujifilm Life Science Corporation, which has an imaging capability with a minimal pixel size of 50 µm and a dynamic range of approximately five orders of magnitude.

Removal of the samples from the IP and transfer of the latter into the image reader was done under strongly subdued red light, as not to impair the recorded signal. In order to have procedural consistency, the first scan was taken exactly one minute after the end of exposure and removal of the samples, each subsequent scan of the same IP was then taken in immediate succession, up to three stacked scans. The internal reproducibility of the measurement protocol has a standard deviation of 0.4%, established on 5 repetitive measurements of 5 samples.

For imaging and qualitative analysis, the sample is placed directly on the IP in order to achieve maximum sharpness, similar to the effect of a photographic contact copy. Autoradiographs of the pressed powder pellets (or any other sample on which the signal is to be used in a quantitative manner) are obtained with a 0.3 mm thick shield of paper (0.8 g cm^{-3}) between samples and IP, acting as an α-particle absorber.

For a qualitative application, it can be beneficial to trim the full greyscale spectrum to the signal latitude recorded from the sample, in order to increase signal to noise ratios. Increasing image contrast curves can also aid illustrative purposes (Figure 3.2), as can inverting the greyscale values.

However, in the case of an intended quantitative use, any image treatment applied to radiographic images must preserve the original signal linearity of the image. This requires that greyscale values from trimmed spectra must be recalculated to the full spectral width in order to be comparable to the measurements from other images. Also, any contrast enhancement done with non-linear input / output curves introduces differential gradation over the remaining spectrum, rendering quantification impossible.

3.5.3 PSL SIGNAL PRODUCTION FROM DIFFERENT TYPES OF RADIATION

While the radiation intensity distribution of a sample is inherently a 3-dimensional property, self-shielding within the sample material and defocusing of radiation contrasts with increasing distance between the emitter and the IP / sample contact surface leads to the recorded image being dominated by the radiation pattern from a layer close to the sample's contact surface. The thickness of this layer is dependant on the material properties of the

sample and the type and energy of the radiation in question. Considering the orders of magnitude of effective ranges of U, Th and K derived α-, β- and γ-rays in quartz as exemplifying values for such radiation ranges in crustal rocks and terrestrial sediments - which make up most of the commonly used sample types – the maximum thickness of this contributing layer lies in the range of < 35 µm (α), < 2 mm (β) and tens of cm (γ).

As any radiation emitted by the sample must also pass the 9 µm Mylar layer of the IP, the thickness of the contributing layer lying in the sample itself (and thus actually containing radionuclides) is only 25 µm or less for α radiation. Due to this and the strong intensity falloff of α radiation in matter, the majority of α particles contributing to the autoradiographic image will originate from only a very small fraction of the sample volume close to the contact surface. Based on the same principle, the effect of a sample's γ emission on the autoradiograph will be rather homogeneous due to its highly penetrative nature, thus simply adding to a uniform base signal in the IP. If a background deduction is made to correct for any signal produced by cosmic radiation, the γ derived uniform signal portion - which extends well beyond the actual sample surface - is also for the largest part being subtracted. As a consequence, with the number of α emitters being subordinate due to a small source volume and γ emission being largely subtracted, β radiation is considered to be the main contributor to the differential signal intensities of the radiographic image. This is corroborated by a shielding experiment, in which a comparative time-series of autoradiographs of two homogenized radiation sources ("RGU-1 Pill" and "RGK-1 Pill", see Table 3.1) were successively exposed with various amounts of shielding between source and IP (Table 3.2).

After adding 0.3 mm of paper ($\rho = 0.8$ g cm^{-3}), a small reduction in PSL signal of around 14% was observed, which is attributed to the complete shielding of the remaining α-particles that previously reached the IP. Subsequently, using 4 mm of aluminium shielding ($\rho = 2.66$ g cm^{-3}) in order to block all β-radiation resulted in a far stronger reduction of the PSL signal of 83% ("RGU-1 Pill") and 95% ("RGK-1 Pill").

Table 3.2: V_{PSL} generated by identical source material with differing amounts of shielding.

Exposure time [h]	no shielding		0.3 mm paper (0.8 g cm^{-3})		4 mm Al (2.66 g cm^{-3})	
	RGU-1 Pill	RGK-1 Pill	RGU-1 Pill	RGK-1 Pill	RGU-1 Pill	RGK-1 Pill
52	*10240*	*9187*	*8762*	*7940*	*1345*	*319*
76	*11233*	*10240*	*9837*	*8899*	*1883*	*517*
124	*12327*	*11357*	*11040*	*10082*	*2720*	*613*

3.6 QUALITATIVE DETERMINATION OF RADIATION INHOMOGENEITY

An example of an autoradiograph of a pegmatitic hardrock specimen (sample "DR076_3") is given in Figure 3.2. There is a clear distinction between the grey rendering of the K-feldspars and the lighter, non radiogenic quartz and plagioclase grains, which show no signal above background. Notable is also the highly heterogeneous distribution of small high-radiation emitters which form black hotspots on the image. Usually these are accessory minerals like zircons, monazites or allanites, which contain high concentrations of U and Th. Their strong radiation emission even causes "bleeding" of their image due to volume effects upon interaction with the imaging phosphor. This can be seen along the right edge of the upper sample, where a radiation halo causes exposure to radially extend beyond the sample edge.

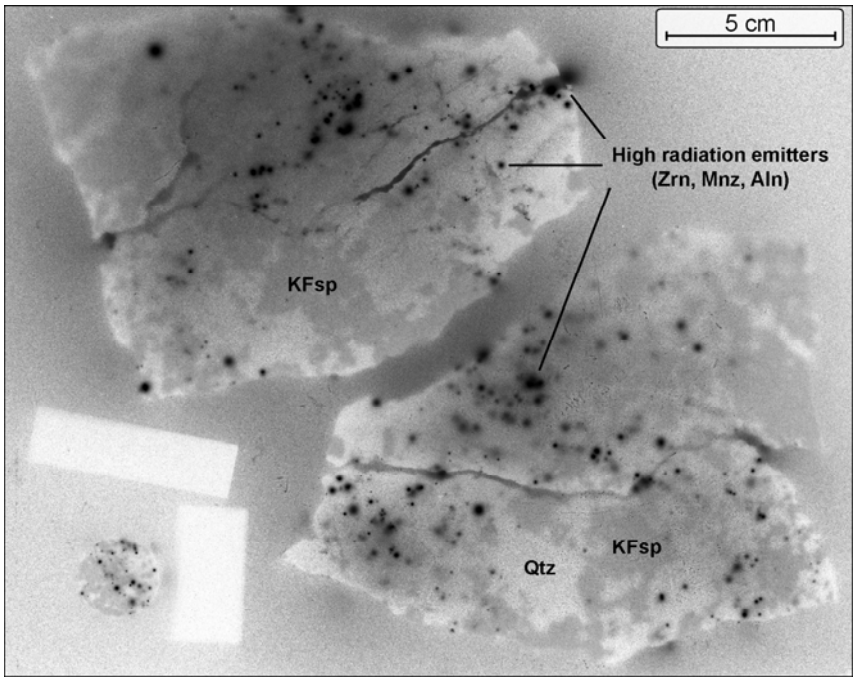

Figure 2.2: Autoradiography of pegmatite sample "DR076_3". Clearly distinguishable are high radiation sources like zircons, monazites or allanites (black hotspots), less radiation emitting K-feldspars (grey) and radiologically inert quartz. The white rectangles are due to PVC shielding blocks and the round sample is an orthogneiss with comparable petrography.

Figure 3.3 shows a comparison between the autoradiograph of a deformed granite slab (Sample "GG_slab_(b)") and the corresponding optical image of the sample surface. The areas of high signal intensity (with the exception of the hotspots) correspond to the location of larger alkali feldspar grains, and Hareyama *et al.* (1998) and Tsuchiya and Hareyama (2001) have shown a basic relationship between increasing K_2O content and increasing PSL signal. The hotspot locations in the autoradiograph cannot be traced to any visible mineral phase in the optical image. This indicates that the constituents causing these radiation inhomogeneities cannot be identified by mere optical observation, especially when the sample must not be subjected to light microscopy.

Concerning unconsolidated samples, Figure 3.4 shows a juxtaposition of autoradiographs from two very different sedimentary materials. Sample "LW2" (Figure 3.4a) is an alpine,

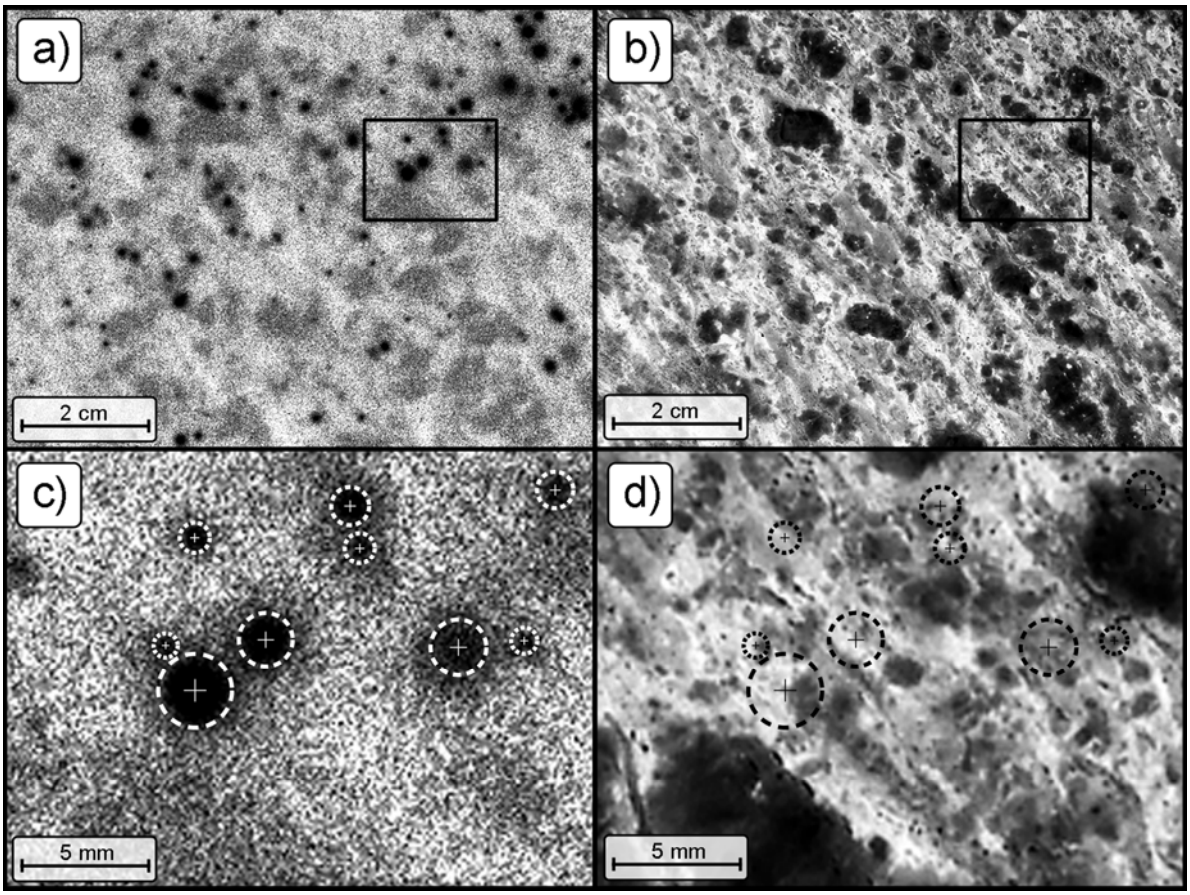

Figure 3.3: Comparison of autoradiography and optical image of a granite slab (sample "GG_slab_(b)"): a) radiographic image showing the distribution and intensity of the photostimulated luminescence; b) optical scanning image of the polished slab surface (inverted greyscale image, dark areas are K-feldspar grains). Framing is identical for both images and the rectangle indicates the section depicted in the close-up images below. c) and d): while the locations of the K-feldspar grains can be traced in the radiography, the sources for the hotspots are not identifiable in the optical image at this magnification.

proglacial sediment derived from a geologically complex source region comprising molasse, limestones and granitic crystalline rocks (which are akin to sample "GG_slab_(b)"). Its sedimentary history is characterized by short transport distances, little sedimentary reworking and minor chemical weathering. This is reflected in the autoradiograph by an increased overall signal level (most of the K-feldspar is still intact), and an inhomogeneous radiation pattern with a significant number of radiation hotspots, indicating that the heavy minerals have not yet been lost to mineral partitioning during transport and sedimentation. It is therefore a representative example of an autoradiograph from a rather immature sediment of very heterogeneous petrographical composition. Such an image gives an indication, that microdosimetry may be a factor to be considered when interpreting OSL data from such a material.

Sample "MS-8" (Figure 3.4b) is an aeolian dune sand from central Australia, representing a very matured sample that experienced important chemical weathering and a long sedimentary history with repeated phases of reworking, (aeolian) transport and redeposition.

With quartz being the dominant mineral constituent and only a negligible amount of feldspar and heavy minerals, the corresponding autoradiograph shows a homogeneous radiation distribution with no discernible hotspots. The overall low radioactivity of this sample necessitated an increase in exposure time in order to record sufficient signal.

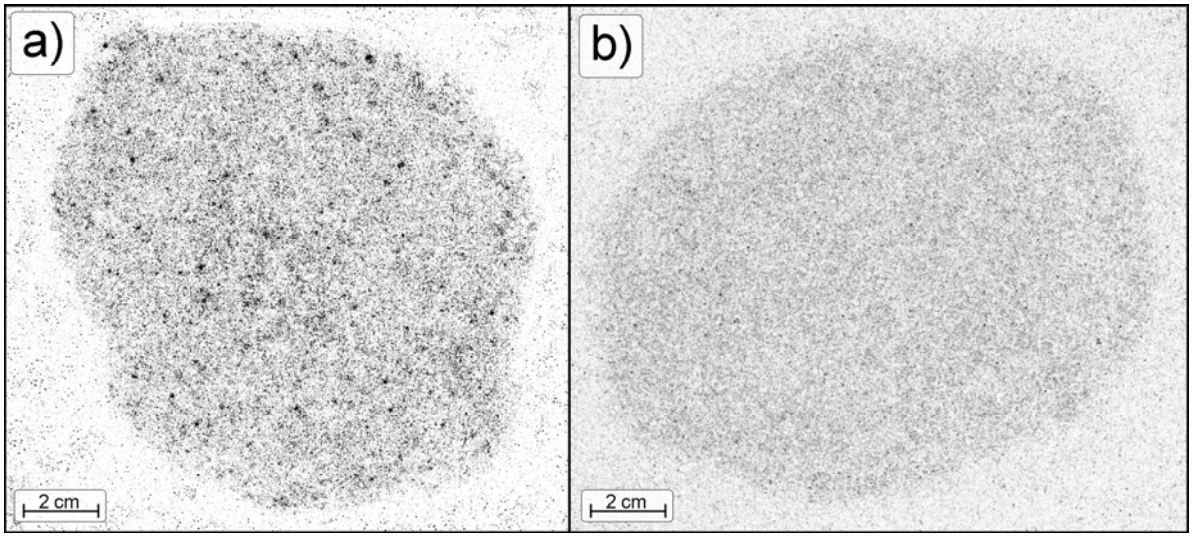

Figure 3.4: Autoradiographs of unconsolidated sand samples. The sand was poured onto the IP and then spread with a spatula by hand to a thickness of 2 – 3 mm. A 12 µm cellophane layer was put between the sample and the IP to facilitate sample removal. a) glacifluvial sample "LW2"; b) aeolian dune sand sample "MS-8". Exposure times were 70.5 h ("LW2") and 112 h ("MS-8") in order to accumulate enough signal in the autoradiograph of the low activity sample "MS-8".

While aeolian dune sands from this region are generally assumed to be well bleached, broad D_E distributions have been reported by Lomax *et al.* (2003) and Lomax *et al.* (2007) for numerous other samples. Without excluding the possibility of post-depositional mixing, microdosimetry is also taken into consideration and Lomax *et al.* (2007) indicate that either high radiation sources like zircons or differential shielding of quartz grains due to carbonate or iron-oxide coating might cause the observed D_E overdispersion. In the case of sample "MS-8", autoradiography allows to exclude the presence of high radiation emitters like zircons as a likely cause for microdosimetry and therefore provides an important information when interpreting the OSL data.

It can be seen that such qualitative screening therefore efficiently gives precursory information whether a sample has to be considered to be variable with regards to dosimetry or not. If, based on these findings, the sample is considered homogeneous in terms of radiation or is discarded altogether, such a qualitative inquiry may suffice. On the other hand, the availability of spatially resolved, relative radiation information evokes a demand for a means of absolute calibration of the information inherent in such images. An established calibration would then allow to just as rapidly obtain absolute dosimetric values.

3.7 FIRST INVESTIGATIONS INTO THE POTENTIAL TO QUANTIFY PSL SIGNALS

As pointed out in the previous section, it would be desirable to have a method available to quantitatively evaluate entire samples or regions of interest in a radiographic image in order to deduce spatially resolved dose rates. To do so, it is necessary to develop a mathematical relationship between the dose emitted from the sample and the signal recorded from the IP in such a region of interest. The complexity and the multitude of physical and chemical factors involved in the production and the reading out of this signal makes a backward calculation model infeasible. We therefore investigate into the potential of experimentally calibrating the signal output by means of calibration standard materials.

While PSL stands for the process of photostimulated luminescence and for the latent image stored in the IP as a non-quantitative entity, the term "PSL-value" has been defined by Mori and Hamaoka (1994) as the "detected photostimulated luminescence value under certain standard conditions of the designated kind of X-ray, radiation amount [and] timing of reading after exposure". As this is therefore simply a question of normalization factor, we use the term "PSL-value" (V_{PSL}) in this paper as the background corrected, averaged greyscale value of a certain area of the resulting image.

3.7.1 THEORETICAL BACKGROUND

Using exposures of one hour, a positive linear relation between PSL signal [given as a.u. mm^{-2}] and specific activity A [given as dpm mm^{-2} per unit mass] was described first by Amemiya and Miyahara (1988) to be a fundamental property of IPs. This relation was found to be different for various radionuclides, giving specific linear factors k_i for different nuclides i and their respective radiation spectrums:

$$V_{PSL_i} = k_i A_i \qquad \textbf{(1)}$$

V_{PSL_i} also correlates positively with exposure time t, albeit not in linear fashion. As the specific activity A_i can be considered to remain constant over the time range of measurement, *(1)* can be extended to:

$V_{PSL_i}(t) = k_i(t)\, A_i$ which can be rewritten as:

$$V_{PSL_i}\, A_i^{-1}(t) = k_i(t) \qquad \textbf{(2)}$$

Thus, if $k_i(t)$ can be formulated (e.g. by regression of a k_i vs. t plot), the specific activity A_i can theoretically be calculated from the V_{PSL_i} of an autoradiograph and its exposure time t.

In the literature, such linear relationship are only described for mono-nuclide radiation (e.g. Amemiya and Miyahara, 1988; Mori and Hamaoka, 1994; Gonzalez *et al.*, 2002) and not for decay chains. In the latter cases – if secular equilibrium is assumed – the resulting linear relationship would be a weighted composite of all the linear relations of the respective nuclides making up the decay chain. Extrapolating, the same concept can be applied to a bulk composition of radionuclides that make up a sample, using a theoretical nuclide as a representative for the entire sample's relative radionuclide composition (note: samples with varying *total* but identical *relative* radionuclide concentrations are therefore represented by the same theoretical nuclide, simply with varying concentration). In this case, the index i denominates the sample composition instead of merely a single radionuclide species and the given formulations can be applied to describe the V_{PSL} generation of a sample with specific activity A as a whole.

3.7.2 ESTABLISHING A CALIBRATION CURVE

A sequence of autoradiographs with varying exposure times was taken from the entire set of calibration pellets in order to get a series of PSL-values variable in exposure time and total activity (Figure 3.5a). As the calibration pellets contain increasing amounts of the same relative mixture of radionuclides, they emit the same radiation spectra. According to *(1)*, the same linear relationship $V_{PSL}(A)$ should apply to all of them. Plotting V_{PSL} against A should therefore result in a set of straight lines going through the origin, with their slopes k given by the varying exposure times as described by *(2)*. Figure 3.5b however shows, that there is an increasing deviation from the postulated linearity of $V_{PSL}(A)$ for longer exposure times, which is attributed to saturation effects. As higher specific activities produce more signal in a given amount of time, they will also cause the IP to go into saturation faster. Therefore, *(1)* becomes less valid with the resulting V_{PSL} approaching

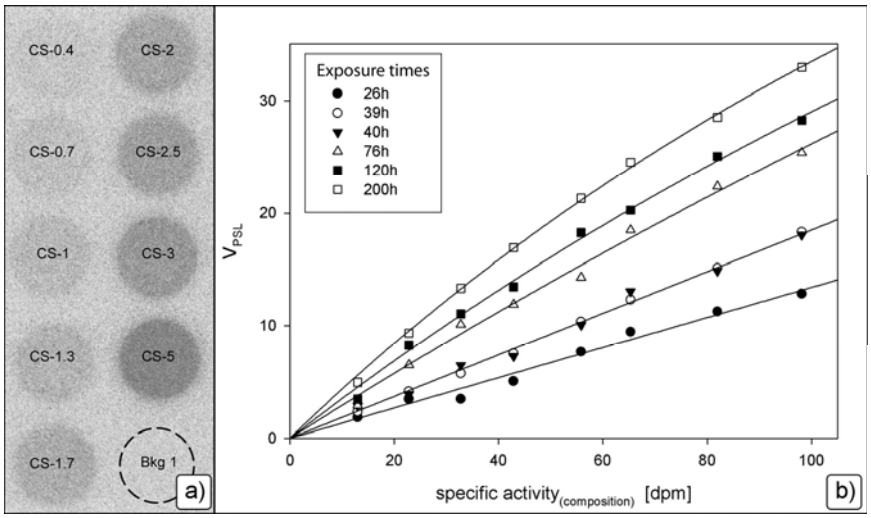

Figure 3.5: a) Stacked image from the 76h exposure showing the increasing PSL densities recorded on the IP with increasing radionuclide concentration in the calibration pellets (contrast enhanced for visualisation). "Bkg 1" indicates a background measurement. b) Correlations between specific activities (based on radionuclide content) and PSL-value for various exposure times.

higher values and the term *k(t)* in *(2)* becomes increasingly influenced by *A*. This is illustrated in Figure 3.6, which is a graphical representation of *(2)* for three calibration pellets of low, medium and high activity. It can be seen that, in the case of our calibration material, the divergence in signal production behaviour due to different specific activities becomes increasingly significant for exposure times above a threshold value of approximately 50 h. A saturating exponential model curve fitted to the mean *k* values of the exposures below that threshold was therefore taken as the functional relation describing *k(t)* for our calibration material (Figure 3.6 inset):

$$k(t) = 0.3484\ (1 - e^{-0.0185\ t}) \qquad \textbf{(3)}$$

In accordance with *(2)*, it is therefore possible to calculate the specific activity of a sample based on the recorded V_{PSL} for a known exposure time.

To test the tolerance of the calibration, specific activities of the entire set of calibration pellets over a wide range of exposure times were calculated using *(3)*. Comparing these to the specific activities from the radionuclide compositions gives an indication about how reliable the calibration works over a comprehensive range of parameters (Figure 3.7). On the low signal side, low exposure time combined with low activities results in considerable scatter, due to bad counting statistics on the resulting low V_{PSL} (Figure 3.7a). Meanwhile, for very long exposures, the varying saturation behaviour for different specific activities becomes apparent (Figure 3.7d). However, exposures of 40 h and 76 h (Figure 3.7b & c) both seem to indicate a range in exposure time in which the calibration seems to work fairly well and the calculated specific activities ratios of all calibration pellets lie within a ± 10% band around unity. Care should therefore be taken to assure that the actual measurement procedure

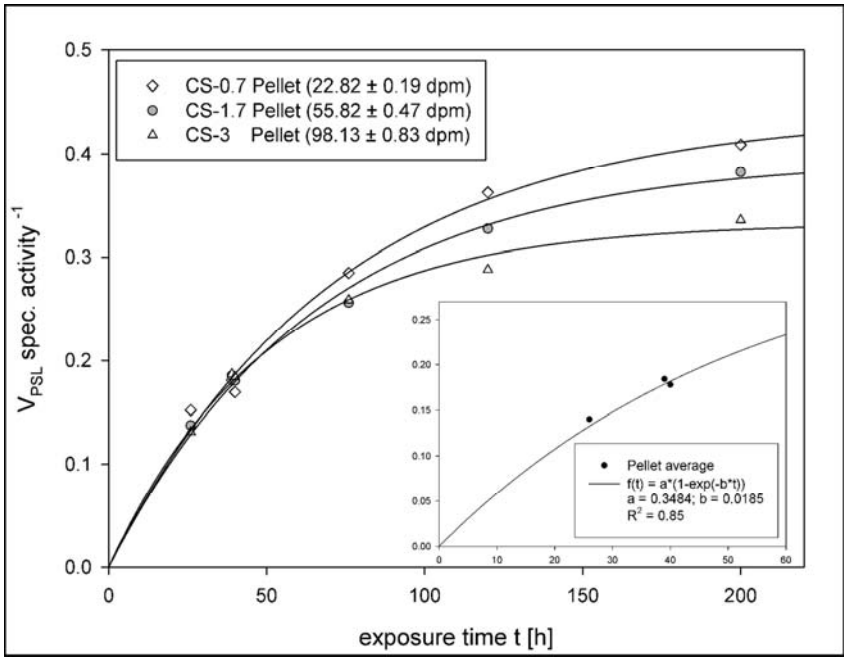

Figure 3.6: Increase of the regression line slopes from Figure 3.5b over time, plotted for a calibration pellet of low, medium and high specific activity. The fitting lines are saturating exponentials, illustrating the influence of specific activity on the saturation behaviour. Inset: saturating exponential curve fit through the calibration pellets mean values. This curve is used as the calibration curve.

applied to the sample is identical to the procedure used when establishing the calibration, and that sample exposures be kept in the range of 40 – 76 h.

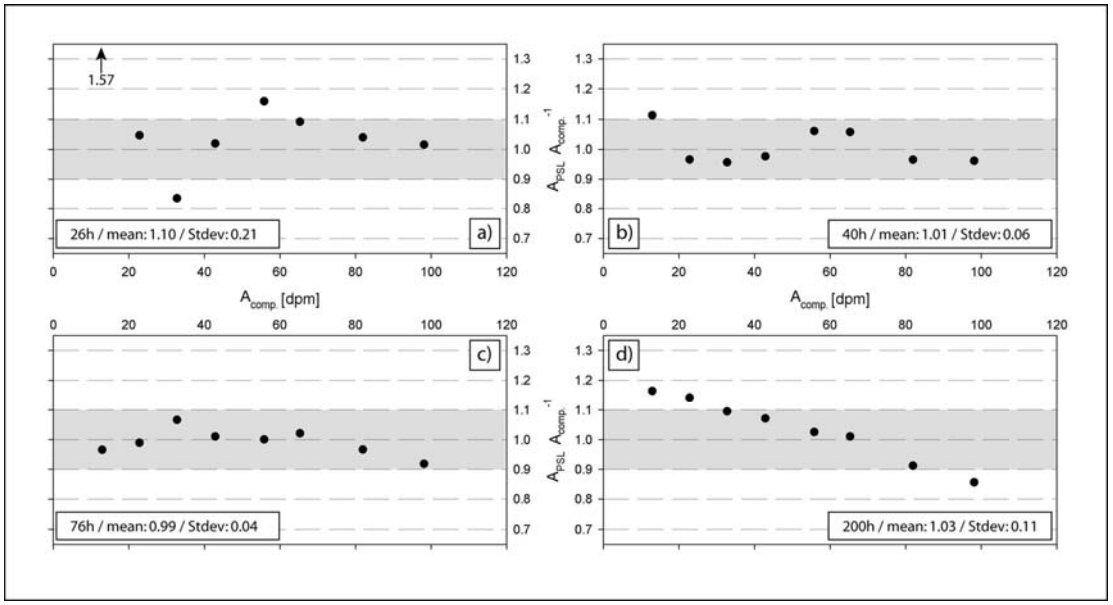

Figure 3.7: Comparison of A_{PSL} / $A_{comp.}$ ratios over the entire range of calibration pellet activities for different exposure times.

3.7.3 APPLICATION TO GEOLOGICAL SAMPLES

The applicability of the method to natural material was tested by applying it to a 50 h exposure, taken from the pressed pellets series of geological samples (Table 3.1). Figure 3.8 shows the correlation between their specific activities based on the nuclide content ($A_{comp.}$) and the specific activities calculated from the PSL-values (A_{PSL}), using *(3)*. With exception of the far outlying values of the samples "Gemmi 1" and "Gemmi 2", the A_{PSL} / $A_{comp.}$ ratios of the geological material plot slightly above unity (mean = 1.12) with a standard deviation of 0.13.

Two aspects must be considered when interpreting these results:

1. The slight overemphasis of the APSL values of the geological material compared to the calibration pellets is seemingly of a systematic nature.
2. The observed spread in the samples is larger than in the calibration pellets. This indicates variations in the APSL of the geological material which seem to exceed the methods intrinsic variability, given by the spread of the calibration pellets (Figure 3.7).

The first point is most likely related to the systematic difference in thickness and density between calibration pellets and geological pellets. As they are thinner, the radionuclide concentration close to the IP is higher in the sample pellets compared to the thicker

calibration pellets. This appears to be only partly compensated by their higher density and hence higher internal attenuation of the emitted radiation.

As to the second point, it has already been discussed that in order to compare two samples quantitatively, the same formulations of *(1)* and *(2)* must apply to both of them. This implies that an absolute calibration could only be made for samples with identical relative radionuclide composition as the calibration material. Comparing the results (Figure 3.8) with the pellet compositions (Table 3.1), it can be seen that the two outliers "Gemmi 1" and "Gemmi 2" indeed show the lowest K / (Th + U) ratios of the geological material. Figure 3.9 plots the samples A_{PSL} / $A_{comp.}$ ratios against the fractions of their specific activity originating from Th + U (X_{Th+U}, with X_{Th+U} + X_K = 1). This corroborates the influence of increasing relative Th and U concentrations on an overestimation of A_{PSL}.

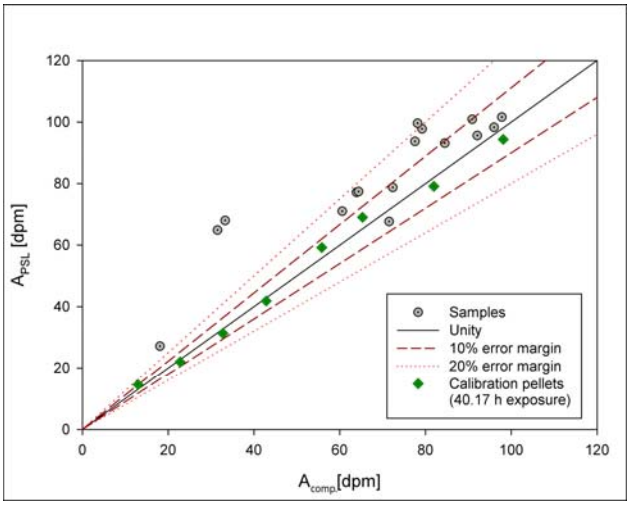

Figure 3.8: Juxtaposition of specific activities calculated from radionuclide content ($A_{comp.}$) and activities calculated from PSL-values (A_{PSL}) for the geological sample pellets. Exposure times were 50 h for the geological samples and 40.17 h for the calibration pellets given to illustrate the spread inherent to the method.

A possible explanation for this observation could be that U emits multiple β-quanta throughout its decay chain which possess lower average energies than the β-quanta emitted by ^{40}K. Tanaka *et al.* (2005) and Chen *et al.* (2008) have shown that PSL generation per electron increases noticeably with decreasing electron energy below 1 MeV, an effect which is attributed to lower energy electrons generating more PSL-signal closer to the IP surface (Thoms, 1996). This in turn leads to a higher signal yield during readout and a relative overestimation of A_{PSL}.

While this demonstrates the need to reconcile radionuclide composition between samples and calibration material, the overall good correlation indicates that the calibration method is fairly tolerant towards this aspect.

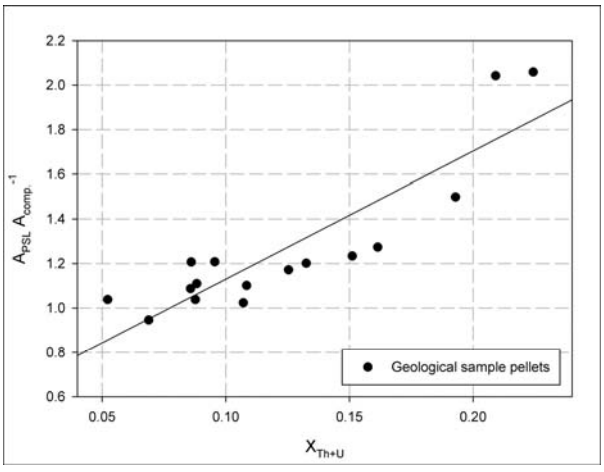

Figure 3.9: A positive correlation between growing relative content in Th + U and excessive A_{PSL} / $A_{comp.}$ ratios illustrates the influence of deviating relative radionuclide compositions for the applicability of the calibration. The abscissa is given as the Th+U fraction of the total U, Th and K content of the samples, with X_{Th+U} + X_K = 1)

3.7.4 THE PROBLEM OF LINKING SPECIFIC ACTIVITY AND DOSE RATES BASED ON PSL-VALUES

In the case of a single, known type of radionuclide and therefore a single, known radiation energy spectrum, the specific activity A is proportional to the emitted dose rate D and $V_{PSL}(A) \approx V_{PSL}(D)$. As β radiation is the principal contributor to the PSL signal, $V_{PSL}(D)$ is strongly influenced by the IPs signal production efficiency per electron (PSL / electron). Two countervailing effects play a role in this: a) below 1 MeV, PSL / electron shows strong variations with electron energy up to a factor of four (Tanaka *et al.*, 2005; Chen *et al.*, 2008), and b) natural β radiation is not discrete, but forms a continuous spectrum over a certain energy range, depending on radionuclide. While the second effect dampens PSL variations introduced by the first effect, equal doses emitted by different radionuclides often still produce differing PSL values. In the case of a mixture of radionuclide species, the resulting β energy spectrum is the integration of the various species' spectra. The more different radionuclides such mixtures incorporate (especially when secular equilibrium is reached), the broader their resulting β spectrum becomes, leading to a decrease in the variation of $V_{PSL}(D)$ between such mixtures. Regardless of that, systematic tests using calibration sequences with fixed dose rates and variable radionuclide compositions would be required in order to establish a quantitative link between dosimetry and PSL-signal.

3.8 CONCLUSIONS

Autoradiography with imaging plates enables the spatially resolved detection and visualisation of radiation inhomogeneities in a wide range of sample types without being destructive to luminescence signals. It is a tool to rapidly assess relative β radiation levels within and between samples, and to provide information about the homogeneity of a given material's radiation field. The procedure does not require elaborate sample processing and provides the results in a graphical manner, which is well suited for interpretation.

Qualitative application of the method to consolidated or hard rock material allows visualization of high radiation areas or layers in a sample. In unconsolidated sediments, the detection of radiation inhomogeneities and hotspots provides important information about whether microdosimetry is to be expected as a likely contributor to a D_E overdispersion.

Information about spatial variability of radiation is essential for any kind of trapped charge dating, especially on material where microdosimetry must be considered a potential problem. It allows for a better constraint of this important parameter, which is too often not properly taken into consideration because it can not be determined with the established method of dosimetry measurement (i.e. gamma-spectrometry).

As such, imaging plate autoradiography of geological materials has its potential application not only in the context of luminescence dating. In the emerging field of speleothem dating by

U-Pb and U-Th series, identifying layers of high radionuclide content is indispensable for successful dating (Cole at al., 2003; Pickering *et al.*, submitted.). Similarly, Electron Spin Resonance (ESR) dating of tooth enamel might profit from a rapid visualisation technique to determine relative radionuclide concentrations in the different tooth components.

A foray into quantitative calibration of the imaging plate is also presented, examining the potential of calculating a samples activity from the greyscale value of the recorded radiographic image. While certain limitations are identified and discussed, verification of the method using 16 geological samples of known specific activities illustrates its general applicability to geological materials. However, to obtain an absolute dosimetric calibration, further research is needed in order to link PSL generation not only to a sample's activity but to its emitted radiation energy. This would eventually enable determining dose rates from an autoradiograph, allowing to calculate spatially resolved D_E or quantify a microdosimetry derived D_E overdispersion.

ACKNOWLEDGEMENTS

A. Dehnert, J. Lomax and D. Steffen are thanked for providing some of the sample material and R. Pickering is greatly acknowledged for the introduction into the radiography lab and many helpful comments on the manuscript. Additional credits go to U. Mäder for the use of the β-scanner facilities and to S. Lowick, T. Rosenberg, J. Giese and A. Voegelin for helpful discussions on various topics. This work was funded by the Swiss National Science Foundation (SNSF), Project No's 200020-105453/1 und 200020-118023/1.

3.9 REFERENCES

AMEMIYA, Y. & MIYAHARA, J. (1988): Imaging Plate Illuminates Many Fields. *NATURE* 336 (6194): 89-90

BATEMAN, M.D., FREDERICK, C.D., JAISWAL, M.K. & SINGHVI, A.K., (2003): Investigations into the potential effects of pedoturbation on luminescence dating. *QUATERNARY SCIENCE REVIEWS* 22 (10-13): 1169-1176.

BRENNAN, B.J. (2006): Variation of the alpha dose rate to grains in heterogeneous sediments. *RADIATION MEASUREMENTS* 41 (7-8): 1026-1031.

CHEN, H., BACK, N.L., BARTAL, T., BEG, F.N., EDER, D.C., LINK, A.J., MACPHEE, A.G., PING, Y., SONG, P.M., THROOP, A. & VAN WOERKOM, L. (2008). Absolute calibration of image plates for electrons at energy between 100 keV and 4 MeV. *REVIEW OF SCIENTIFIC INSTRUMENTS* 79 (3).

COLE, J.M., NIENSTEDT, J., SPATARO, G., RASBURY, E.T., LANZIROTTI, A., CELESTIAN, AJ., NILSSON, M. & HANSON, G.N. (2003): Phosphor imaging as a tool for in situ mapping of ppm levels of uranium and thorium in rocks and minerals. *CHEMICAL GEOLOGY* 193 (1-2): 127-136.

DULLER, G.A.T., BØTTER-JENSEN, L. & MURRAY, A.S. (2000): Optical dating of single sand-sized grains of quartz: sources of variability. *RADIATION MEASUREMENTS* 32 (5-6): 453-457.

GALBRAITH, R.F., ROBERTS, R.G., LASLETT, G.M., YOSHIDA, H. & OLLEY, J.M. (1999): Optical dating of single and multiple grains of quartz from Jinmium rock shelter, northern Australia - Part 1: Experimental design and statistical models. *ARCHAEOMETRY* 41: 339-364.

GONZALEZ, A.L., LI, H., MITCH, M., TOLK, N. & DUGGAN, D.M. (2002): Energy response of an imaging plate exposed to standard beta sources. *APPLIED RADIATION AND ISOTOPES* 57 (6): 875-882

GREILICH, S., GLASMACHER, U.A. & WAGNER, G.A. (2002): Spatially resolved detection of luminescence: a unique tool for archaeochronometry. *NATURWISSENSCHAFTEN* 89 (8): 371-375.

GREILICH, S., GLASMACHER, U.A. & WAGNER, G.A. (2005): Optical dating of granitic stone surfaces. *ARCHAEOMETRY* 47: 645-665.

HAREYAMA, M., TSUCHIYA, N. & TAKEBE, M. (1998): Two-dimensional measurement of natural radioactivity of rocks by photostimulated luminescence. *WATER-ROCK INTERACTION, ROTTERDAM.*

HAREYAMA, M., TSUCHIYA, N., TAKEBE, M. & CHIDA, T. (2000): Two-dimensional measurement of natural radioactivity of granitic rocks by photostimulated luminescence technique. *GEOCHEMICAL JOURNAL* 34 (1): 1-9.

IAEA REPORT RL 148. (1987): Preparation of Gamma-ray Spectrometry Reference Materials RGU-1, RGTh-1 and RGK-1. Report – IAEA/RL/148, *VIENNA*

LOMAX, J., HILGERS, A., WOPFNER, H., GRÜN, R., TWIDALE, C.R. & RADTKE, U. (2003): The onset of dune formation in the Strzelecki Desert, South Australia. *QUATERNARY SCIENCE REVIEWS* 22 (10-13): 1067-1076

LOMAX, J., HILGERS, A., TWIDALE, C.R., BOURNE, J.A. & RADTKE, U. (2007): Treatment of broad palaeodose distributions in OSL dating of dune sands from the western Murray Basin, South Australia. *QUATERNARY GEOCHRONOLOGY* 2 (1-4): 51-56.

MATSUDA, T., ARAKAWA, S., KODA, K., TORII, S. & NAKAJIMA, N. (1993): New technical developments in the FCR9000. *FUJI COMPUTED RADIOGRAPHY TECHNICAL REVIEW NO 2* (Fuji Photo Film)

MAYYA, Y.S., MORTHEKAI, P., MURARI, M.K. & SINGHVI, A.K. (2006): Towards quantifying beta microdosimetric effects in single-grain quartz dose distribution. *RADIATION MEASUREMENTS* 41 (7-8): 1032-1039.

MIYAHARA, J. (1989): The Imaging Plate: A new radiation image sensor. *CHEMISTRY TODAY* No. 223: 29-36

MORI, K. & HAMAOKA, T. (1994): IP Autoradiography System (BAS). *PROTEIN, NUCLEIC ACID AND ENZYME* 39 (11): 11.

MURRAY, A.S. & WINTLE, A.G. (2000): Luminescence dating of quartz using an improved single-aliquot regenerative-dose protocol. *RADIATION MEASUREMENTS* 32 (1): 57-73.

NATHAN, R.P., THOMAS, P.J., JAIN, M., MURRAY, A.S. & RHODES, E.J. (2003): Environmental dose rate heterogeneity of beta radiation and its implications for luminescence dating: Monte Carlo modelling and experimental validation. *RADIATION MEASUREMENTS* 37 (4-5): 305-313

OLLEY, J.M., CAITCHEON, G.G. & ROBERTS, R.G. (1999): The origin of dose distributions in fluvial sediments, and the prospect of dating single grains from fluvial deposits using optically stimulated luminescence. *RADIATION MEASUREMENTS* 30 (2): 207-217.

PICKERING, R., KRAMERS, J.D., PARTRIDGE, T., KODOLANYI, J., & PETTKE, T. (Submitted) Uranium-lead dating of calcite-aragonite layers in low-uranium speleothems from South Africa by MC-ICP-MS. *QUATERNARY GEOCHRONOLOGY.*

PREUSSER, F., BLEI, A., GRAF, H. & SCHLÜCHTER, C. (2007): Luminescence dating of Wurmian (Weichselian) proglacial sediments from Switzerland: methodological aspects and stratigraphical conclusions. *BOREAS* 36 (2): 130-142.

ROWLANDS, J.A. (2002): The physics of computed radiography. *PHYSICS IN MEDICINE AND BIOLOGY* 47 (23): R123-R166.

SALIS, M. (2003): On the photo-stimulated luminescence of BaFBr : Eu+2 phosphors. *JOURNAL OF LUMINESCENCE* 104 (1-2): 17-25

SCHWEIZER, S. (2001): Physics and current understanding of X-ray storage phosphors. *PHYSICA STATUS SOLIDI A - APPLIED RESEARCH* 187 (2): 335-393.

SEIBERT, J.A. (1997): Computed radiography: technology and quality assurance. In: FREY, G.D. & SPRAWLS, P. (eds.), *THE EXPANDING ROLE OF MEDICAL PHYSICS IN DIAGNOSTIC IMAGING FOR AAPM.* Madison: Advanced Medical Publishing. 37-83

SPAETH, J.M. (2001): Recent developments in X-ray storage phosphor materials. *RADIATION MEASUREMENTS* 33 (5): 527-532.

TAKAHASHI, K. (2002): Progress in science and technology on photostimulable BaFX : Eu2+ (X = Cl, Br, I) and imaging plates. *JOURNAL OF LUMINESCENCE* 100 (1-4): 307-315.

TANAKA, K.A., YABUUCHI, T., SATO, T., KODAMA, R., KITAGAWA, Y., TAKAHASHI, T., IKEDA, T., HONDA, Y. & OKUDA, S. (2005): Calibration of imaging plate for high energy electron spectrometer. *REVIEW OF SCIENTIFIC INSTRUMENTS* 76 (1)

THOMS, M. (1996): The quantum efficiency of radiographic imaging with image plates. *NUCLEAR INSTRUMENTS & METHODS IN PHYSICS RESEARCH SECTION A - ACCELERATORS SPECTROMETERS DETECTORS AND ASSOCIATED EQUIPMENT* 378 (3): 598-611.

TSUCHIYA, N. & HAREYAMA, M. (2001): Two-dimensional measurement of natural radioactivity of some Archean and Proterozoic rocks from South Africa. *MEMOIRS. NATIONAL INSTITUTE OF POLAR RESEARCH* (Special Issue 55): 167-177.

VANDENBERGHE, D., HOSSAIN, S.M., DE CORTE, F. & VAN DEN HAUTE, P. (2003): Investigations on the origin of the equivalent dose distribution in a Dutch coversand. *RADIATION MEASUREMENTS* 37 (4-5): 433-439.

CHAPTER 4

Variable fading rates in K-feldspar caused by different IRSL components and implications for g-value determination

Daniel Rufer, Sally E. Lowick, Frank Preusser & Mareike Trauerstein

Institute of Geological Sciences, University of Bern, Switzerland

Submitted to:
Radiation Measurements, 2009

"Truth in science can be defined as the working hypothesis best suited to open the way to the next better one."

Konrad Z. Lorenz (1903 - 1989), Zoologist

VARIABLE FADING RATES IN K-FELDSPAR CAUSED BY DIFFERENT IRSL COMPONENTS AND IMPLICATIONS FOR G-VALUE DETERMINATION

4.1 ABSTRACT

The approaches currently available to correct for anomalous fading of feldspar infrared stimulated luminescence (IRSL) signals depend on accurate determination of a sample's fading rate. Fading rates are usually determined using delayed measurements with increasing pauses between preheat and IRSL measurement. Following such fading rate determinations, a deviation from the expected logarithmic signal decay was observed for the shortest measurement delays. By the fitting of IRSL decay curves to three components, it was possible to show that the relative behaviour of these components was responsible for the unexpected signal decay rate for the shortest pauses. Application of a certain minimum delay before IRSL measurement avoids the inclusion of an unstable signal and allows the accurate determination of feldspar fading rates.

Keywords: anomalous fading, IRSL, feldspar, fading rate, component fitting

4.2 INTRODUCTION

It is well known that feldspar can underestimate luminescence ages due to anomalous fading (e.g. Wintle, 1973). The loss in the natural luminescence signal responsible for this is understood as the result of quantum mechanical tunnelling, and is seen to follow a logarithmic decay on laboratory timescales (Visocekas, 1979). Based on this, various correction methods have been proposed (Huntley and Lamothe, 2001; Lamothe *et al.*, 2003; Wallinga *et al.*, 2007; Kars *et al.*, 2008), to determine the fading rate, which is expressed as percentage of signal loss per decade (g-value; Aitken, 1985) and extrapolated into the past. Thomsen *et al.* (2008), however, have demonstrated that measured g-values are dependent on experimental parameters, and Huntley (2006) also provides mathematical arguments that fading rates should change for both short and long fading times. In this study, we present g-value measurements, where the measured fading rates trend towards highly increased values if measurement delays are kept very short. The implications of this observation for g-value determinations and fading corrections are discussed.

4.3 MATERIALS AND METHODS

This study was conducted on a set of four K-feldspar samples covering a wide geographic range as well as diverse source regions and sedimentary environments: a glaciofluvial

deposit from the Kamaka site, North Westland, New Zealand (Preusser *et al.*, 2005); a fluvial terrace sediment from Pisco valley, Peru (Steffen *et al.*, 2009); an Eemian fluvial sediment from the Luthern valley, central Switzerland (Preusser *et al.*, 2001) and a Late Pleistocene aeolian deposit from the "Middle aeolianite", Uniabmund, Namibia.

IRSL measurements were carried out on Risø DA-20 TL/OSL readers fitted with internal $^{90}Sr/^{90}Y$ beta sources, using a combination of a Schott BG39 and a LOT/Oriel D410/30 interference filter. After bleaching in the reader, a constant regeneration dose of ~95 Gy was applied, followed by immediate preheating of the sample. Using increasing pauses after preheating, the samples were then measured at 40°C, followed by the measurement of a test dose (Table 4.1, Table 4.2). It is important to note that all measurements were carried out using the "run 1 at a time" option of Sequence Editor in order to be able to measure with very short delays. Checks for phosphorescence emissions were made by replacing the pause in the sequence by IRSL measurements using no stimulation, but no signal above the usual dark count level was recorded.

Table 4.1: The measurement protocol used for fading rate determination. Measurements were made using the "run 1 at a time" option of Sequence Editor.

Step	Action
1	Regeneration dose, 800 s (~95 Gy) [a]
2	Preheat 290°C for 60 s
3	Variable pause [b]
4	IR stimulation, 40°C for 300 s
5	Test dose, 180 s (~21 Gy)
6	Preheat 290°C, 60 s
7	IR stimulation, 40°C for 300 s, 5 channels s^{-1}
8	Repeat step 1-7 with increasing pause

[a] No regeneration dose is given in the first cycle in order to bleach the sample.

[b] Replaced by no-stimulation IRSL for phosphorescence checks.

Fading rates were determined according to Huntley and Lamothe (2001); the g-value is deduced from the slope of the regression line on a plot of IRSL intensities against the log of time elapsed since irradiation (plus half of the irradiation time to account for fading during irradiation (see Auclair *et al.*, 2003), both normalized to the corresponding values of the immediate measurement (I/I_c vs. $\log(t^*/t_c)$). While t_c can be chosen arbitrarily (allowing for t* values to be lower than t_c), for this study it is always used for the immediate measurement (i.e. the measurement with the lowest t*).

Table 4.2: The measurement protocol used for fading rate determination. Measurements were made using the "run 1 at a time" option of Sequence Editor.

Pause [s]	*0*	*60*	*120*	*240*	*480*	*900*	*1500*	*2400*
t* [s]	*602*	*620*	*682*	*801*	*1042*	*1463*	*2065*	*2968*

4.4 RESULTS AND DISCUSSION

Figure 4.1 shows the results from fading experiments for the four samples. All data is normalized to the immediate measurement taken at t_c = 602 s, which is the shortest possible t* based on the chosen dose and preheat (Table 4.2). The signal used was integrated over the first second (5 channels) of the IRSL signal, following Wallinga *et al.* (2000). It can be seen, that the resulting fading curves do not follow the predicted linear fit in semi-logarithmic plots, as is required following the theory of logarithmic decrease of the fading signal with time (Huntley and Lamothe, 2001). Instead, towards the shortest t* they increasingly deviate from the expected fit. This phenomenon seems to be independent of the sample and its source material (Figure 4.1) and, furthermore, measurement of the same sample on different readers, where beta sources vary ~30% in intensity, indicates that there is also no correlation between irradiation dose rate and the observed signal behaviour.

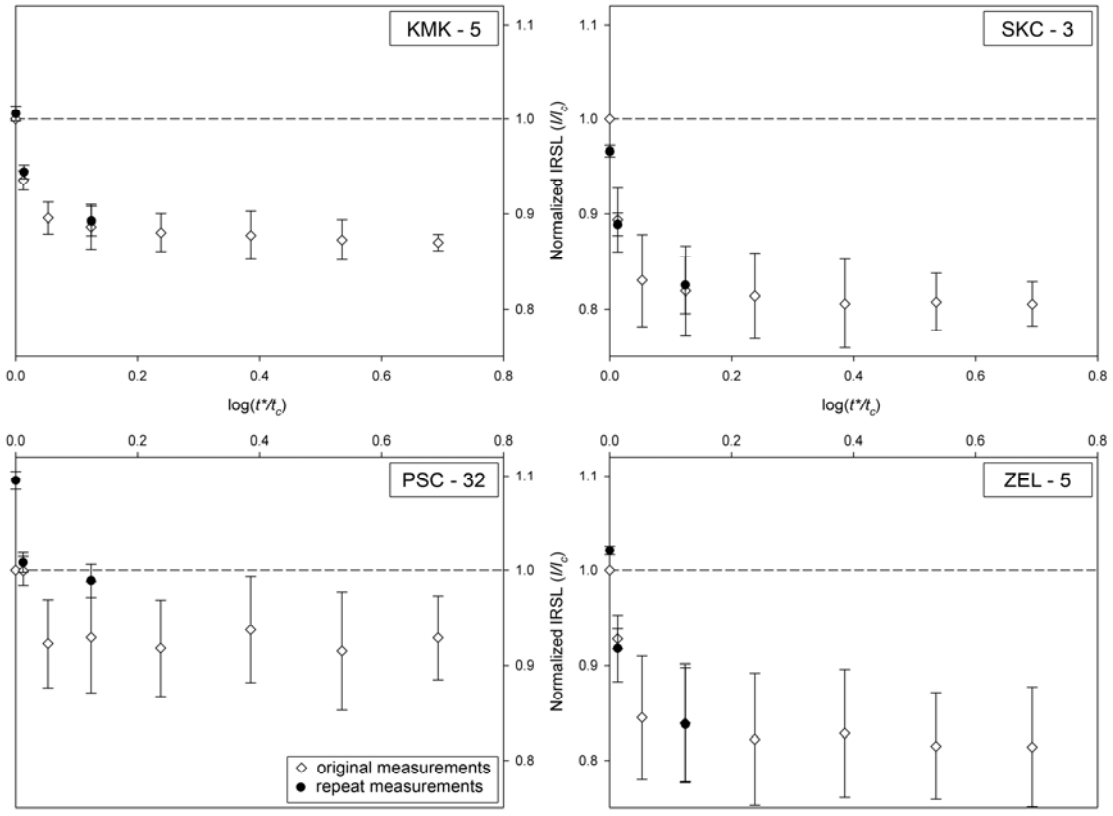

Figure 4.1: Anomalous fading results for the samples used in this study. The repeat measurements were obtained after the last original measurement; with the exception of sample PSC-32, no sensitivity change is observed. The ordinate is given as sensitivity corrected IRSL signal measured after t normalized to the immediate measurement at t_c. Experimental parameters: t_c = 602 s, used signal integral = 1 s (channels 1-5).*

With this in mind, all further observations will be illustrated using sample KMK-5. It is evident that determining a fading rate based on linear fitting of these datasets will not yield

useful results, as the g-values would depend on how much of the curve is used for fitting. However, the curve's tendency to a linear behaviour for longer t* indicates that the unusual behaviour is limited to short delays, suggesting that it may be linked to an IRSL signal instability which gradually disappears over the first few fading steps. Therefore, if only the latter measurement pauses were used (which would implicate normalisation to the signal of a higher t_c), linearity of fit appears to be satisfied.

Using longer signal integrals, the effect becomes less pronounced (Figure 4.2), indicating that it is not only linked to short measurement delays, but also that it is affected differently by different parts or components of the decay curve. This observation is in agreement with the findings of Thomsen *et al.* (2008), who observed changing fading rates as a function of increasing stimulation time.

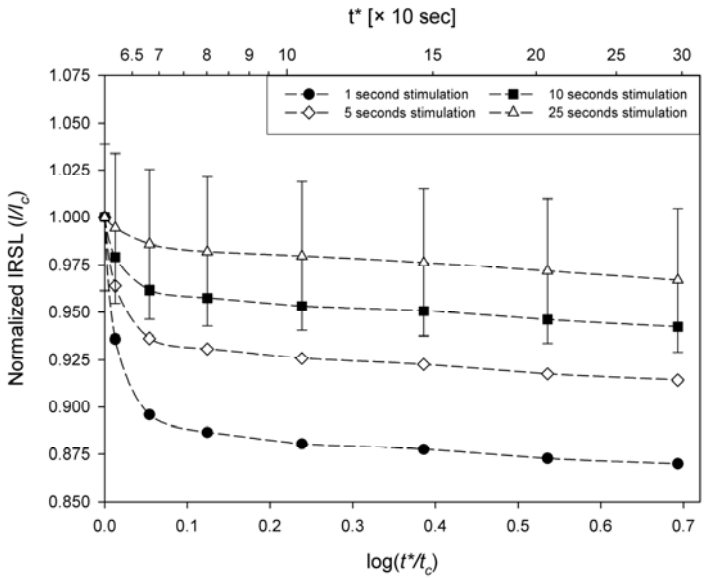

Figure 4.2: Fading plots for sample KMK-5 using signal integrals of 0, 1, 5, 10 and 25 seconds. Normalization for all curves is to their respective immediate measurement taken at t_c = 602 s. For clarity, errors (1 σ std-err, n= 3) are only given for the 25 s stimulation curve but are similar for all others.

Using both linearly modulated (LM) and time resolved IRSL, it has been shown that the decay curves of K-feldspars can be fitted to three components (Bulur and Göksu, 1999; Tsukamoto *et al.*, 2006). In order to characterize the fading behaviour of our sample, deconvolution, i.e. component fitting, was undertaken on the continuous wave (CW)-IRSL decay curves measured in the fading tests using Sigmaplot. All decay curves fitted well (average R^2 = 0.99) to three components with photoionisation cross-sections (σ) of 4.08 × 10^{-18} cm^2, 7.40 × 10^{-19} cm^2 and 5.138 × 10^{-20} cm^2, where the third component is to a large part comprised of background. It is not possible to make a direct comparison of these values to those of Bulur and Göksu (1999), who recorded LM-IRSL decay curves using a broadband visible filter. Figure 4.3 shows that the decay curves recorded following all measurement pauses (defined by their increasing t*) exhibit a contribution from the same three components. The relative contribution of the components changes with increasing t*, with the first and third components displaying a relative decrease, while the second component increases. These relative changes are most pronounced for low t* steps and the three curves asymptotically approach a stable configuration after a pause of at least 480 s (equivalent t* = 1042 s). The decay curves can, almost independently of t*, be divided into distinct regions, each dominated by one of the

components. It must be kept in mind, however, that these positive and negative changes are of a relative nature only. On an absolute scale, the overall signal (the sum of the three components) decreases from one measurement pause to the next. Therefore, the overall signal sampled in an integral that lies within the region dominated by the first component will categorically decrease with increasing t*, but the rate of this decrease will be high for the low t* pauses and abate to a constant value for t* pauses greater than 1042 s. Although only one delayed measurement was made after 30 days, when comparing this to an immediate measurement, Tsukamoto *et al.* (2006) were able to show that their 'first' component was less stable. For a sampling integral dominated by the second component, the decreasing signal will show a lower initial rate of decrease, which then rises to a final value. The third component only becomes dominant after a prolonged stimulation time that is usually of little interest, and we concentrate therefore on the first two components. As the g-value is a measure of the rate of signal decrease with time, the different components

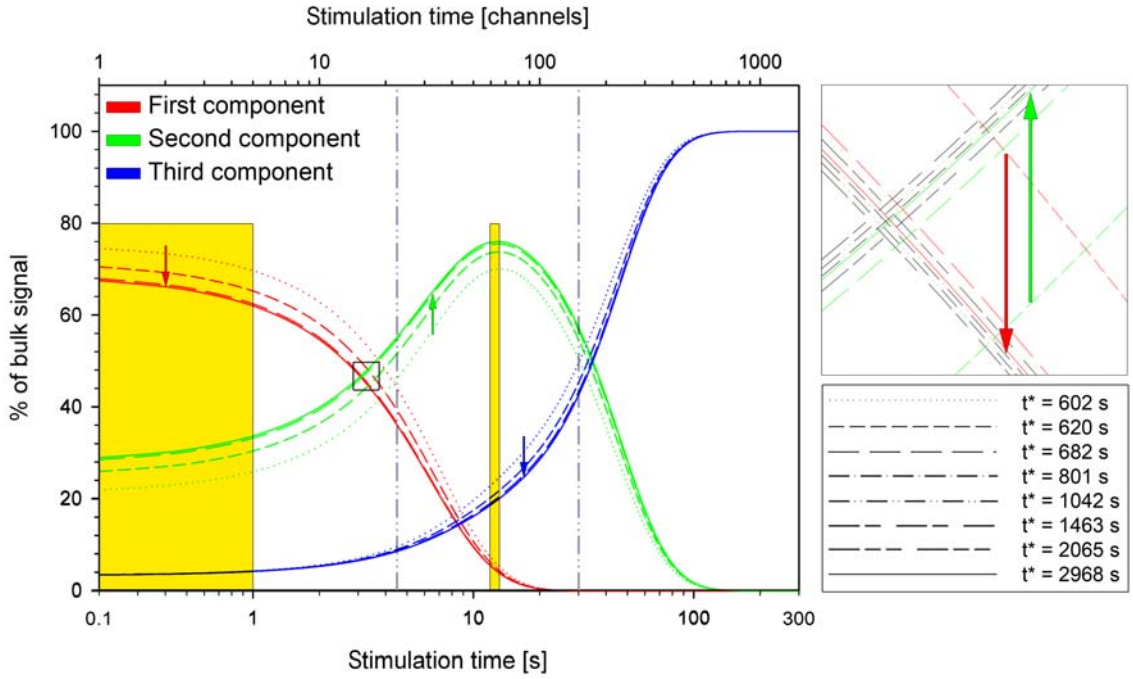

Figure 4.3: All continuous-wave IRSL decay curves from sample KMK-5 for each of the delays in the fading measurements were fitted to three components; the relative contribution to the bulk signal vs. time is plotted. The curves of the individual components show initial changes in their relative positions but asymptotically approach stable values for increasing t (a higher resolution of this is shown to the right). These changes are negative for the first and third components, contrary to a positive change for the second component, as indicated by the arrows. The vertical grey lines separate the regions in which the decay curve is dominated by each of the components. The yellow areas mark the signal integrals for the first and 13th second.*

contribute differently to the fading rate. The resulting overall g-value is the result of the combined effects of the two components integrated over the chosen signal integral. Particularly for low t*, the varying ratio of these contributions will lead to varying overall

g-values. This is illustrated in Figure 4.4: for the first second of the decay curve (A) - dominated by the first component - the fading rate for the entire set of measurement pauses shows a high value of 11.7 ± 1.65 % per decade. If the first measurement pause (zero seconds pause, t* = 602 s) is not taken into consideration, the dataset is normalized to the new immediate measurement after a pause of 60 seconds (t* = 620 s, thus t_c = 620 s), and the resulting g-value is reduced to 7.2 ± 1.64. For further increases in t_c, the measured g-values trend towards a value around 2.5 % per decade after a t_c of 1042 s. For the 13th second of the decay curve (B), dominated by the second component, the behaviour is reversed and the g-values rise from a negative value of -1.6 % per decade for t_c = 602 s towards the same value of around 2.5 % per decade, again after a t_c of 1042 s. These "final" g-values coincide with the average g-value of 2.6 ± 0.2 obtained from linear fitting of the individual curves in Figure 4.2, if only the measurement pauses beyond a t_c of 1042 s are considered. The interrelation of the signal components is no longer subject to change with increasing t* for this choice of t_c (Figure 4.3). As a consequence, this g-value remains independent of both the choice of t* (for t* ≥ t_c) and the chosen integral. Thus, for sample KMK-5, keeping the initial delay to a minimum of at least 480 seconds between the end of preheating and beginning of the IRSL measurement (equivalent to a t_c of at least 1042 s) avoids the problem of aberrant fading behaviour for short pauses and allows the determination of a reasonable g-value. Interestingly, this required minimum initial threshold is very similar for the other samples investigated, as is already evident in Figure 4.1.

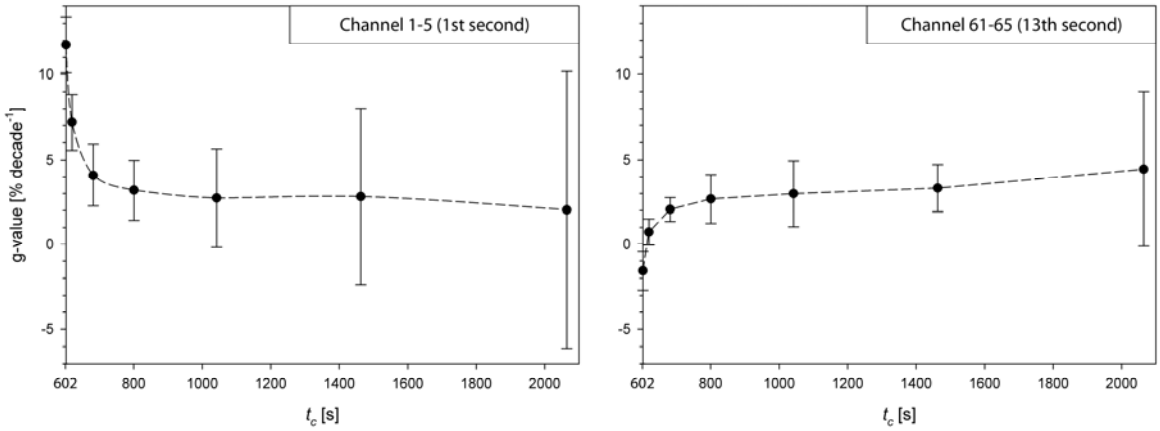

Figure 4.4: Sample KMK-5 fading rates as a function of t_c for a signal integral dominated by the first component (A) and the second component (B). When increasing t_c, only those fading steps with $t^* \geq t_c$ are used for fading rate evaluation. Errors are given as 1 σ std-err (n = 3, which explains the overall large errors). The increase in error towards higher t_c is due to high tc fading rates being defined by ever less points (only 2 for t_c = 2065 s). This lack of constraint leads to a large scatter of the g-values for the individual aliquots and consequentially a large error on the average values. Extending t^* in order to have at least a 5 point fit for the highest t_c and using a higher number of aliquots would greatly reduce errors.

While using a very late part of the decay curve (where the first component has disappeared and the remaining components show opposite behaviour) also yields constant g-values, this is impractical due to low signal levels, bad counting statistics and, most likely, problems with partial bleaching.

4.5 CONCLUSIONS

It has been demonstrated that fading rate determinations, according to Huntley and Lamothe (2001), can result in aberrant g-values if the t_c of the immediate measurement is too short. This is due to the presence of at least two different components in the IRSL signal, having differing fading characteristics. While their behaviour initially differs, these relative changes are most pronounced for low t_c steps, and are seen to approach a stable configuration over time. For the samples investigated in this study, taken from fluvial, glaciofluvial and aeolian sites around the globe, this stable point appears to be reached after 480 s between the end of preheating and the start of the IRSL measurement (corresponding to a t_c of 1042 s). It therefore appears imperative that any IRSL measurements, not only in the context of fading determinations, should be made after a certain minimal delay and that this is applied to all IRSL measurements conducted on a sample. This precludes the use of "run 1 at a time" measurement sequences without appropriate delays.

ACKNOWLEDGEMENTS

A. Dehnert, M. Suchy, T. Rosenberg and I. Schindelwig are gratefully thanked for helpful discussions and comments on the manuscript. This work was funded by the Swiss National Science Foundation (SNSF), Project No's 200020-105453/1, 200020-118023/1, 206021-117374, 200020-121671 and 200020-121680.

4.6 REFERENCES

AITKEN, M.J. (1985): Thermoluminescence Dating. *ACADEMIC PRESS, LONDON.*

AUCLAIR, M., LAMOTHE, M. & HUOT, S. (2003): Measurement of anomalous fading for feldspar IRSL using SAR. *RADIATION MEASUREMENTS* 37 (4-5): 487-492.

BULUR, E. & GÖKSU, H.Y. (1999): Infrared (IR) stimulated luminescence from feldspars with linearly increasing excitation light intensity. *RADIATION MEASUREMENTS* 30 (4): 505-512.

HUNTLEY, D.J. (2006): An explanation of the power-law decay of luminescence. *JOURNAL OF PHYSICS - CONDENSED MATTER* 18 (4): 1359-1365.

HUNTLEY, D.J. & LAMOTHE, M. (2001): Ubiquity of anomalous fading in K-feldspars and the measurement and correction for it in optical dating. *CANADIAN JOURNAL OF EARTH SCIENCES* 38 (7): 1093-1106.

KARS, R.H., WALLINGA, J. & COHEN, K.M. (2008): A new approach towards anomalous fading correction for feldspar IRSL dating - tests on samples in field saturation. *RADIATION MEASUREMENTS* 43 (2-6): 786-790.

LAMOTHE, M., AUCLAIR, M., HAMZAOUI, C. & HUOT, S. (2003): Towards a prediction of long-term anomalous fading of feldspar IRSL. *RADIATION MEASUREMENTS* 37 (4-5): 493-498.

PREUSSER, F., ANDERSEN, B.G., DENTON, G.H. & SCHLÜCHTER, C. (2005): Luminescence chronology of late pleistocene glacial deposits in North Westland, New Zealand. *QUATERNARY SCIENCE REVIEWS* 24 (20-21): 2207-2227.

PREUSSER, F., MÜLLER, B.U. & SCHLÜCHTER, C. (2001): Luminescence dating of sediments from the Luthern Valley, central Switzerland, and implications for the chronology of the last glacial cycle. *QUATERNARY RESEARCH* 55 (2): 215-222.

STEFFEN, D., SCHLUNEGGER, F. & PREUSSER, F. (2009): Drainage basin response to climate change in the Pisco valley, Peru. *GEOLOGY* 37 (6): 491-494.

THOMSEN, K.J., MURRAY, A.S., JAIN, M. & BØTTER-JENSEN, L. (2008): Laboratory fading rates of various luminescence signals from feldspar-rich sediment extracts. *RADIATION MEASUREMENTS* 43 (9-10): 1474-1486.

TSUKAMOTO, S., DENBY, P.M., MURRAY, A.S. & BØTTER-JENSEN, L. (2006): Time-resolved luminescence from feldspars: New insight into fading. *RADIATION MEASUREMENTS* 41 (7-8): 790-795.

VISOCEKAS, R. (1979): La luminescence de la calcite après irradiation cathodique: thermoluminescence et luminescence par effet tunnel. *PH.D. THESIS, UNIVERSITÉ DE PIERRE ET MARIE CURIE, FRANCE.*

WALLINGA, J., BOS, A.J.J., DORENBOS, P., MURRAY, A.S. & SCHOKKER, J. (2007): A test case for anomalous fading correction in IRSL dating. *QUATERNARY GEOCHRONOLOGY* 2 (1-4): 216-221.

WALLINGA, J., MURRAY, A. & WINTLE, A. (2000): The single-aliquot regenerative-dose (SAR) protocol applied to coarse-grain feldspar. *RADIATION MEASUREMENTS* 32 (5-6): 529-533.

WINTLE, A.G. (1973): Anomalous Fading of Thermoluminescence in Mineral Samples. *NATURE* 245 (5421): 143-144.

CHAPTER 5

Late Quaternary volcanic history of the Vakinankaratra volcanic field (central Madagascar): insights from luminescence dating of phreatic eruptions

Daniel Rufer [a], Frank Preusser [a], Edwin Gnos [b],
Guido Schreurs [a] & Alfons Berger [c]

[a] Institute of Geological Sciences, University of Bern, Switzerland
[b] Muséum d'histoire naturelle de Genève, Switzerland
[c] Department of Geography and Geology, University of Copenhagen, Denmark

To be submitted to:
Bulletin of Volcanology

"He also had one volcano that was extinct. But as he said, "One never knows!" So he cleaned out the extinct volcano, too.

If they are well cleaned out, volcanoes burn slowly and steadily, without any eruption. Volcanic eruptions are like fire in a chimney.

On our earth, we are much too small to clean out our volcanoes. That is why they bring no end of trouble upon us."

From "The Little Prince", 1943, Antoine de Saint-Exupéry (1900 - 1944), Writer and aviator

LATE QUATERNARY VOLCANIC HISTORY OF THE VAKINANKARATRA VOLCANIC FIELD (CENTRAL MADAGASCAR): INSIGHTS FROM LUMINESCENCE DATING OF PHREATIC ERUPTIONS

5.1 ABSTRACT

For the first time, luminescence dating has been successfully applied to date phreatic explosion deposits from the Quaternary Vakinankaratra volcanic field in the central Madagascar highlands. This region of intracontinental, rift-related volcanism, resulting from the south-eastwards extension of the East-African Rift system is assumed to have been active up into the Holocene, although there is very little data available on the volcanic eruptions, particularly with regard to numerical ages. Establishing a chronostratigraphic framework of the young volcanic activity is therefore not only a prerequisite for further research, but is also an important aspect for volcanic hazard assessment in this densely populated region. The article gives an overview of the explosive phreatic activity in the area and illustrates various aspects of the method. The numerical ages produced for at least four phreatic deposits are the only currently available numerical ages for the Quaternary volcanic history in the Vakinankaratra so far, and indicate that the eruptive activity of the volcanic field started in the Late Pleistocene.

Keywords: luminescence dating; Quaternary volcanism; geochronology; Madagascar; Ankaratra; phreatic explosion

5.2 INTRODUCTION

Situated in the central Madgascar highlands, the Ankaratra, Lac Itasy and Vakinankaratra volcanic fields are examples of intracontinental, rift-related volcanism (Figure 5.1, Geological Map in *APPENDIX B*). Caused by asthenospheric bulging (Rakotondraompiana *et al.*, 1999) and extensional reactivation of Precambrian and old Phanerozoic tectonic structures and zones of weaknesses, they are a result of the south-eastwards extension of the East-African Rift system (Mougenot *et al.*, 1986; Kusky *et al.*, 2007). Together with a high seismic activity (Bertil and Regnoult, 1998) and extensional graben structures (e.g. Ankay-Alaotra rift, Piqué *et al.*, 1999), they manifest widespread intracontinental rifting in Madagascar.

Unfortunately, there is very little data available about these volcanic provinces, particularly with regard to numerical dating of the Late Quaternary volcanic activity of the Vakinankaratra volcanic field (Figure 5.2). While a better constraint on the young eruptive history is a prerequisite for a wide range of research topics, establishing a chronostratigraphic record of volcanic activity is also fundamental for volcanic hazard

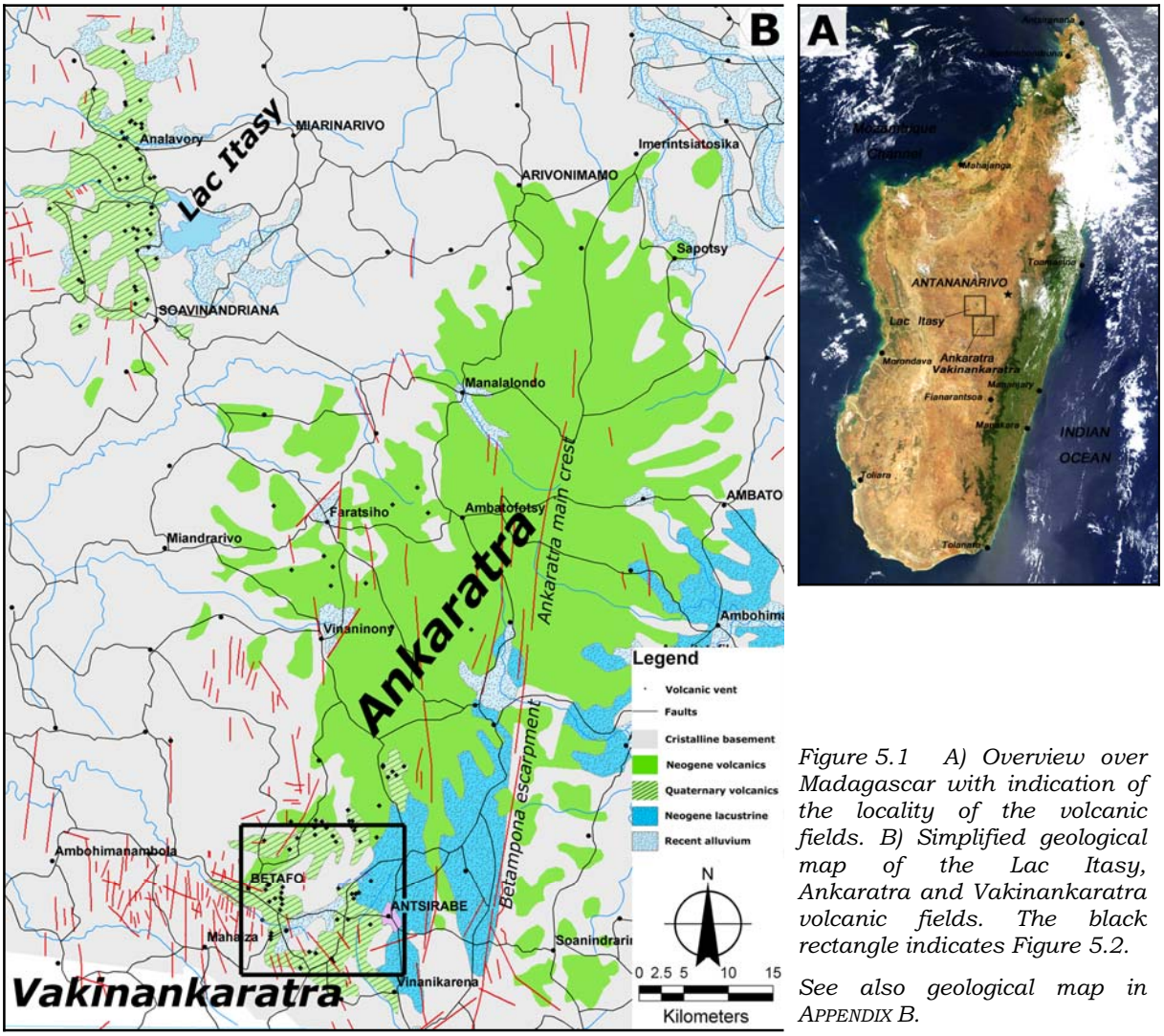

Figure 5.1 A) Overview over Madagascar with indication of the locality of the volcanic fields. B) Simplified geological map of the Lac Itasy, Ankaratra and Vakinankaratra volcanic fields. The black rectangle indicates Figure 5.2.

See also geological map in APPENDIX B.

assessment. This is particularly important as these young volcanic regions are, due to the high fertility of the volcanic soils, amongst the most densely populated areas in Madagascar.

Initial attempts to date the predominantly basanitic to tephritic material using the $^{39}Ar/^{40}Ar$ technique failed due to the young age of the material, overall low potassium concentrations in whole rock samples and a distinct lack of measurable K-feldspars. Unfortunately alternative methods for directly dating young volcanic rocks are rather scarce and most of them possess some inherent pitfalls (cf. Fattahi and Stokes, 2003). Based on the deliberations given by Rufer *et al.* (submitted a), luminescence dating was undertaken on a series of phreatic explosion deposits from the Vakinankaratra volcanic field. This article will give an introduction into the geology and the volcanological setting of the region and present first numerical ages for phreatic explosion horizons obtained with this new luminescence method.

5.3 GEOLOGICAL SETTING

Situated in an intraplate context in the south-western Indian Ocean, Madagascar is a continental island (de Wit, 2003) that stretches 1600 km north-south and at its widest point measures nearly 600 km across. It features an east-west asymmetric topography, with a broad axial zone where the mean elevation is about 1200 m.a.s.l. This High Plateau is flanked to the east by a steep escarpment, whereas to the west it gradually slopes towards the Late Palaeozoic and Mesozoic Morondava and Mahajanga basins. The elevated interior of the island consist almost exclusively of high-grade metamorphic Precambrian basement. Extensive erosional remnants of Upper Cretaceaous flood basalts associated with the breakup between Madagascar and India can be traced across large sections of the coast. As a consequence of the youngest plate reorganization in the Indian Ocean, which started ~34 Ma ago with the opening of the Red Sea and the initiation of the East African Rift system, Madagascar has come under an extensional regime since the mid Miocene (Bertil and Regnoult, 1998), leading to the development of the intracontinental volcanic fields (Figure 5.1).

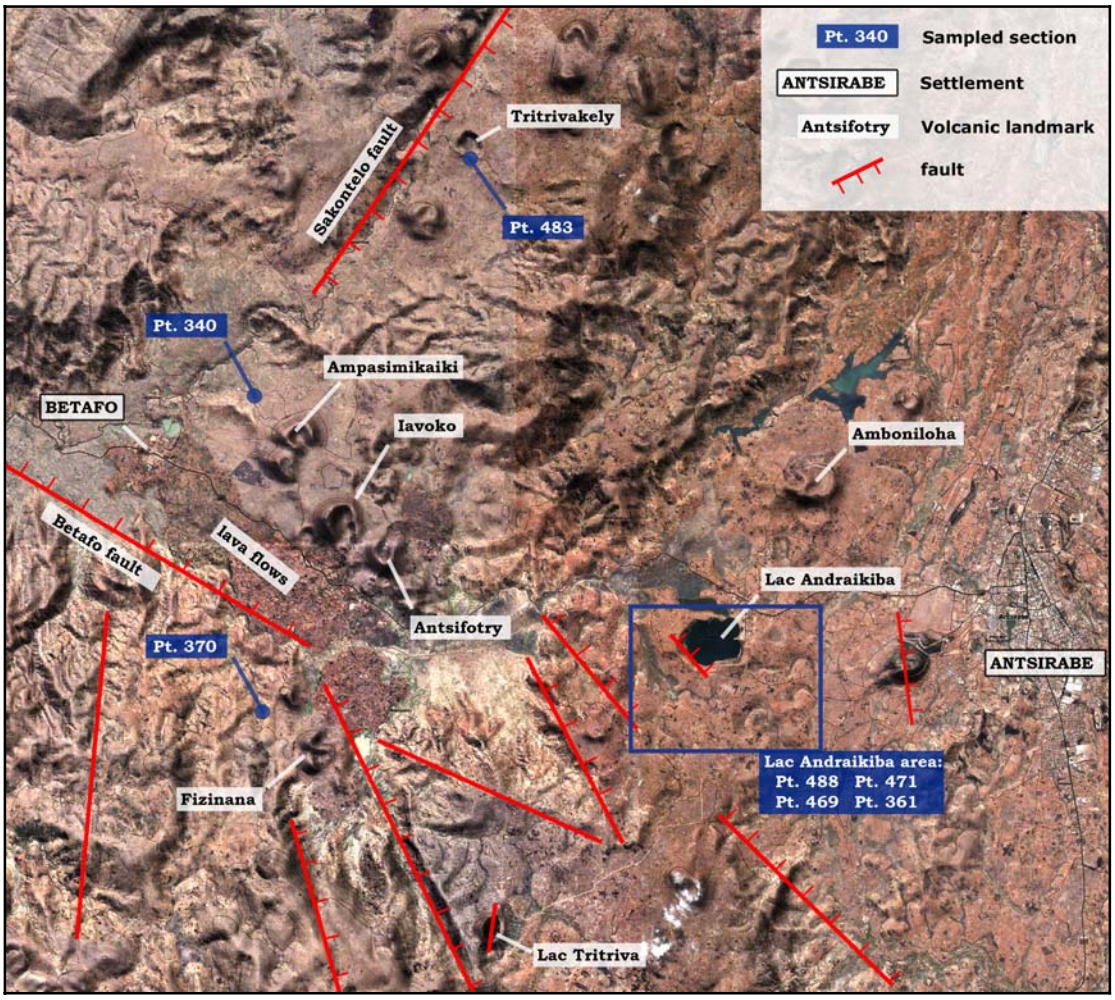

Figure 5.2 Aerial view over the Antsirabe-Betafo region of the Vakinankaratra volcanic field including locations of sampled sections. The blue rectangle indicates Figure 5.9. See also geological map in APPENDIX B.

The Ankaratra massif covers a surface of approximately 3800 km², between 18°56' to 19°57' S and 46°46' to 47°30' E and extends over 100 km in north-south direction (Woolley, 2001). It is dominated by extensive flood basalts, most of which originated from along the main crest of the massif, which strikes N20°E and continues to the south in the large Betampona escarpment, a west dipping normal fault deliminating a half graben structure containing the Ambohimiarivo basin, one of the large Neogene alluvial basins in the highlands. To the north, the volcanic field features large ankaratrite (olivine-nepheline basalt) flows and a number of acidic to intermediate extrusions as well as intramontane tectonic basins (e.g. Vinaninony and Faratsiho basin) can be found chiefly in the western part of the massif.

The Lac Itasy volcanic field lies approximately 40 km to the north-west of the Ankaratra massif and covers some 300 km² (Woolley, 2001). It constitutes primarily of numerous domes, scoria cones and lava flows of trachytic to basanitic composition overlying Precambrian basement. A number of late stage hydroclastic explosions craters formed a series of maar craters, often cutting existing trachytic domes. Both the Ankaratra and the Lac Itasy field overly the old Precambrian basement.

The Vakinankaratra volcanic field is situated in the south-western extension of the Ankaratra massif (Figure 5.1 & Figure 5.2), where it partially overlies the older volcanic material. As Vakinankaratra is a geographical denomination, literally meaning "divided by Ankaratra", it is often used to describe all volcanic vents south of the Ankaratra massif. On one hand, this includes older, acidic extrusions along the Betampona rift shoulder, on the other hand it complicates a division between e.g. felsic projections of the latest stage of the actual Ankaratra field along its south-western edge and younger, mafic material attributed to the Vakinankaratra field in the same region. As this study focuses on the Latest Pleistocene to Holocene volcanism in the region Antsirabe-Betafo, the denomination Vakinankaratra volcanic field is here used to describe this youngest volcanic activity, which is primarily dominated by basanitic to tephritic strombolian cones and flows in the region between Antsirabe, Lac Tritriva, and Betafo, as well as along the Sakontelo fault north-east of Betafo. While the crystalline basement is the same as in the other volcanic areas, parts of the Vakinankaratra substratum also consist of older basalt flows from the Ankaratra massif.

5.3.1 PHREATIC ERUPTIONS IN THE VAKINANKARATRA VOLCANIC FIELD

Phreatic eruptions occur through mechanical mixing of magma with water (e.g. at the contact between ascending magma and the phreatic nappe), triggering a chain of reactions resulting in almost instantaneous vaporization and volumetric expansion of large amounts of water. The ensuing explosions often form distinct volcanosedimentary deposits ranging from proximal high energy surges to distal airfall deposits (Figure 5.3 & Figure 5.4). In the case of phreatic eruptions, which are defined as steam explosions primarily within the country rock above a magmatic heat source (MacDonald, 1972), the ejected mass contains

only a negligible amount of juvenile material, contrary to phreatomagmatic eruptions, where new magma is disintegrated as well. The composition of phreatic explosion deposits can therefore be considered representative of the average basement rock composition.

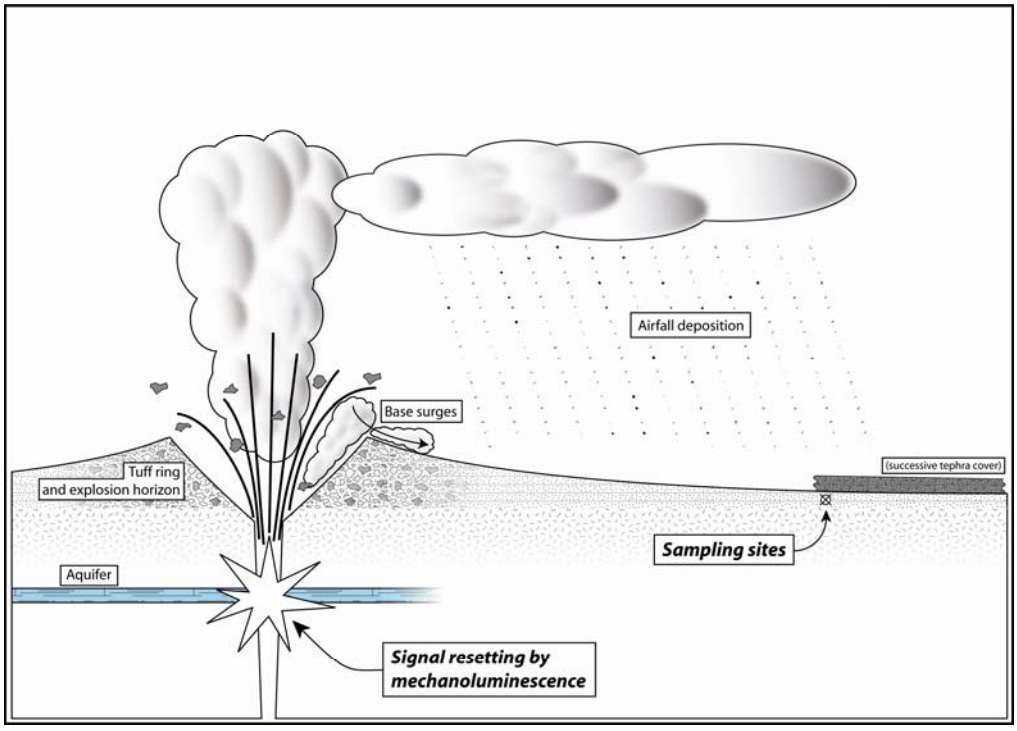

Figure 5.3 Schematic cross-section through a phreatic explosion crater with an indication of the relevant sites and processes for luminescence dating of phreatic deposits.

In the Antsirabe-Betafo area, several maar craters attest to such phreatic activity. Most of the identified phreatic craters lie in the eastern part of the Vakinankaratra volcanic field, with Lac Andraikiba being the most prominent member and the only one containing a perennial crater lake. Two unnamed, morphologically older craters of apparently purely phreatic origin lie approximately 1 km east of Lac Andraikiba and between Lac Andraikiba and Lac Tritriva (Figure 5.2). Futher phreatic craters might subsequentially be overprinted by strombolian cones (e.g. in the Amboniloha volcanic complex, see 5.6.1). In the western part of the volcanic field there is no clear occurrence of phreatic craters. Even though Lac Tritrivakely crater, north-east of Betafo (Figure 5.2), is sometimes being described as a maar crater (e.g. Gasse *et al.* (1994) and Williamson *et al.* (1998)), the phreatic deposits found at this location are not linked to the crater itself. Mottet (1980b) therefore describes it rather as an intermediate between a strombolian cone and an explosive (not necessarily phreatic) crater.

It should be noted, that Lac Tritriva in the southern part of the volcanic field, is generally not considered to be a phreatic crater (Mottet, 1980b and Petit, 1998), even though its diatreme shaped form and profound depth over 600 ft (> 182 m) (Sibree, 1891) may induce

such an interpretation. Despite the occurrence of numerous basement blocks in the surrounding tephra deposits, there is no evidence of a purely phreatic or phreatomagmatic explosion deposit. The unusual shape and depth of the crater is explained by tectonic activity along a roughly N-S trending assumedly subvertical fault (Mottet, 1980b).

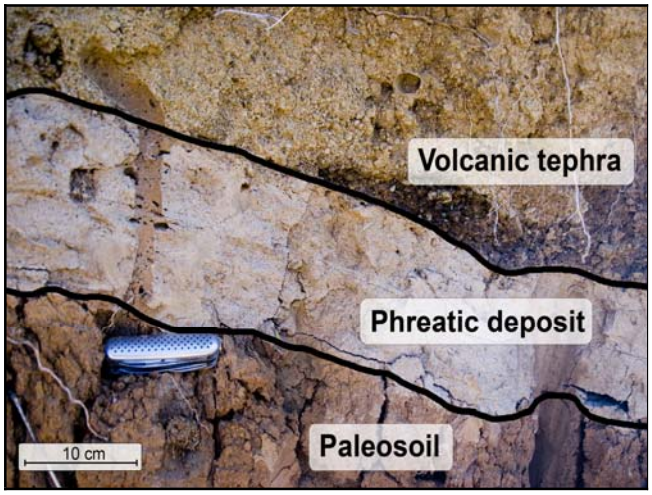

Figure 5.4 Outcrop photograph of a phreatic explosion deposit intercalated between a paleosoil from an strongly weathered lava flow and overlying tephritic tephra. The explosion layer has a sandy grain size and is finely layered; its constituents are derived from granitic rocks. The black lines between the units are for illustrative purposes only.

Phreatic eruptions deposits can be found over wide parts of the volcanic field (Figure 5.2 & Figure 5.9). They provide clearly identifiable horizons which extend far beyond the confined eruption range of cinder cones or fissure vents. While their stratigraphic correlation between outcrops is often possible, so far only one layer has been successfully correlated with its source (Lac Andraikiba).

5.4 EXISTING CHRONOSTRATIGRAPHY

There is a notable scarcity of absolute age data of the volcanic history both of the Miocene to Pliocene activity of the main Ankaratra massif, as well as of the Late Pleistocene to Holocene volcanism in the Vakinankaratra. Particularly for the latter there are no ages of directly dated volcanic material.

Various earlier interpretations (e.g. Lacroix, 1912; Lacroix, 1921-1923; Brenon and Bussiere, 1959; and Alsac, 1963) divide the volcanic history of the main Ankaratra massif into multiple phases and assign them to geological epochs based on intercalations of volcanic material with Neogene lacustrine sediments (Bussiere, 1957). It must be noted, however, that the absolute age ranges of the Cenozoic geological epochs have been revised repeatedly since these publications appeared (for a discussion concerning the attribution of an absolute date to the Pliocene, see Mottet (1980a), p. 232). Unless numerical ages are provided, these age ranges must therefore be considered under this aspect.

Mottet (1980a,b) and Petit (1998) subdivide the volcanic history of the main Ankaratra massif into three main phases:

- An initial Late Miocene to Pliocene episode dominated by effusion of the extensive flood basalts (Petit, 1998). It is assumed that pre-existing Precambrian lineaments and zones

of weaknesses served as pathways for the fissural eruptions of these sheet flows (Mottet, 1980a). Several ages for these flood basalts are in circulation: Bardintzeff *et al.* (2001) and Bardintzeff *et al.* (2002) give an age range of 27.9 – 3.1 Ma (no individual dates or method indicated); Petit (1998) gives an age range between 6-8 Ma and 2.7 Ma (no individual dates or method indicated) and Mottet (1980a) reports a K-Ar age of 6.76 Ma (no errors given).

- A second phase with frequent eruptive activity and subsequent emplacement of a large volume of ankaratrites along the modern Ankaratra main crest as well as numerous trachytic extrusions in the entire volcanic field. This phase is accompanied by the formation of several intramontaneous basins of volcano-tectonic nature (e.g. "cuvette de Vinaninony", "cuvette de Faratsiho" (Mottet, 1980a) (Figure 5.1).
- A third phase dominated by locally occurring large andesitic flows and trachy-andesitic extrusions and, in the southern part of the field, leucocrate tephra emissions (Mottet, 1980a). Absolute ages are given in Petit (1998) as 1.7 - 1.4 Ma for the andesitic flows and as 0.8 Ma for the tephra deposits (all ages without mention of the method, no errors given). Mottet (1980a) reports K-Ar ages of 1.71 Ma and 1.44 Ma for two andesitic flows (no errors given).

It should be noted, that the K-Ar ages must be considered with caution, as the method does not control influences of alteration and excess argon (e.g. Faure, 1986). Particularly the problem of alteration is indicated by Mottet (1980a, p. 222).

While activity in the Vakinankaratra field is often considered to simply be the latest phase of volcanic activity in the Ankaratra region, it is here treated separately due to its geographical constraint as well as its restricted prevalent type of eruption processes (see section *5.3*).

Mottet (1980b) gives an age estimate of < 50 ka for the volcanic structures in the region Antsirabe – Betafo (Figure 5.2) with individual estimates of 6 to 5 ka for the Iavoko cone and 4 to 2 ka for the youngest Antsifotra cone. The only numerical (albeit indirect) age is provided by a volcanic tephra layer found at 1175 cm depth in a drillcore from lake Tritrivakely, a crater, situated approximately 8 km NE of Betafo, dated between 36.2 ± 1.2 ka and 34.7 ± 1 ka using radiocarbon dating on diatomaceous clay and peat layers found below and above the tephra layer (Gasse and Van Campo, 2001). For four additional tephra layers, found at deeper levels of the core (2654 cm, 3675 cm, 3685 cm and 3720 cm), no physical datings are available. However, based on "tentative" (sic.) model correlations between the Tritrivakely record and the Vostok temperature curve (Jouzel *et al.*, 1993), these tephra deposits would fall into age ranges of 98.5 – 87 ka (2654 cm) and 143 - 124 ka (3675 cm, 3685 cm and 3720 cm).

These ages are in the same order as two K-Ar ages of 70.0 ± 3.5 ka and 57.0 ± 3.0 ka, determined on basanites and trachytes respectively, from the contemporaneous (e.g. Petit, 1998) Lac Itasy volcanic field (Ratsimbazafy and Rakoto, 1997).

While this suggests an age range spanning the Latest Pleistocene to the Holocene for the volcanic activity in the Antsirabe-Betafo region, the presence of only one single indirect age for the associated volcanic deposits also illustrates very strongly the need for further dating results to better constrain the young volcanic history of this region.

5.5 METHODOLOGY

5.5.1 INTRODUCTION TO LUMINESCENCE DATING

Luminescence dating techniques allow the determination of the time that has elapsed since quartz or feldspar grains have last been exposed to daylight, heat or mechanical stress. When undisturbed, the sample accumulates a signal induced by natural radioactivity, both ambient and internal (in the case of K-feldspar) as well as from cosmic radiation. The ionizing radiation causes excitation of atoms within the crystal lattices of the samples' quartz and feldspar grains, leading to the formation of activated electrons at higher energy states and a corresponding electron hole. While the majority of these electrons fall back and recombine instantaneously, some are captured at lattice defects in so called electron traps. While energetically shallow traps can only keep their charge for a short amount of time, the electrons in deeper traps remain stable over geological timescales, leading to an accumulation of filled traps. When exposed to a particular stimulation energy (e.g. light, heat or mechanical stress), these trapped electrons can escape the energy-trough of the trap and recombine with an electron hole under emission of the stored energy in the form of luminescence. Based on the form of stimulation, it is differenciated between i.a. optically stimulated luminescence (OSL), infrared stimulated luminescence (IRSL), thermo-luminescence (TL) and mechanoluminescence.

Any measured luminescence signal is therefore representative for the amount of traps filled since the last resetting. After measuring the natural luminescence signal of a sample, it is repeatedly bleached, irradiated and measured with increasing radiation doses, resulting in an internal signal/dose calibration curve. This allows the calculation of the paleo-dose (also called equivalent dose) D_E which was required to produce the initially measured natural luminescence signal. After determining the doserate D* to which the sample was subject, the age T of the last resetting event can be calculated as

$$T = D_E / D^*$$

A more comprehensive and detailed introduction into the topic is given by e.g. Preusser *et al.* (2008).

5.5.2 LUMINESCENCE DATING OF PHREATIC EXPLOSION DEPOSITS

One of the principal motivations behind using phreatic explosion deposits for luminescence dating of volcanic eruptions lies in trying to avoid problems usually encountered when dating volcanic quartz, feldspar or glass (see Rufer *et al.*, submitted a), or in environments, where these phases are too scarce to be effectively sampled. It furthermore allows dating of a type of volcanic activity that often occurs early in a new eruptive cycle of a centre and therefore represents an important chronostratigraphic marker.

Signal resetting of such materials is potentially different to fluvial or aeolian sediments, where signal resetting occurs by exposure to light and is therefore strongly dependant on transport time and factors like turbidity of the transporting medium. In phreatic explosion deposits, the materials experience resetting of their luminescence signals due to mechanical stress during the violent explosive fragmentation in the phreatic eruption (Rufer *et al.*, submitted a).

5.5.3 SAMPLE PREPARATION AND EXPERIMENTAL PARAMETERS

Sample processing and measurements were carried out under subdued red light. After gravimetric determination of the moisture content, the samples were dried, sieved and the 100-150 µm fraction was selected for further processing. Subsequent to removal of the magnetic fraction with a neodymium hand magnet, the samples were subjected to a 10% hydrochloric acid and a 35% H_2O_2 wash in order to remove carbonate and organic material. A two step density separation using LST (a solution of lithium heteropolytungstates in water; the specific gravities used were 2.58 g cm^{-3} and 2.70 g cm^{-3}) was employed to isolate the quartz and feldspar fractions, with the quartz being subsequently etched in 40% hydrofluoric acid (Mejdahl, 1985). The quartz separates were further treated with

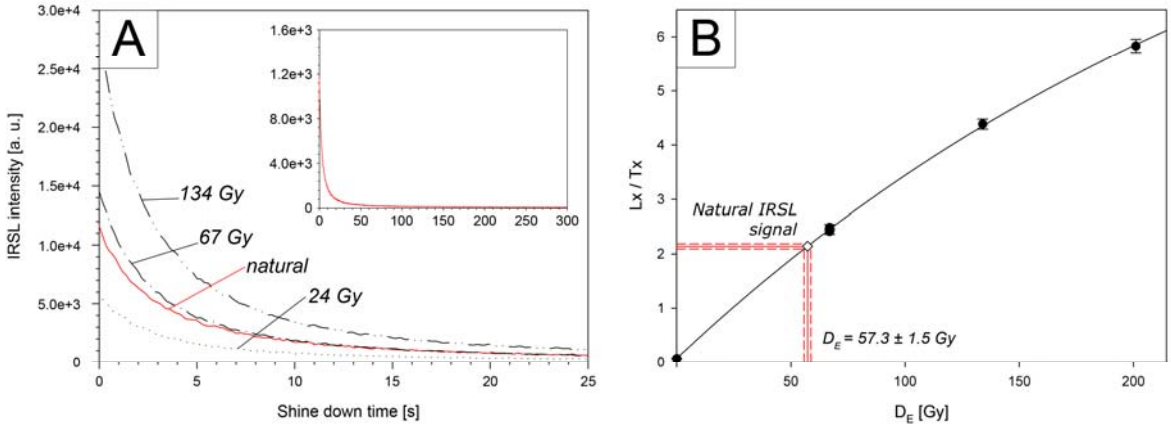

Figure 5.5 A) Representative IRSL shine down curve (sample DR483_1) for the natural and three regenerative doses, given in the initial 25 s signal integral used for the measurements. Inset: natural signal plotted over the entire 300 s stimulation time. B) A typical IRSL dose response curve (sample DR483_1)

hydrofluorosilicic acid (H_2SiF_6) for one week in order to eliminate any remaining feldspar contamination (Steffen *et al.*, 2009). No acid etching was used on the feldspar separates, because this would most probably not remove a uniform surface layer (Duller, 1992). An alpha efficiency value of 0.07 ± 0.02 was assumed (Preusser, 1999).

Measurements were carried out on Risø DA-20 TL/OSL readers fitted with internal $^{90}Sr/^{90}Y$ beta sources, using a combination of a Schott BG39 and a LOT/Oriel D410/30 interference filter and a Hoya U340 UV-transmitting filter for the IRSL and blue OSL measurements respectively.

For the feldspar samples, equivalent doses (D_E) were determined following the single-aliquot regenerative-dose (SAR) approach of Wallinga *et al.* (2000). The samples were stimulated by IRSL diodes at 40°C for 300 s (Figure 5.5) and the initial 25 s of the measurement were used. Background subtraction was made using the last 25 s. Based on preheat tests (Figure 5.6), a preheat temperature of 290°C was determined and subsequently applied for either 10 s or 60 s on both regenerative and test dose. No influence of preheat time on the measured D_E could be determined with exception for three samples (DR DR471_2, DR340_1 and DR483_2), where the deviation probably caused by bad statistics on the 60 second preheat D_E determination due to a low number of aliquots (Figure 5.7). As a consequence, ages in the text are given as averages between the two types of measurements as indicated by the column Age_{avg} in Table 5.2. Dose recovery tests all yielded a recovered dose within 10% of the given dose.

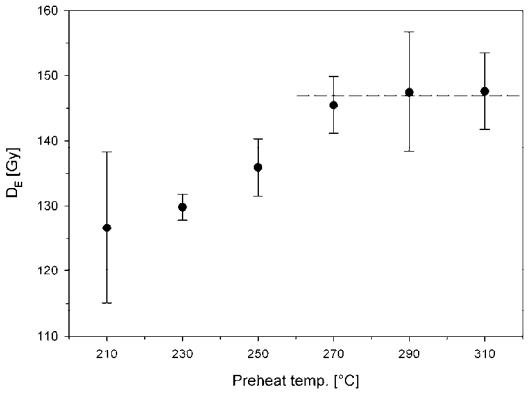

Figure 5.6 Plot of equivalent dose (D_E) versus preheat temperature showing a plateau from 270°C to 310°C for a three aliquot average of sample DR370_1.

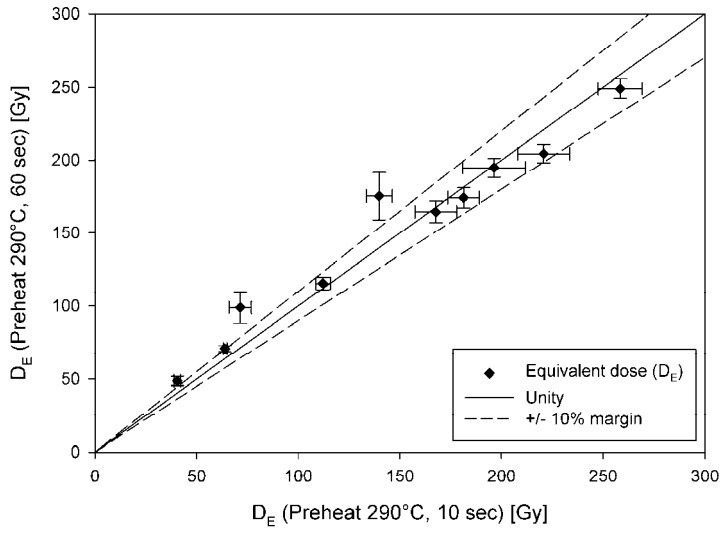

Figure 5.7 The comparison between D_E obtained after preheating at 290°C for 10 s and 60 s shows an overall good fit close to unity. The three outlying samples above the 10% discrepancy margin all have a low number of aliquots measured for the 60 s preheat (DR483_2, DR340_1 & DR471_2; see Table 5.1).

For the quartz samples, D_E determination resulted in uncontrollable scatter and irreproducible results. The shine

down curves reveal a notably slower decay and higher overall background compared to the signal from the Risø calibration quartz, a well behaving sample that is dominated by a fast component (Figure 5.8). As feldspar contamination can be excluded due to the chemical treatment of the quartz separates, these curves most likely indicate a relatively weak or absent fast component (see Steffen *et al.*, 2009). The reason for this adverse behaviour of quartz in our samples is not yet clear. In order to circumvent potential problems with these samples, priority was therefore given to the feldspar samples and all data presented in this paper is from feldspar-IRSL measurements.

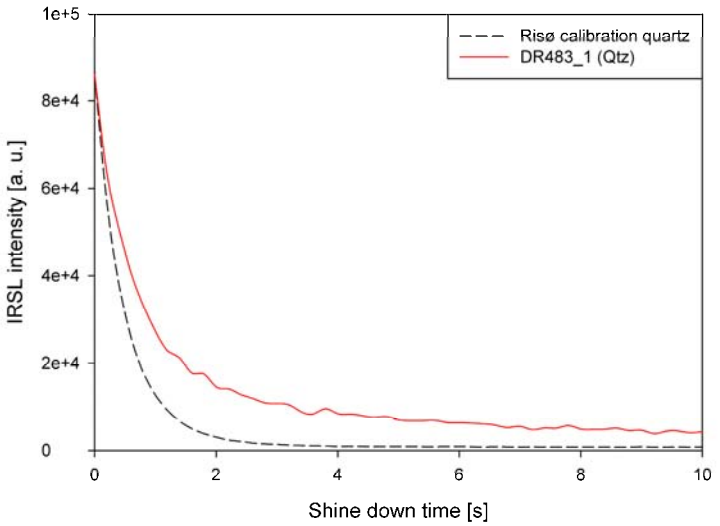

Figure 5.8 Comparison of the decay curves from two quartz samples. While the Risø calibration quartz shows "normal" signal decay behaviour and reaches background levels after a few seconds, sample DR483_1 (taken as representative of the entire sample suite) exhibits a much slower decay, suggesting that the fast component may not be the dominant signal contributor.

Dose rate determinations were made from U, Th and K contents measured using high resolution gamma spectrometry on material taken from the immediate surrounding of the luminescence samples. For samples taken from layers less than 30 cm thick, or samples taken from near the contact to another layer, the adjacent layers were sampled as well and their influence on dosimetry was taken into account using the infinite layer model built into the ADELE software (Kulig, 2005). This is particularly important due to the generally significant differences in radionuclide composition between the sampled material and e.g. underlying paleosoils and overlying basanitic tephra. Cosmic dose rates were calculated based on present day overburden. As this covering material consist entirely of low density volcanogenic tephra and its weathering products (paleosoils and modern soil), cosmic dose rate can contribute up to 12% of the total dose rate, particularly in samples with low overall dose rate. The overall low density of the cover material also leads to the cosmic dose rate being relatively insensitive to variations in overburden thickness.

5.5.4 DETERMINATION OF SAMPLE MOISTURE CONTENTS

Moisture content is one of the key parameters for accurate age determinations, as it significantly attenuates the environmental dose rate. While the moisture content of a material at the time of sampling can easily be determined gravimetrically, estimating a time integrated water content spanning the entire time range of the sample since its last

deposition can be difficult. As our samples were taken at the end of the dry season in a period of several weeks of no rainfall, we use the actually measured moisture content ($moist_{meas}$) as the minimal boundary condition (Table 5.1).

The gravimetrically compacted samples were then saturated with water and let to drip through a sieve for several hours in order to measure the retained capillary water content. This is not directly comparable to a true determination of the sample's field capacity (Israelson and West, 1922) and overestimates the water content due to factors like sample disturbance and shortened drainage time (normally 2-3 days). However, the obtained values of 36-47%$_{H_2O}$ for saturation content are in an acceptable range for sandy soils and the drained values of 23-29%$_{H_2O}$ are therefore taken as conservative maximum values for water content in the field under wet conditions. Furthermore, Randriantsoa (2001) reports water saturation levels dropping to 75% (relative to a near surface measurement) at depths larger than 10 cm for volcanic soils in the region of Betafo during the wet season. This was taken into account and the maximum moisture ($moist_{max}$) contents were calculated for each sample as *0.75 × drained water content*, giving the maximum boundary condition for the respective sample (Table 5.1). Pluviometric data given in Zebrowski and Ratsimbazafy (1979) for the meteorologic station in Antsirabe shows an averaged (over 25 years) annual rainfall of 1466 mm, around 87 % of which falls between Mid-October to Mid-April. It can clearly be distinguished between a six month dry period with average monthly rainfall of less than 22 mm and a six month wet period where monthly rainfalls are in excess of 300 mm. Similar results are given for the station in Betafo. Based on these numbers annually averaged water contents ($moist_{avg}$) were calculated as $(6 \times moist_{meas} + 6 \times moist_{max}) / 12$ and assigning an estimated ± 5% uncertainty (Table 5.1). These numbers were subsequently used in the age calculations.

5.5.5 DETERMINATION OF INTERNAL K CONTENT OF THE FELDSPAR SEPARATE

Each sample was analyzed on a Zeiss EVO 50 XVP scanning electron microscope using Energy Dispersive X-ray spectroscopy (EDX). K-feldspar grains were identified optically using a combination of backscattered electron (BSE) imaging and EDX element mapping of i.a. K, Na and Ca in order to distinguish them from e.g. plagioclase. Element mapping indicates that Na- and Ca-feldspars are only minor constituents relative to K-feldspar. Multiple EDX measurements were then taken on several K-feldspar grains per sample to determine the average internal K content in the K-feldspars of that sample (given as K_{Fsp} in Table 5.1). It is noted, that most of these values are lower than the value of 12.5 ± 0.5% suggested by Huntley and Baril (1997), which is often found in the literature as a surrogate value.

Table 5.1 *Summary data of IRSL dating for the entire suite of phreatic explosion horizon samples.*

Area		Sample	K_{Fsp} [a] [%]	K [%]	Th [ppm]	U [ppm]	$Moist_{meas.}$ [b] [%]	$Moist_{avg.}$ [c] [%]	Depth [m]	D_{Fsp} [d] [Gy ka^{-1}]
Lac Andraikiba	Upper	DR361_3	12.5 ± 0.6	0.84 ± 0.02	21.91 ± 0.26	7.13 ± 0.05	7.7	12.5 ± 2.5	0.50	4.51 ± 0.41
		DR471_2	9.5 ± 1.0	1.05 ± 0.02	20.53 ± 0.45	3.80 ± 0.06	7.6	13.5 ± 2.7	0.75	3.72 ± 0.43
		DR469	11.2 ± 1.0	1.00 ± 0.03	20.97 ± 0.80	4.20 ± 0.13	10.5	15.5 ± 3.1	0.85	3.80 ± 0.34
	Lower	DR488	9.0 ± 1.4	0.24 ± 0.01	4.54 ± 0.28	7.74 ± 0.08	18.7	20.2 ± 4.0	0.90	3.08 ± 0.28
		DR361_2	10.5 ± 0.8	0.23 ± 0.01	5.88 ± 0.24	4.77 ± 0.05	5.4	11.4 ± 2.3	0.71	2.70 ± 0.27
		DR361_1	11.4 ± 0.9	0.23 ± 0.01	4.63 ± 0.16	5.56 ± 0.03	18.7	20.0 ± 4.0	0.80	2.60 ± 0.21
		DR471_1	10.9 ± 1.6	0.22 ± 0.01	6.56 ± 0.23	1.54 ± 0.05	7.9	13.7 ± 2.7	2.10	1.94 ± 0.22
Ampasimi-kaiki		DR340_1	11.4 ± 1.3	0.41 ± 0.01	7.99 ± 0.19	0.96 ± 0.05	3.1	11.8 ± 2.4	0.20	1.79 ± 0.27
		DR340_2	11.6 ± 0.6	0.76 ± 0.02	6.04 ± 0.20	0.89 ± 0.04	9.2	14.8 ± 3.0	2.00	2.09 ± 0.16
Fizinana		DR370_2	11.3 ± 0.6	1.37 ± 0.03	7.79 ± 0.11	1.47 ± 0.03	4.6	14.8 ± 3.0	1.45	2.46 ± 0.19
		DR370_1	8.4 ± 0.5	1.73 ± 0.04	11.25 ± 0.19	2.37 ± 0.05	3.5	14.2 ± 2.8	2.10	3.08 ± 0.28
Lac Tritrivakely		DR483_2	11.8 ± 0.1	1.80 ± 0.04	4.20 ± 0.19	0.60 ± 0.02	8.5	14.1 ± 2.8	0.80	2.56 ± 0.22
		DR483_1	9.9 ± 1.1	2.10 ± 0.04	4.10 ± 0.11	0.50 ± 0.01	11.3	15.5 ± 3.1	2.30	2.63 ± 0.17

[a] Internal K concentration of the sample's K-feldspar grains.

[b] Gravimetrically measured moisture content of the sample at time of sampling (end of dry season)

[c] Average moisture content of the sample; used for age determinations. For calculation see text.

[d] Total dose rate used for age determinations; includes internal, environmental (including layers) and cosmic dose rate.

5.5.6 CORRECTIONS FOR ANOMALOUS FADING

It is a known phenomenon in luminescence dating that samples can underestimate their true ages due to continuous loss of signal over time, a process called anomalous fading (Wintle, 1973). It arises, because some of the trapped electrons in a sample are situated in traps that are unstable over geological timescales and will be lost before the sample is taken. The natural signal of the sample is therefore derived only from stable traps. The laboratory induced signal, however, will originate from both stable and unstable traps, due to the far shorter timescale involved, resulting in a higher signal yield from a laboratory dose than from a natural dose of the same intensity. This leads to the paleodose, and consequentially the sample's age, being underestimated. Various approaches to determine the rate of this signal loss, the g-value (Aitken, 1985), and calculate corrected ages have been proposed by Huntley and Lamothe (2001), Lamothe *et al.* (2003) Wallinga *et al.* (2007) and Kars *et al.* (2008).

In this study, fading corrected ages were calculated after Lamothe *et al.* (2003), based on fading rates determined after Rufer *et al.* (submitted b). Due to analytical problems, g-values could only be obtained for samples DR488 (5.6 ± 1.4%/decade), DR483_1 (7.4 ± 1.0%/decade), DR370_1 (5.3 ± 0.9%/decade) and DR469 (5.6 ± 1.1%/decade). An averaged g-value of 6.0 ± 0.5%/decade was therefore used for all samples. Table 5.2 lists both uncorrected and corrected ages, while in the text the fading corrected values are given.

5.6 SITES AND DATING RESULTS

Phreatic explosion layers were sampled in three main areas: Lac Andraikiba in the eastern part; Fizinana and Ampasimikaiki, to the south-east and north-east of Betafo, in the western part; and at Lac Tritrivakely in the northern part of the volcanic field (Figure 5.2, Table 5.3). The stratigraphic relations in each area will be discussed and combined with the obtained luminescence ages (Table 5.2).

5.6.1 LAC ANDRAIKIBA AREA

Lac Andraikiba, situated approximately 7 km due west of Antsirabe is a maar crater that is presently filled by a lake of roughly 1 km diameter (Figure 5.2, Figure 5.9). The lake is reported to be "of profound depth" (Sibree, 1891), but no bathymetric data is available. The crater is encircled by a ring of volcanoclastic deposits with an average height of 50 m and characterized by steep interior (~70°) and shallow external slopes (20-25°).

The largest part of the crater wall is made up of the maar explosion material, which forms a strongly heterogeneous deposit with a highly elevated contribution of crystalline basement material. It is unsorted and contains a wide range of component sizes, ranging from meter sized blocks down to a fine grained, sandy matrix material. Basement clasts include

Table 5.2 Equivalent doses (D_E) and luminescence ages. Values with indices 60 or 10 indicate measurements made with 60 s preheat or 10 s respectively. N is the number of aliquots measured. Age_{avg} is the average between Age_{60} and Age_{10} using error-propagation. Corrected ages base on Age_{avg}.

Area		Sample	$D_{E\,60}$ [Gy]	N_{60}	D_{E10} [Gy]	N_{10}	Age_{60} [ka]	Age_{10} [ka]	Age_{avg} [ka]	Corr. Age_{avg} [ka]
Lac Andraikiba	Upper	DR361_3	204.4 ± 6.3	22	220.7 ± 12.8	11	45.3 ± 3.2	48.9 ± 4.2	47.1 ± 2.6	63.9 ± 3.5
		DR471_2	175.3 ±16.1	8	139.8 ± 6.4	34	47.1 ± 5.2	37.6 ± 2.8	37.6 ± 2.8 [b]	50.7 ± 3.8
		DR469	174.1 ± 6.8	13	181.3 ± 7.8	12	45.9 ± 3.6	47.8 ± 3.8	46.8 ± 2.6	63.2 ± 3.5
	Lower	DR488	248.9 ± 6.7	19	258.3 ± 10.9	24	80.9 ± 6.4	84.0 ± 7.2	82.4 ± 4.8	113.9 ± 6.6
		DR361_2	194.7 ± 6.5	27	196.3 ± 15.4	10	72.1 ± 4.8	72.7 ± 7.1	72.4 ± 4.3	99.6 ± 5.9
		DR361_1	209.6 ± 7.5	28	n.a.	n.a.	80.5 ± 6.0	n.a.	80.5 ± 6.0 [a]	110.2 ± 8.2
		DR471_1	242.5 ± 8.9	25	n.a.	n.a.	125.2 ± 13.5	n.a.	125.2 ± 13.5 [a, c]	175.8 ± 19.0
Ampasimi-kaiki		DR340_1	98.9 ±10.7	3	71.4 ± 5.6	12	55.3 ± 7.3	39.9 ± 4.3	39.9 ± 4.3 [b]	54.0 ± 5.8
		DR340_2	115.6 ± 4.4	26	112.2 ± 3.6	20	55.7 ± 3.8	54.1 ± 3.5	54.9 ± 2.6	73.9 ± 3.5
Fizinana		DR370_2	159.1 ± 6.2	31	n.a.	n.a.	64.7 ± 4.3	n.a.	64.7 ± 4.3 [a]	89.0 ± 5.9
		DR370_1	164.5 ± 7.4	11	167.7 ± 10.3	12	53.3 ± 3.7	54.4 ± 4.4	53.8 ± 2.9	73.0 ± 3.9
Lac Tritrivakely		DR483_2	48.7 ± 3.1	3	40.5 ± 1.6	12	19.0 ± 1.5	15.8 ± 0.9	15.8 ± 0.9 [b]	20.7 ± 1.2
		DR483_1	70.9 ± 2.2	23	63.9 ± 0.9	24	26.9 ± 1.7	24.3 ± 1.4	25.6 ± 1.1	33.7 ± 1.4

[a] The only available age is given, not an average.

b The statistically arguable age (due to low n) is not considered in the average.

[c] For a discussion of this age, see 5.6.1.

primarily migmatites, quartzites, gneisses and micaschists. Part of these rocks show signs of calcination, which indicates elevated temperature gradients prior to the eruption (Mottet, 1980b). There is also a notable contribution of basaltic clasts, which originate from the explosive fragmentation of an older basaltic flow ("Vinaninkarena flow", Mottet, 1980b) overlying the basement at the time of the Andraikiba eruption. This lava flow outcrops discontinuously along the lake shore and is strongly weathered into a thick lateritic paleosoil of several meters thickness, directly underlying the phreatic explosion deposits. In some places, ejected basaltic blocks can be found impacted into the basalt-derived laterite. There is no indication of a juvenile magmatic fraction in the maar explosion deposits, indicating a purely phreatic eruption process. They are locally covered by black, basanitic to tephritic tephra, which Mottet (1980b) attributes to the Antsifotry cone east of Betafo (Figure 5.2).

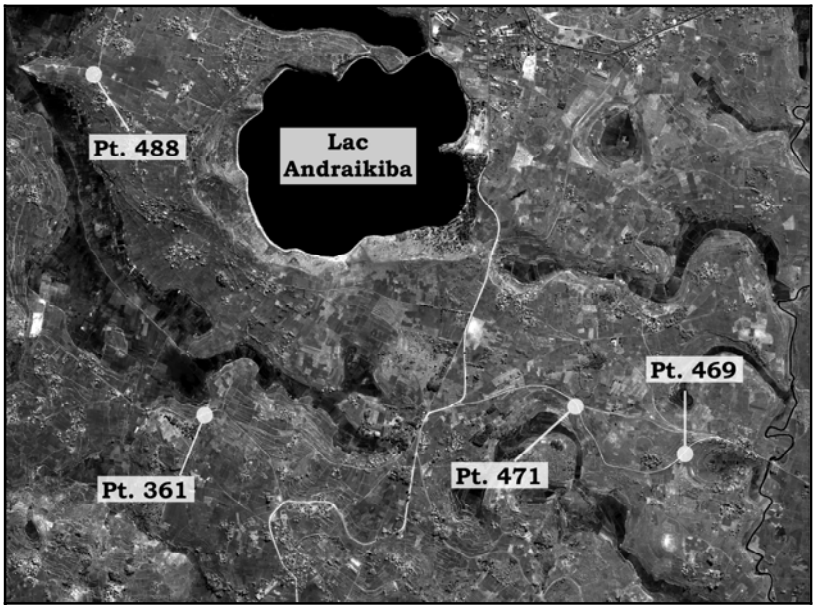

Figure 5.9 Locations of the sampled sections in the Lac Andraikiba area. The section profiles are given in Figure 5.10.

Tectonic activity posterior to the eruption caused a relative subsidence of the eastern part of the crater periphery along a NW-SE trending normal fault situated along the south-western lakeshore. Similarly oriented faults are observed in the entire eastern part of the volcanic field, where they can form steps in morphology. They are mainly recognized by sudden changes in altitude of the contact between the already mentioned Vinaninkarena basalt flow (which outcrops regularly in the south-eastern part of the volcanic field) and its overlying deposits.

We sampled four profiles within a 2 km radius of the crater (Figure 5.9). All sampled profiles feature the basal contact to the old basalt flow, succeeded by a series of two phreatic explosion layers and capped by the black lapilli which grade into the modern soil (Figure 5.10).

The lower phreatic explosion layer (samples DR488, DR361_1, DR361_2, DR469) generally consists of sandy material containing primarily a mineral assemblage representative for the overall granitoid basement composition (Nédélec *et al.*, 1995). Sorting and banking is generally poor or entirely absent. Towards the top of the layer, most outcrops show

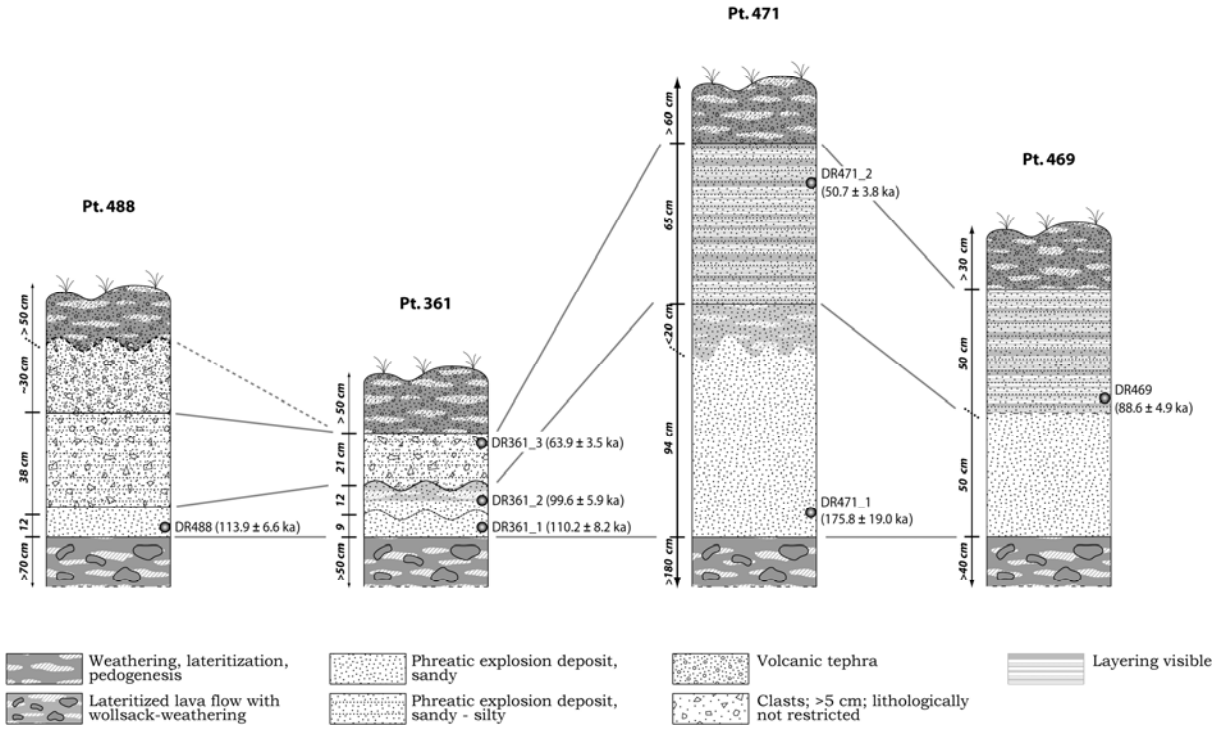

Figure 5.10 Stratigraphic sections in the Lac Andraikiba area. For profile locations, see Figure 5.3

increased weathering and beginning soil formation, facilitating the differentiation to the overlying upper explosion layer, which shows similar characteristics but has a slightly finer overall grain size (sandy to silty). In the southeastern outcrops (Pt. 471 and Pt. 469; samples DR471_2 and DR469) the upper layer is characterized by a clearly visible banking in the cm range and contains no rock fragments. Towards the northwestern outcrops (Pt. 361 and Pt. 488, sample DR361_3), the relative amount and size of lithic clasts (both basement and old basaltic material) increases up to 5 cm at Pt. 361 and up to 30 cm at Pt. 488, accompanied by a strong reduction in banking (Figure 5.10).

While the upper explosion layer can be traced to the Lac Andraikiba maar explosion, the geographical origin of the lower explosion layer is not clear. A possible candidate would be the Amboniloha volcanic complex, approximately 4 km to the north east (Figure 5.2). There, a phreatic explosion layer crops out along the flank of one of the older cones. Compositionally similar to the proximal Lac Andraikiba explosion deposits, it also exhibits a high fraction of large crystalline and old basalt blocks, suggesting a proximal deposit. This explosion layer is directly overlain by unsorted deposits of black tephra containing juvenile volcanic bombs and clasts of decimeter scale, with some of these blocks containing xenoliths of crystalline material identical to the underlying explosion horizon. It is assumed that these overlying volcanics originate from the nearby Amboniloha cones. This is corroborated by the fact that material from the explosive layer is not found on the surface of a late stage basanitic flow from this vent. Mottet (1980b), correlates this youngest Amboniloha tephra with an outcrop on the south eastern lake shore of Lac Andraikiba,

where ash and tephra layers underlie the phreatic explosion deposit. A similar ash and tephra sequence between the weathered old basalt flow and the overlying phreatic explosion deposits can be found in an isolated outcrop along the western lake shore (coordinates: 19° 52.329' E, 46°57.836' S), although it is not entirely clear whether these two outcrops are correlatable as the same units. Regardless, this would indicate the following relative chronological sequence in the Lac Andraikiba area: old, basaltic laterite; Amboniloha explosion deposits; Amboniloha tephra; Andraikiba explosion deposits; Antsifotry tephra.

Luminescence ages for the lower deposits lie between 113.9 ± 6.6 ka and 99.6 ± 5.9 ka for outcrops Pt. 488 and Pt. 361, while at outcrop Pt. 471 the age is 175.8 ± 19.5 ka (Table 5.2). The significance of this latter, significantly older age is unclear. While the sampled layer apparently lies in the same stratigraphic position as samples DR488 and DR361_1 it has a significantly different U/Th ratio. This, and the fact that there is no compelling reason to discard this age based on analytical problems, might indicate the presence of an older layer at this location. Further datings in this or immediately neighboring sections would be desirable to better constrain this problem. The upper layer gives ages between 63.9 ± 3.5 ka and 50.7 ± 3.8 ka for the Lac Andraikiba related maar deposits (Table 5.2).

Considered relatively, the obtained ages are in stratigraphic order and appear to be correlatable with individual stratigraphic units. The observed pedogenesis in the lower layer accords with the observed hiatus in the absolute ages between the lower and upper phreatic deposit.

5.6.2 LAC TRITRIVAKELY

This volcanic crater is situated approximately 9 km north-northeast of Betafo in a chain of several large strombolian cones along the eastward facing, N30°E oriented Sakontelo normal fault, which is the tectonic delimination of the granitic Vavato massif to the west and northwest (Figure 5.2). It contains an intermittent lake of approximately 300 m diameter and has a sedimentary infill consisting of at least 40 m depth (which is the length of the core taken by Gasse and Van Campo (2001)). Reported sediment thickness values vary between 50 m (Sifeddine *et al.*, 1995) and 90 m (Gasse and Van Campo, 2001), however no measurement method is mentioned, and Rakoto *et al.* (1997) calculated a poorly constrained maximum thickness of 39 m based on geoelectrics. With exception of the south-eastern side, the crater is encircled by a 50-80 m high basaltic tuff ring which contains blocks of migmatitic basement material, identical to the Vavato migmatites in the region (Mottet, 1980b). While there is no identifiable phreatic explosion deposit that could be linked to Tritrivakely itself, two phreatic explosion layers outcropping in several locations along the inner part of the southern rim were identified. Both layers are of predominantly sandy grain size and consist primarily of quartz, feldspar and partially oxidized, reddish mica, although rare basaltic clasts (<5 mm) can be found. The upper layer has a thickness of approximately

60 cm and exhibits banking on a cm scale, while the lower layer is more massive and exceeds 1 m in thickness. Due to their position inside the crater rim, coupled with their small, homogeneous grain size and absence of any larger clasts, they are interpreted as being of external – albeit as yet unknown - origin.

The obtained luminescence ages, give an age of 33.7 ± 1.4 ka for the lower and 20.7 ± 1.2 ka for the upper explosion deposit (Table 5.2). On the steeper parts of the volcanic rampart, no clearly identifiable remains of these explosion deposits can be found, which is most likely a consequence of an efficient erosion of the only lightly consolidated deposit. Due to this and the fact that the phreatic deposit blanketed the entire crater, a sand layer should also be evident in the crater infill sediments, both from the primary sedimentation event as well as due to later reworking of such material from the rampart.

The stratigraphic record from the drillcore shows a sandy section between 4.5 and 3 m depth overlain only by peat deposits (Gasse and Van Campo, 2001), which we interpret to be a possible equivalent to the sampled horizons. This layer is reported to show a partition between a lower part consisting of sand with intercalated clay and an upper, purely sandy part. This would coincide with our identification of two separate deposits. ^{14}C ages on Cyperaceae throughout the entire height of the sandy layer give ages between 19.2 ± 0.2 and 6.3 ± 0.1 cal. kyr B.P. (Gasse and Van Campo, 2001). This spans an almost identical amount of time between the lowest and highest ^{14}C age (12.9 ka) as between the lower and the upper phreatic deposit (13 ka). In terms of chronological position, however, there is no overlap, as the ^{14}C age range follows immediately after the luminescence age range. While erosion and resedimentation of the circumjacent phreatic deposits into the lake may account for a smearing out of the lower age boundary in the drillcore, the upper age limit should be similar due to the contemporaneous initial deposition on the surrounding area as well as into the crater lake. Despite this misfit, the rather close chronological proximity of the luminescence ages to the ^{14}C ages is encouraging.

5.6.3 FIZINANA AND AMPASIMIKAIKI AREAS

Similar to the volcanoes around Lac Tritrivakely in terms of their morphologically older appearance, the twin cones of Ampasimikaiki, due east of Betafo, lie in the south-western continuation of the Sakontelo fault trace (Figure 5.2). They are amongst the oldest edifices in the region of the Betafo basin, which is a tectonic subsidence basin situated at the intersection between the Sakontelo fault (normal fault to the east) and the Betafo fault, which is a northward dipping normal fault striking roughly WNW-ESE (Mottet, 1980b). Further volcanic complexes bordering this basin are the younger cones of the Iavoko complex and the stratigraphically youngest Antsifotry cone and its associated flow, all to the south-east of Ampasimikaiki. Along the eastern extension of the Betafo fault lies the extensive Fizinana volcanic complex, which is dominated by the two large Fizinana cones,

the younger of which is presumably comparable in age to Iavoko (Mottet, 1980b). The Fizinana area also features quite a large number of smaller cones, ranging from morphologically far older cones to small secondary vents seemingly contemporaneous to the main Fizinana cones. Both the Iavoko and the Fizinana complex sourced large basanitic flows which infill large parts of the Betafo basin (Figure 5.2).

As such, the Betafo area provides an important volcanostratigraphic record linking the older volcanic events along the Sakontelo area with the younger strombolian activity along the edges of the Betafo basin, followed by the volumetrically important effusive features, up to the latest strombolian and terminally effusive volcanic activity of the Antsifotry.

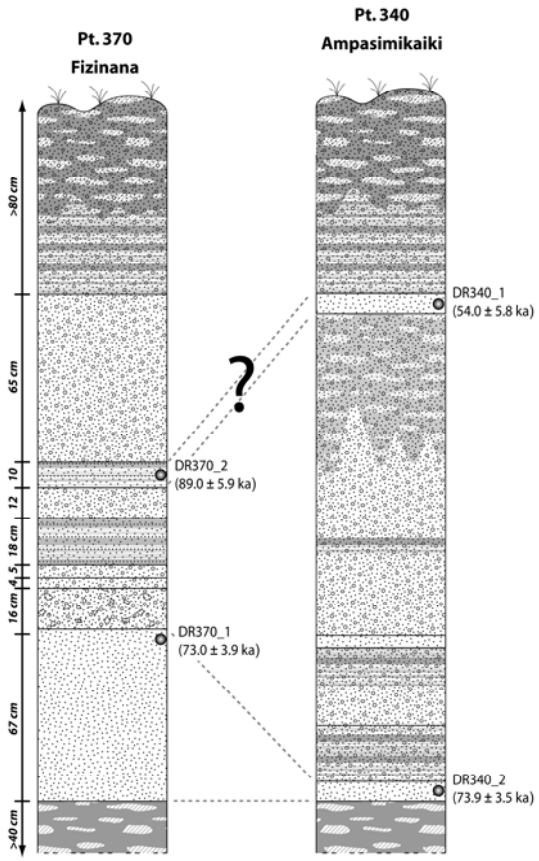

Figure 5.11 Stratigraphic section of the Fizinana and Ampasimikaiki outcrops (Figure 5.2). The section of Pt. 340 is not to scale, but the sampled phreatic explosion layers are 2-5 cm (DR340_2) and 5-10 cm thick (DR340_1). Units identical to Figure 5.10.

Two phreatic explosion deposits are found in most stratigraphically appropriate outcrops both near the Ampasimikaiki and the Fizinana cones and were sampled at Pt. 340 and Pt. 370 respectively (Figure 5.2 & Figure 5.11). Being anterior to the large flows in the Betafo basin, however, these layers could not be continuously traced between the two areas. Both to the south as well as to the north, the stratigraphically lower deposit directly overlies an old laterite with a thickness of at least several meters. This is indicative that the phreatic deposits in both cases were deposited after a prolonged phase with no volcanic sedimentation in their respective vicinity, which might hint at a stratigraphic link.

At the Fizinana section (Pt. 370) this lower deposit (sample DR370_1) is overlain by a series of tephra sequences, the lowermost of which contains small basement clasts. The source of these deposits is not yet clear, but is at the moment tentatively linked to the older cone immediately north of the Fizinana main cones, based on an increase in thickness of these tephra layers, as well as an increase in relative amount and size of the crystalline clasts towards the cone. These tephra layers are followed by a second, finely layered explosion horizon which locally appears to show signs of pedogenesis. This layer has, however, only been identified in two other, nearby outcrops and its extent or stratigraphic role is unclear. Following a sequence of dark lapillis, the upper explosion horizon is the stratigraphically

highest explosion horizon in the Fizinana area (sample DR370_2). It is capped by tephra deposits originating from the younger of the main Fizinana cones and possibly also from Antsifotry (Mottet, 1980b).

At the Ampasimikaiki section (Pt. 340), the lower explosion layer (sample DR340_2) consists of a layered sandy deposit, consisting primarily of quartz, feldspar, mica, pyroxene and hornblende. It also contains a small fraction of volcanic material in the form of volcanic ash particles of less than 2 mm grain size. The explosion deposit is followed by a series of tephra and volcanic ash layers, none of which contain basement clasts or volcanic bombs. The mostly unsorted tephra layers show a predominant grain size between 0.5 and 3 cm and the entire sequence grades up into a brownish paleosoil of variable thickness. This sequence originates from the Ampasimikaiki cones, as it can be traced upslope with increasing thickness and grainsize. Overlying the paleosoil is the upper explosion deposit (sample DR340_1) of similar composition and characteristics as the lower explosion layer, which is in turn capped by another sequence of dark tephra, interspersed with layers of finer, volcanic ash, grading up into the modern soil. It can be assumed that these uppermost tephra layers originate from Iavoko and Antsifotry, the latter being mentioned by Mottet (1980b).

The origin of the explosion layers is not clear. The generally elevated thickness between 25 and 67 cm of the lower deposit found in the Fizinana outcrops may indicate a more proximal setting compared to the only 2-5 cm thick layer in the Ampasimikaiki area, but a potential source has not yet been identified. The upper deposit has a similar thickness of 5-10 cm in both areas. It is therefore possible that the source might be farther away.

Luminescence ages for the lower deposit are almost identical for both areas: 73.9 ± 3.5 ka for Ampasimikaiki and 73.0 ± 3.9 ka for Fizinana. The matching ages in combination with the fact that the lower layer forms the lowermost unit directly on an older laterite strongly suggests that this layer forms a stratigraphic link between the northern and the southern part of the Betafo basin.

In the Ampasimikaiki section, the upper layer yields an age of 54.0 ± 5.8 ka, which is in stratigraphic order and accommodates for the existing paleosoil between the two explosion deposits. While this is similar to the ages from the upper Andraikiba unit, it would probably be presumptuous to make a correlation based on this single sample. In the Fizinana section, the obtained age is 89.0 ± 5.9 ka.

Table 5.3 Coordinates of the sampled sections and samples.

Section	Samples	Coordinates [WGS 1984 UTM, Zone 38S]	Elevation [m.a.s.l.]
Pt. 340	DR340_1 DR340_2	19° 49.793' S, 46° 52.578' E	1540
Pt. 361	DR361_1 DR361_2 DR361_3	19° 53.161' S, 46° 57.718' E	1560
Pt. 370	DR370_1 DR370_2	19° 53.251' S, 46° 52.727' E	1600
Pt. 469	DR469	19° 53.249' S, 46° 59.159' E	1511
Pt. 471	DR471_1 DR471_2	19° 53.074' S, 46° 58.860' E	1539
Pt. 483	DR483_1 DR483_2	19° 46.796' S, 46° 55.201' E	1800
Pt. 488	DR488	19° 52.195' S, 46° 57.382' E	1552

5.7 CONCLUSIONS

This study provides the first direct ages of phreatic explosion deposits and demonstrates the cardinal applicability of feldspar IRSL dating in this context. The study also provides a set of twelve ages for at least three phreatic explosion deposits as well as for the Lac Andraikiba maar explosion. These are the only direct ages for the Quaternary volcanism in the Vakinankaratra volcanic field and apart from the chronostratigraphic record of the Lac Tritrivakely drillcore the only numerical ages for this volcanic field so far.

The obtained ages are (with one exception) in stratigraphic order and stratigraphically correlatable layers show matching ages. This relative conformance clearly indicates that the method works, but also, that additional, independent ages are required, with the goal to calibrate the results of this method with other chronostratigraphies. So far, comparing the luminescence ages with the ^{14}C ages from the Tritrivakely drillcore does not result in a fit, but the close chronological proximity of the two age ranges is encouraging.

Our study shows that the phreatic eruptions in the Antsirabe-Betafo region, and therefore the onset of the eruptive activity in this young volcanic field started in the Late Pleistocene. The age of the Lac Andraikiba maar explosion could be constricted to lie between 50.7 ka and 63.9 ka, and an older phreatic eruption deposit in the same area was similarly dated to lie between 99.6 ka and 113.9 ka. In the area of the Betafo basin, a phreatic explosion layer underlying the volcanic deposits of the young strombolian cones was dated to lie at approximately 73 ka. At Lac Tritrivakely, two allochthonous phreatic deposit yielded ages between 33.7 ka and 20.7 ka.

These ages provide an upper age limit to the subsequently developed strombolian cones and associated young lava flows. Field indications like the extraordinary low grade of weathering on these young volcanic edifices indicate ongoing activity probably up into the Holocene. Further age determinations on the latest volcanic manifestations like the Antsifotry lava flow (e.g. using embedded xenoliths as suggested by Rufer *et al.* (submitted a)) would allow bracketing the young volcanic history of the Vakinankaratra volcanic field.

ACKNOWLEDGEMENTS

Dr. Sönke Szidat is thanked for the high-resolution gamma spectrometry measurements and Dr. Marco Herweg is acknowledged for the introduction into using the SEM. M. Suchy, J. Giese, I. Schindelwig, S. E. Lowick and D. Steffen are gratefully thanked for helpful discussions and comments. This work was funded by by the Swiss National Science Foundation (SNSF), Project No's 200020-105453/1, 200020-118023/1 and 206021-117374.

5.8 REFERENCES

AITKEN, M.J. (1985): Thermoluminescence Dating. *ACADEMIC PRESS, LONDON*

ALSAC, C. (1963): Contribution a l'étude du volcanisme du sud-ouest de l'Ankaratra a Madagascar. *COMPTES RENDUS DE LA SEMAINE GÉOLOGIQUE DE MADAGASCAR:* 125-128.

BARDINTZEFF, J.M., BONIN, B., LIEGEOIS, J-P., BELLON, H. & RASAMIMANANA, G. (2001): Madagascar volcanic provinces: isotopic evidence. *EUROPEAN UNION OF GEOSCIENCES XI,* 8-12. April, Strasbourg, France.

BARDINTZEFF, J.M., LIEGEOIS, J-P., BONIN, B., BELLON, H. & RASAMIMANANA, G. (2002): Les sources mantelliques sous Madagascar. *19. RÉUNION SCIENCES DE TERRE,* Nantes, France.

BERTIL, D. & REGNOULT, J.M. (1998): Seismotectonics of Madagascar. *TECTONOPHYSICS* 294 (1-2): 57-74.

BRENON, P. & BUSSIERE, P. (1959): Le volcanisme à Madagascar. *BULLETIN VOLCANOLOGIQUE* 21: 77-93.

BUSSIERE, P. (1957): Le massif volcanique de l'Ankaratra. *TRAVAUX DU BUREAU GÉOLOGIQUE* 83: 118-126.

DE WIT, M.J. (2003): Madagascar: Heads it's a continent, tails it's an island. *ANNUAL REVIEW OF EARTH AND PLANETARY SCIENCES* 31: 213-248.

DULLER, G.A.T. (1992): Luminescence chronology of raised marine terraces, south-west North Island, New Zealand. *UNPUBLISHED PH.D. THESIS*, University of Wales, Aberystwyth

FATTAHI, M. & STOKES, S. (2003): Dating volcanic and related sediments by luminescence methods: a review. *EARTH-SCIENCE REVIEWS* 62 (3-4): 229-264.

FAURE, G. (1986): Principles of isotope geology : 2nd edition. *JOHN WILEY & SONS*, New York

GASSE, F., CORTIJO, E., DISNAR, J.R., FERRY, L., GIBERT, E., KISSEL, C., LAGGOUNDEFARGE, F., LALLIERVERGES, E., MISKOVSKY, J.C., RATSIMBAZAFY, B., RANAIVO, F., ROBISON, L., TUCHOLKA, P., SAOS, J.L., SIFFEDINE, A., TAIEB, M., VAN CAMPO, E. & WILLIAMSON, D. (1994): A 36-Ka Environmental Record in the Southern Tropics - Lake Tritrivakely (Madagascar). *COMPTES RENDUS DE L'ACADEMIE DES SCIENCES - SERIE II* 318 (11): 1513-1519.

GASSE, F. & VAN CAMPO, E. (2001): Late Quaternary environmental changes from a pollen and diatom record in the southern tropics (Lake Tritrivakely, Madagascar). *PALAEOGEOGRAPHY PALAEOCLIMATOLOGY PALAEOECOLOGY*, 167 (3-4): 287-308.

HUNTLEY, D.J. & BARIL, M.R. (1997): The K content of the K-feldspars beeing measured in optical dating or in thermoluminescence dating. *ANCIENT TL* 15 (1): 11-14.

HUNTLEY, D.J. & LAMOTHE, M. (2001): Ubiquity of anomalous fading in K-feldspars and the measurement and correction for it in optical dating. *CANADIAN JOURNAL OF EARTH SCIENCES* 38 (7): 1093-1106.

ISRAELSON, O.W. & WEST, F.L. (1922): Water holding capacity of irrigated soils. *UTAH STATE AGRICULTURAL EXPERIMENT STATION BULLETIN* 183: 1–24.

JOUZEL, J., BARKOV, N.I., BARNOLA, J.M., BENDER, M., CHAPPELLAZ, J., GENTHON, C., KOTLYAKOV, V.M., LIPENKOV, V., LORIUS, C., PETIT, J.R., RAYNAUD, D., RAISBECK, G., RITZ, C., SOWERS, T., STIEVENARD, M., YIOU, F. & YIOU, P. (1993). Extending the Vostok Ice-Core Record of Paleoclimate to the Penultimate Glacial Period. *NATURE* 364 (6436): 407-412.

KARS, R.H., WALLINGA, J. & COHEN, K.M. (2008): A new approach towards anomalous fading correction for feldspar IRSL dating -- tests on samples in field saturation. *RADIATION MEASUREMENTS* 43 (2-6): 786-790.

KULIG, G. (2005): Erstellung einer Auswertesoftware zur Alterbestimmung mittels Lumineszensverfahren unter spezieller Berücksichtigung des Einflusses radioaktiver Ungleichgewichte in der 238U-Zerfallsreihe. *UNPUBLISHED BSC-THESIS*, Technical University Bergakademie Freiberg, Freiberg

KUSKY, T.M., TORAMAN, E. & RAHARIMAHEFA, T. (2007): The Great Rift Valley of Madagascar: An extension of the Africa-Somali diffusive plate boundary? *GONDWANA RESEARCH* 11 (4): 577-579.

LACROIX, A. (1912): Les volcans du centre de Madagascar: Le massif de L'Itasy. *SÉANCE DE L'ACADÉMIE FRANCAISE DU 5. FÉVRIER*.

LACROIX, A. (1921-1923): La Minéralogie de Madagascar. Paris

LAMOTHE, M., AUCLAIR, M., HAMZAOUI, C. & HUOT, S. (2003): Towards a prediction of long-term anomalous fading of feldspar IRSL. *RADIATION MEASUREMENTS* 37 (4-5): 493-498.

MACDONALD, G.A. (1972): Volcanoes. Prentice-Hall, Englewood Cliffs, N.J.

MEJDAHL, V. (1985): Thermoluminescence dating of partially bleached sediments. *NUCLEAR TRACKS AND RADIATION MEASUREMENTS (1982)*, 10 (4-6): 711-715.

MOTTET, G. (1980a): L'Ankaratra et ses bordures (Madagascar): recherches de géomorphologie volcanique. - Tome I, le Massif de l'Ankaratra. *PHD-THESIS*, Université de Lyon, Lyon

MOTTET, G. (1980b): L'Ankaratra et ses bordures (Madagascar): recherches de géomorphologie volcanique. - Tome II, les bordures et le volcanisme quaternaire : le

volcanisme du massif des Vavavato, le Vakinankaratra, le massif de l'Itasy. *PHD-THESIS*, Université de Lyon, Lyon

MOUGENOT, D., RECQ, M., VIRLOGEUX, P. & LEPVRIER, C. (1986): Seaward extension of the East African Rift. *NATURE* 321 (5): 599-603.

NÉDÉLEC, A., STEPHENS, W.E. & FALLICK, A.E. (1995): The Panafrican Stratoid Granites of Madagascar: Alkaline Magmatism in a Post-Collisional Extensional Setting. *JOURNAL OF PETROLOGY* 36 (5): 1367-1391.

PETIT, M. (1998): Présentation physique de la grande île Madagascar. FTM - *INSTITUT GÉOGRAPHIQUE ET HYDROGRAPHIQUE NATIONAL*, Antananarivo

PIQUÉ, A., LAVILLE, E., CHOTIN, P., CHOROWICZ, J., RAKOTONDRAOMPIANA, S. & THOUIN, C. (1999): Neogene and present extension in Madagascar: structural and geophysical data. *JOURNAL OF AFRICAN EARTH SCIENCES* 28 (4): 975-983.

PREUSSER, F. (1999): Lumineszenzdatierungen fluviatiler Sedimente - Fallbeispiele aus der Schweiz und Norddeutschland. *KÖLNER FORUM FÜR GEOLOGIE UND PALÄONTOLOGIE* 3: 63.

PREUSSER, F., DEGERING, D., FUCHS, M., HILGERS, A., KADEREIT, A., KLASEN, N., KRBETSCHEK, M., RICHTER, D. & SPENCER, J.Q.G. (2008): Luminescence dating: basics, methods and applications. *E & G QUARTERNARY SCIENCE JOURNAL* 57 (1/2): 95-149.

RANDRIANTSOA, M.M. (2001): Rôle de la matière organique dans la fertilité phosphorique d'un sol ferrallitique des Hautes Terres malgaches. *DEA DE L'INSTITUT NATIONAL POLYTECHNIQUE DE LORRAINE*. CIRAD-TAFA, 26p.

RAKOTO, H., RANAIVO-NOMENJANAHARY, F., RATSIMBAZAFY, J.B., ALBOUY, Y., JEAN-JACQUES, S. & MICHEL, M. (1997): Réinterprétation par inversion bayésienne des sondages électriques sur le lac Tritrivakely (Madagascar). *COLLOQUE GEOFCAN, GÉOPHYSIQUE DES SOLS ET DES FORMATIONS SUPERFICIELLES.*

RAKOTONDRAOMPIANA, S.A., ALBOUY, Y. & PIQUÉ, A. (1999): Lithospheric model of the Madagascar island [western Indian ocean]: a new interpretation of the gravity data. *JOURNAL OF AFRICAN EARTH SCIENCES* 28 (4): 961-973.

RATSIMBAZAFY, J.B. & RAKOTO, H. (1997): Mesures d'aimantation et de datation de quelques échantillons de roches dans la région volcanique de l'Itasy. *ACTES DES JOURNÉES SCIENTIFIQUES RIFTING MALGACHE:* 112-122.

RUFER, D., PREUSSER, F., GNOS, E. & SCHREURS, G. (submitted a): New approaches for dating young volcanic eruptions by luminescence methods. *SUBMITTED TO GEOCHRONOMETRIA*.

RUFER, D., LOWICK, S.E., PREUSSER, F. & TRAUERSTEIN, M. (submitted b): Variable fading rates in K-feldspar caused by different IRSL components and implications for g-value determination. *SUBMITTED TO RADIATION MEASUREMENTS*.

SIBREE, R.J. (1891): The volcanic lake of Tritriva, Central Madagascar. *PROCEEDINGS OF THE ROYAL GEOGRAPHIC SOCIETY AND MONTHLY RECORD OF GEOGRAPHY, NEW MONTHLY SERIES* 13 (8): 477-483.

SIFEDDINE, A., LAGGOUNDEFARGE, F., LALLIERVERGES, E., DISNAR, J.R., WILLIAMSON, D., GASSE, F. & GIBERT, E. (1995): Lacustrine Organic Sedimentation in the Southern Tropical Zone in the Last 36000 Years (Lake Tritrivakely, Madagascar). *COMPTES RENDUS DE L'ACADEMIE DES SCIENCES - SERIE II - FASCICULE A - SCIENCES DE LA TERRE ET DES PLANETES* 321 (5): 385-391.

STEFFEN, D., PREUSSER, F. & SCHLUNEGGER, F. (2009): OSL quartz age underestimation due to unstable signal components. *QUATERNARY GEOCHRONOLOGY* 4 (5): 353-362.

WALLINGA, J., MURRAY, A. & WINTLE, A. (2000): The single-aliquot regenerative-dose (SAR) protocol applied to coarse-grain feldspar. *RADIATION MEASUREMENTS* 32 (5-6): 529-533.

WALLINGA, J., BOS, A.J.J., DORENBOS, P., MURRAY, A.S. & SCHOKKER, J. (2007): A test case for anomalous fading correction in IRSL dating. *QUATERNARY GEOCHRONOLOGY* 2 (1-4): 216-221.

WILLIAMSON, D., JELINOWSKA, A., KISSEL, C., TUCHOLKA, P., GIBERT, E., GASSE, F., MASSAULT, M., TAIEB, M., VAN CAMPO, E. & WIECKOWSKI, K. (1998): Mineral-magnetic proxies of erosion/oxidation cycles in tropical maar-lake sediments (Lake Tritrivakely, Madagascar): paleoenvironmental implications. *EARTH AND PLANETARY SCIENCE LETTERS* 155 (3-4): 205-219.

WINTLE, A.G. (1973): Anomalous Fading of Thermoluminescence in Mineral Samples. *NATURE* 245 (5421): 143-144.

WOOLLEY, A.R. (2001): Alkaline Rocks and Carbonatites Of The World, Part 3: Africa. *THE GEOLOGICAL SOCIETY PUBLISHING HOUSE*, Bath, U.K.

ZEBROWSKI, C. & RATSIMBAZAFY, C. (1979): Carte Pédologique de Madagascar à 1/100.000 - Notice explicative No. 83.

CHAPTER 6

Conclusions

"Life is the art of drawing sufficient conclusions from insufficient premises."

Samuel Butler (1835 - 1902), Novelist

CONCLUSIONS

The present work is an explorative study in applications of luminescence dating techniques to Quaternary volcanic eruptions. It discusses crystalline xenoliths as a potential target material for dating young lava flows, and introduces imaging plate autoradiography to the field of luminescence dating as a tool for microdosimetry assessment.
More importantly, it successfully demonstrates the applicability of luminescence dating to phreatic explosion layers and presents the first recorded direct ages of such volcanic deposits. These are also the first and only direct ages for the Late Quaternary volcanism in the Vakinankaratra volcanic field in central Madagascar.
This illustrates the huge potential of this new method for volcanology and geochronology, as it enables direct numerical dating of a type of volcanic deposit which has not been successfully directly dated by any other method so far.

Investigations into new fields and methods always lead to new questions, and over the course of this work, a number of open problems and venues for further research were identified.

While luminescence dating of phreatic explosion deposits was successful for feldspar IRSL, it has also disclosed that quartz from the same samples show an adverse behaviour for OSL dating. This raises the question whether or not this phenomenon is related to crystallographic material changes in the quartz crystal due to the intense mechanical stress during fragmentation. Is it a ubiquitous phenomenon in shocked quartz, and at what levels of shock does it occur, if it is not a gradual process? A systematic study, probably including both experimental shock experiments as well as comparative studies with other naturally shocked quartz samples, could provide important new insight into the behaviour of this important dosimeter under such conditions.

Although imaging plate autoradiography could be introduced as a an expedient screening tool for qualitative assessment of potential microdosimetry in a sample, its quantitative application is currently still relying on using calibration materials with broadly similar relative radionuclide concentrations as the samples. This restriction would most likely fall away if a calibration could be obtained between signal value and radiation energy, unlike the current calibration, which is between signal value and sample activity. This could be achieved by using calibration series of mono-nuclidic emitters, in which case the resulting signal values could be directly correlated to both activity and emitted energy. Such a

calibration would then allow the determination of spatially resolved D_Es or the quantification of a microdosimetry related D_E overdispersion.

The resetting potential of crystalline xenoliths in lava flows has been demonstrated, and a screening method to allow focussing on microdosimetrically unproblematic samples is at hand. The next will be to apply luminescence dating to xenoliths sampled from known-age lava flows in order to refine the methodological aspects, with the goal that the technique can – at a later stage – be confidently applied to samples of unknown age.

The obtained ages for the phreatic explosion deposits from the Vakinankaratra field are an important first step, but further research is clearly required in order to establish a comprehensive chronology of the young volcanic history of this area. Future work should be directed towards improving stratigraphic correlations over the entire volcanic field, in order to gain a more reliable stratigraphic control on numerical ages of the phreatic deposits. Additionally, efforts to date the late stage lava flows would result in complementary ages to the phreatic explosion deposits, providing an age bracket for the volcanic activity in the Vakinankaratra field. Potential methods would include terrestrial cosmogenic nuclides on the lava itself, luminescence dating of fluviatile sediments overflown by lava flows, or – as a future prospect – luminescence dating of embedded xenoliths.

Last but not least, luminescence dating of phreatic explosion deposits must be applied to a wide range of eruptions of different geological settings and known age in order to thoroughly test the method, so that it can be improved further and hopefully become a useful standard technique in the field of volcanic geochronology.

APPENDIX A

Conference contributions

"Science is facts; just as houses are made of stones, so is science made of facts; but a pile of stones is not a house and a collection of facts is not necessarily science."

Jules Henri Poincaré (1854 - 1912), Mathematician and Physicist

CENOZOIC ALKALINE VOLCANISM IN CENTRAL MADAGASCAR IN THE CONTEXT OF INTRACONTINENTAL RIFTING

Rufer Daniel, Schreurs Guido, Berger Alfons, Gnos Edwin & Villa Igor
Insitute of Geological Sciences, University of Berne, Switzerland

The youngest plate reorganization in the Indian Ocean started ~34 Ma ago with the opening of the Red Sea and the formation of the East African Rift, and since the mid Miocene, Madagascar has come under an extensional tectonic regime (Bertil & Regnoult, 1998). Multiple indications for this east-west extension can be observed on the central highlands of the island: a high seismic activity with normal fault focal mechanisms and distribution preferentially along pre-existing tectonic trends (Bertil & Regnoult, 1998); gravimetric and seismic data indicating a thinned crust and lithosphere, related to asthenospheric upwelling (Rakotondraompiana et al. 1999); extensional structures (e.g. grabens and basins, Piqué et al. 1999) as well as extensive Tertiary to Quaternary volcanism. Such young volcanic fields can be found in the central highlands (Lac Itasy and Ankaratra) as well as in the north of the island (Nosy Be, Massif d'Ambre and Tsaratanana).

The focus of our study lies on the volcanic province of the central highlands (Figure 1) with the goal of better understanding the younger tectonic history of central Madagascar and to gain insight into the early stages of intracontinental rifting. A detailed petrological and geochemical study of the alkaline volcanic rock sequence of these young fields should yield information about its source, magmatic processes and mantle evolution in a region where asthenospheric upwelling under an old continental lithosphere takes place. Dating of the volcanic deposits will allow to establish a temporal framework for these processes, permitting us to link the volcanic activity with the young tectonic history.

Existing age data suggest two main volcanic episodes in the upper Miocene (11-9 Ma) and the Quaternary - both of which seem to correlate between the volcanic provinces of the central highlands and the north of the island. The age record for the central highlands is still especially sparse and it is unclear whether we deal with a continuous volcanic activity or discrete stages. The larger Ankaratra field (Figure 1) can be subdivided into an assumed Neogene part, consisting mainly of basaltic and phonolitic flows and tuffs and less abundant trachytic plugs, and a Quaternary part, which includes mainly basanitic and tephritic flows and tuffs with a noted absence of trachytic material. The smaller Lac Itasy field (Figure 1) is dominated by basanitic to tephritic material that forms small flows and tuff cones, larger phonolitic flows and trachytic domes. This field is of as yet unknown age, but probably not older than Quaternary.

First geochemical data show an alkaline volcanism of peraluminous type for both regions. The Quaternary Lac Itasy field yields comparable patterns to the Neogene part of Ankaratra with decreasing Cr, Ni, MgO and TiO_2 contents and increasing Al_2O_3 and incompatible elements vs. SiO_2 concentration. This is indicative of fractionation of Cpx, Fsp and Ti-magnetites. In comparison, the Quaternary Ankaratra rocks show different patterns in comparison with the neighbouring Neogene Ankaratra volcanic rocks as well as the Quaternary Lac Itasy volcanics, pointing to an influence by primitive material and an

increasing degree of melt production. This is reflected by higher Ni and Cr concentrations as well as increasing CaO/TiO_2 and decreasing Al_2O_3 vs. SiO_2.

While the reasons for the chemical differences between the contemporaneous Lac Itasy and the Quaternary parts of the Ankaratra region remains to be investigated, these findings could corroborate the geophysical indications of an asthenospheric upwelling under the central highlands of Madagascar.

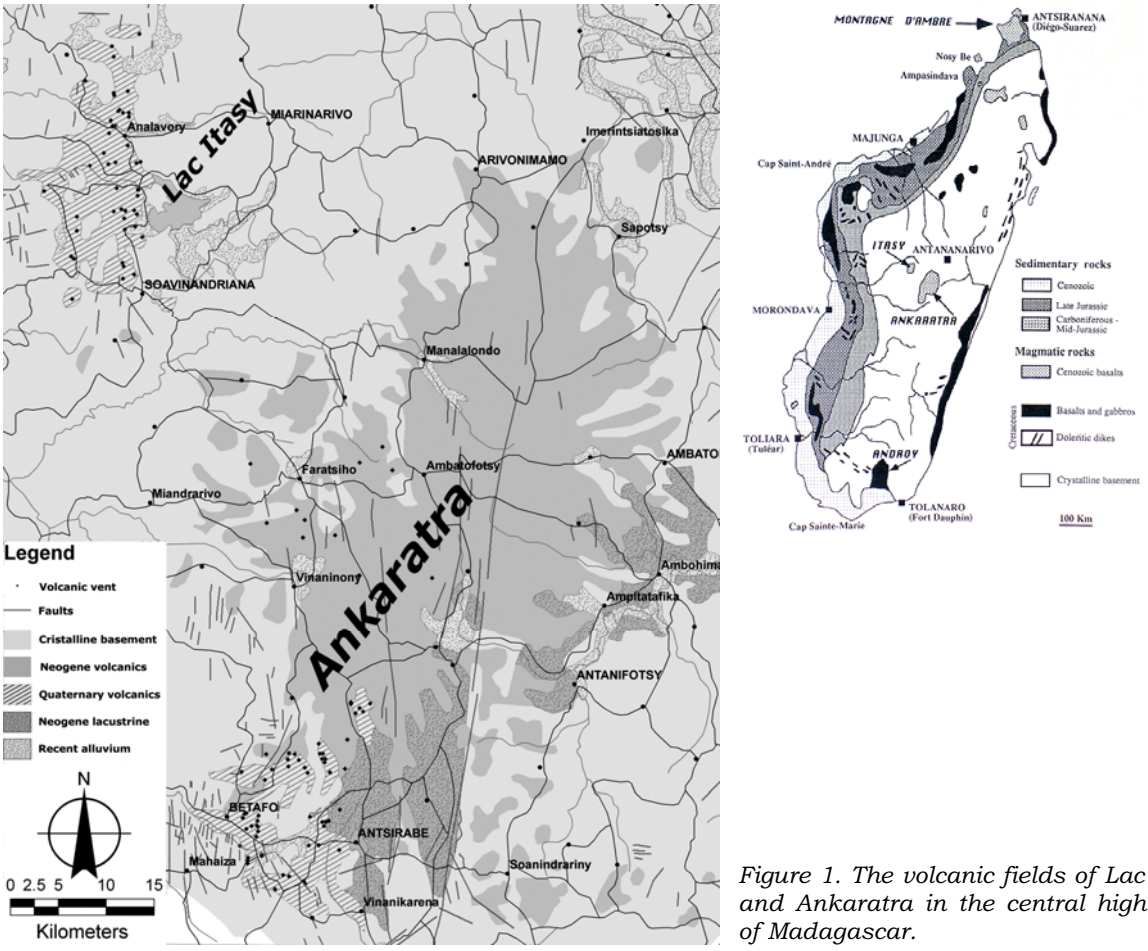

Figure 1. The volcanic fields of Lac Itasy and Ankaratra in the central highlands of Madagascar.

REFERENCES

BERTIL, D. & REGNOULT, J.M. (1998): Seismotectonics of Madagascar. *TECTONOPHYSICS* Vol. 294, 57-74.

RAKOTONDRAOMPIANA S.A. ET AL. (1999): Modèle de lithosphere pour l'île de Madagascar (océan Indien occidental): nouvelle interprétation des données gravimétriques. *JOURNAL OF AFRICAN EARTH SCIENCES* Vol. 28 No. 4, 961-973.

PIQUÉ A. ET AL. (1999): L'extension à Madagascar du Néogene à l'Actuel: arguments structuraux et géophysiques. *JOURNAL OF AFRICAN EARTH SCIENCES VOL.* 28 No. 4, 975-983.

PROPOSING TL ON CRUSTAL XENOLITHS AS A TOOL FOR DATING QUATERNARY ALKALINE VOLCANIC ROCKS.

Rufer Daniel & Frank Preusser

Insitute of Geological Sciences, University of Berne, Switzerland

Obtaining accurate ages for young volcanic eruptions is an important factor in geomorphic, tectonic and climatic studies, as well as an integral prerequisite for hazard assessments. Unfortunately, the available methods for directly dating volcanic rocks of quaternary, especially late Pleistocene to Holocene age, are rather scarce and possess some inherent pitfalls. Most radioactive decay systems have stringent requirements concerning aspects like closed system behaviour, useful estimations of initial ratios (e.g. U/Th disequilibrium series) or minimal accumulation of radiogenic daughter isotopes needed for accurate and precise measurements. Other methods rely on the presence of a datable component (e.g. organic material for radiocarbon dating, quartz for cosmogenic nuclides). Besides, there is also but little overlap in the datable time ranges between the different methods, leading to problems in correlating ages from different methods or the impossibility to obtain an age should one method fail. This problematic is especially severe in the case of young intracontinental alkaline volcanism, where the absence of high K content phases like Sanidine in the less evolved rocks makes accurate and precise K/Ar and $^{40}Ar/^{39}Ar$ measurements difficult. The abundance of xenocrysts together with open system behaviour of phlogopite concerning U most often also prevents dating by ^{230}Th-^{238}U.

Luminescence dating would be a potential target technique for acquiring ages in the timeframe in question, and Tsukamoto et al. (2007) have shown that red isothermal TL on volcanic quartz can be used to date rhyolitic tephras back to 388 ± 25 ka. However, as the absence of volcanic quartz in alkaline volcanic rocks prevents the direct application of this method, we propose to apply TL dating to crystalline xenoliths embedded in the volcanic deposits, in order to date the last heating event which should be contemporaneous with the eruption and deposition of the volcanic host material.

Precursory tests indicate that Quartz grains from the xenoliths are capable of holding a TL signal and that at least the 320-350°C peak appears to be suitable for TL measurements. There are however still open questions concerning differences in the thermal spectra for grains from different types of xenoliths, as well as some unusual behaviour concerning dose response curves and changes in sensitivity for parts of the thermal spectrum.

Due to the strong inhomogeneities between xenolith and surrounding material as well as between the various mineral phases of the xenolith, dosimetry measurements and calculations are far less straightforward than with more homogenous sandy sediments. Furthermore, due to the potential presence of high radiation sources (e.g. zircons) in the xenolith, microdosimetric aspects have to be taken into consideration. Sample preparation itself is strongly dominated by the fact that we deal with a crystalline rock from which selected suitable quartz grains need to be extracted without destroying the stored natural signal due to exposure to heat or light during cutting and crushing.

REFERENCES

TSUKAMOTOS., MURRAY A.S., HUOT S., WATANUKI T., DENBY P.M., BØTTER-JENSEN L. (2007): Luminescence property of volcanic quartz and the use of red isothermal TL for dating tephras. *RADIAT. MEAS.* 42: 190-197.

1st International Symposium on Luminescence, Bern, Switzerland. July 3-6th, 2007

DETECTION AND MEASUREMENT OF SPATIALLY RESOLVED DOSE RATES USING IMAGING PLATES

D. Rufer and F. Preusser

Institute of Geological Sciences, University of Bern, Switzerland

Significant variation in D_E is a phenomenon that is often observed in luminescence dating. If these spreads in D_E cannot be attributed to variations in luminescence properties, incomplete bleaching or post-depositional mixing (Lomax et al., 2007), they often have microdosimetric influences as their origin. As these variations ore often perceived only after the D_E measurement, the determination of quantity and distribution of minerals that might cause such influences can only be done on different material than the D_E measurements were carried out on.

In the case of unconsolidated material, spatial dose rate distributions are statistical properties linked to the relative concentrations of the various particle types and dose rates in the sediment. It is therefore admissible to assess dose rate distributions on a different subspecimen of the measured material, under the premise of sample homogeneity. Kalchgruber et al., (2003) describe a method using Al_2O_3 : C grains intermixed with the sample to determine dose rate distributions, and Monte-Carlo models to quantify such effects on single grains in heterogeneous sediments have been suggested by Mayya et al., (2006). However, for solid samples used in spatially resolved OSL or TL measurements (Greilich et al., 2005; Rufer and Preusser, 2007), information about spatial distribution of dose rates must be obtained on the same material as to be used for DE measurements, prior to it's (inherently destructive) processing for quartz or feldspar separation. This is due to the circumstance that in solid, natural rock material dosimetric contributions are directly tied to the petrographical configuration, which often is neither sufficiently homogeneous within a subsample, nor between subsamples. Unfortunately, most of the commonly used techniques for radioactive element mapping (e.g. electron microprobe) as well as optical determination of potentially high dose rate mineral phases are destructive towards the luminescence signals and must therefore be discarded.

In this study we illustrate the use of autoradiography of geological samples with imaging plates as a tool to document and measure spatial dose rate distributions. Although imaging plates have long been established as a tool in medicinal sciences, only few experiments were conducted applying them to geological problems (e.g. Hareyama et al., 2000). We advocate their application to qualitatively appraise heterogeneous dosimetry and now propound a method to use imaging plates to quantitatively determine spatially resolved dose rates and their distribution, as well as providing a means to efficiently assess the dosimetry of a large number of samples within a relatively short amount of time.

REFERENCES

GREILICH, S., GLASMACHER, U.A. AND WAGNER, G.A., 2005. Optical dating of granitic stone surfaces. *ARCHAEOMETRY*, 47: 645-665.

HAREYAMA, M., TSUCHIYA, N., TAKEBE, M. AND CHIDA, T., 2000. Two-dimensional measurement of natural radioactivity of granitic rocks by photostimulated luminescence technique. *GEOCHEMICAL JOURNAL*, 34(1): 1-9.

KALCHGRUBER, R., FUCHS, M., MURRAY, A.S. AND WAGNER, G.A., 2003. Evaluating dose-rate distributions in natural sediments using alpha-Al2O3 : C grains. *RADIATION MEASUREMENTS*, 37(4-5): 293-297.

LOMAX, J., HILGERS, A., TWIDALE, C.R., BOURNE, J.A. AND RADTKE, U., 2007. Treatment of broad palaeodose distributions in OSL dating of dune sands from the western Murray Basin, South Australia. *QUATERNARY GEOCHRONOLOGY*, 2(1-4): 51-56.

MAYYA, Y.S., MORTHEKAI, P., MURARI, M.K. AND SINGHVI, A.K., 2006. Towards quantifying beta microdosimetric effects in single-grain quartz dose distribution. *RADIATION MEASUREMENTS*, 41(7-8): 1032-1039.

RUFER, D. AND PREUSSER, F., 2007. Proposing TL on crustal xenoliths as a tool for dating Quaternary alkaline volcanic rocks. *INTERNATIONAL SYMPOSIUM ON LUMINESCENCE 2007, BERN, SWITZERLAND.*

2nd International Symposium on Luminescence, Port Elizabeth, South Africa. June 29 – July 4, 2008

and

12th International Conference on Luminescence and Electron Spin Resonance Dating, Beijing, China. September 18-22, 2008

LUMINESCENCE DATING OF PHREATOMAGMATIC ERUPTIONS FROM CENTRAL MADAGASCAR

*G. Schreurs, *D. Rufer and F. Preusser*

Institute of Geological Sciences, University of Bern, Switzerland

The Ankaratra volcanic field in central Madagascar is closely linked to extensional tectonics that affects the area since the middle Miocene. This intracontinental rifting in Madagascar possibly represents a continuation of the East African Rift (Bertil and Regnoult, 1998). The latest phase of the rift-related volcanism in central Madagascar occurred in the southern part of the Ankaratra volcanic field during the late Quaternary. The existing dates for the eruptions in this region are only of indirect nature or based on geomorphological observations and absolute ages are lacking. It is therefore of great interest to directly date the Quaternary volcanism in order to establish a reliable temporal framework for the youngest neotectonic and magmatic events in central Madagascar.

The alkaline ultramafic volcanic rocks are mostly silica undersaturated and the bulk of the alkaline feldspars occur as microcrysts in an aphanitic matrix. Thus neither quartz nor suitable feldspars are available for luminescence dating. However, at least one phreatomagmatic eruption occurred during the early stages of many of the volcanic centres. Due to the nature and the immense energy release of the explosive eruptions, large volumes of crystalline basement material were disintegrated and ejected as ash and sand sized particles over large areas of several tens to hundreds of square kilometres. The bleaching potential during the relatively long aerial transit-time of up to several hours (Bonadonna et al., 2005) and the potential resetting of the luminescence signal by hydrostatic pressure or frictional heating during the eruption (Zöller et al., 2007) suggests that quartz or feldspar grains from this kind of deposit might be suitable for luminescence dating.

In this study we test the potential of OSL for directly dating phreatomagmatic explosion layers from late Quaternary eruptions from the Ankaratra volcanic field. Multiple feldspar samples from several volcano-stratigraphically linked explosion horizons were studied by single aliquot regenerative IRSL. The quartz samples were not measured, as they exhibited an unusually low saturation level for laboratory irradiation, the cause of which is not clear, but might be related to the violent fragmentation process of the eruption.

REFERENCES

BERTIL, D. AND REGNOULT, J.M., 1998. Seismotectonics of Madagascar. *TECTONOPHYSICS*, 294(1-2): 57-74.

BONADONNA, C. ET AL., 2005. Probabilistic modeling of tephra dispersal: Hazard assessment of a multiphase rhyolitic eruption at Tarawera, New Zealand. *JOURNAL OF GEOPHYSICAL RESEARCH-SOLID EARTH*, 110(B3).

ZOELLER, L. ET AL., 2007. The partial heat - longest plateau technique for TL dating of Middle and Upper Quaternary volcanic eruptions. *CHEMICAL GEOLOGY*, submitted.

12th International Conference on Luminescence and Electron Spin Resonance Dating, Beijing, China. September 18-22, 2008

PROPOSING IR STIMULATED LUMINESCENCE TO DATE QUATERNARY PHREATOMAGMATIC ERUPTIONS FROM CENTRAL MADAGASCAR

Rufer Daniel, Preusser Frank & Schreurs Guido

Institut für Geologie, Universität Bern, Baltzerstrasse 1 + 3, CH-3012 Bern

The Ankaratra volcanic field in central Madagascar is closely linked to extensional tectonics that affects the area since the middle Miocene. This intracontinental rifting in Madagascar possibly represents a continuation of the East African Rift (Bertil and Regnoult, 1998). The latest phase of the rift-related volcanism in central Madagascar occurred in the southern part of the Ankaratra volcanic field during the late Quaternary. The existing dates for the eruptions in this region are only of indirect nature or based on geomorphological observations and absolute ages are lacking. It is therefore of great interest to directly date the Quaternary volcanism in order to establish a reliable temporal framework for the youngest neotectonic and magmatic events in central Madagascar.

Unfortunately, the available methods for directly dating volcanic rocks of quaternary, especially late Pleistocene to Holocene age, are rather scarce and possess some inherent pitfalls like the necessitation of closed system behaviour, usable estimations of initial ratios (U/Th disequilibria) or finding suitable sample material (e.g. organics for ^{14}C). The young age and the geochemical and petrological composition causes further problems for radiogenic dating with K/Ar or Ar/Ar methods, as the bulk of the potassium is dispersed in the vitreous to aphanitic matrix and a noted absence of juvenile Sanidine is observed.

Luminescence dating would be a potential target technique for acquiring ages in the timeframe in question, and Tsukamoto et al. (2007) have shown that red isothermal TL on volcanic quartz can be used to date rhyolitic tephras back to 388 ± 25 ka. However, as the alkaline ultramafic volcanic rocks of the Ankaratra region are mostly silica undersaturated and alkaline feldspars are scarce or occur only as microcrysts in aphanitic matrix, neither quartz nor suitable feldspars are available for luminescence dating. However, at least one phreatomagmatic eruption occurred during the early stages of many of the volcanic centres. Due to the nature and the immense energy release of the explosive eruptions, large volumes of crystalline basement material were disintegrated and ejected as ash and sand sized particles over large areas of several tens to hundreds of square kilometres. The bleaching potential during the relatively long aerial transit-time of up to several hours (Bonadonna et al., 2005) and the potential resetting of the luminescence signal by hydrostatic pressure or frictional heating during the eruption (Zöller et al., 2007) suggests that quartz or feldspar grains from this kind of deposit might be suitable for luminescence dating.

In this study we test the potential of IR stimulated luminescence (IRSL) for directly dating phreatomagmatic explosion layers from late Quaternary eruptions from the Ankaratra volcanic field. Multiple feldspar samples from several volcano-stratigraphically linked explosion horizons were studied by single aliquot regenerative IRSL. The quartz samples were not measured, as they exhibited an unusually low saturation level for laboratory irradiation, the cause of which is not clear, but might be related to the violent fragmentation process of the eruption.

REFERENCES

BERTIL, D. AND REGNOULT, J.M. 1998: Seismotectonics of Madagascar. *TECTONOPHYSICS*, 294(1-2): 57-74.

BONADONNA, C., CONNOR, C. B., HOUGHTON, B. F., CONNOR, L., BYRNE, M., LAING, A., HINCKS, T. K. 2005: Probabilistic modeling of tephra dispersal: Hazard assessment of a multiphase rhyolitic eruption at Tarawera, New Zealand. *JOURNAL OF GEOPHYSICAL RESEARCH-SOLID EARTH,* 110(B3).

TSUKAMOTO S., MURRAY A.S., HUOT S., WATANUKI T., DENBY P.M., BØTTER-JENSEN L. 2007: Luminescence property of volcanic quartz and the use of red isothermal TL for dating tephras. *RADIAT. MEAS.* 42, 190-197.

ZOELLER, L., BLANACHARD, H., MCCAMMON, C. 2007: The partial heat - longest plateau technique for TL dating of Middle and Upper Quaternary volcanic eruptions. *CHEMICAL GEOLOGY,* submitted.

6th Swiss Geoscience Meeting, Lugano, Switzerland. 21st– 23rd November 2008

APPENDIX B

Geological map: West of Antsirabe

(the map can be found in the pouch
at the rear of the thesis)

Alfons Berger[a], Edwin Gnos[b], Michel A. F. Rakotondrazafy[c],
Daniel Rufer[d] & Guido Schreurs[d]

[a] Department of Geography and Geology, University of Copenhagen, Denmark
[b] Muséum d'histoire naturelle de Genève, Switzerland
[c] Département des Sciences de la Terre, Université Antananarivo, Madagascar
[d] Institute of Geological Sciences, University of Bern, Switzerland

"The great men of science are supreme artists."

Martin H. Fischer (1879 - 1962), Physician and author

APPENDIX C

Sample locations

"Data is a precious thing and will last longer than the systems themselves."

Tim Berners-Lee (born 1955), Inventor of the World Wide Web

Table C.1 Sample list including lithologies and sample source from field seasons 2005 and 2007 plus field visit 2008. Lithological assignation based on field observations. Coordinates are Universal Transverse Mercator (UTM), southern hemisphere, zone 38, WGS 84. Luminescence: L = sampling in the dark, G = sample for γ-spectrometry, L/G = dark sample plus γ-spectrometry sample taken.

Sample	L / G	UTM X	UTM Y	m.a.s.l.	Lithology	Source
DR 001		606766.769	7824708.988	2216	basalt	small flow or plug
DR 002		705582.727	7833740.495	n.r.	Phonolite	small flow or plug
DR 003_1		706932.889	7838891.909	1918	basalt	small plug (?)
DR 003_2		706932.889	7838891.909	1918	basalt	flow, discordant over DR 003_1
DR 004_1		707030.836	7838888.943	1953	Sanidine crystals	from light ash layer
DR 004_2		707030.836	7838888.943	1953	volcanic tuff	weathered, overlying DR 004_1
DR 007		711747.283	7843452.018	1881	basalt (?)	flow, weathered
DR 010		720390.496	7800452.620	1597	basalt	flow or small plug
DR 014		742536.184	7796128.750	1931	phonolite	scattered blocks (> 1 m)
DR 017		742792.245	7797030.723	2128	trachyte	summit of large plug
DR 021		743523.381	7797242.448	1890	gneiss	basement
DR 027		706286.071	7800855.202	1526	phonolite + peridotite xenolith	flow
DR 034_1		698648.701	7801329.921	1527	basalt	flow
DR 034_2		698648.701	7801329.921	1527	basalt + basement xenolith	flow
DR 034_3		698648.701	7801329.921	1527	basalt + basement xenolith	flow
DR 035_1		612976.273	7897033.345	1303	trachyte	not in-situ
DR 035_2		612976.273	7897033.345	1303	gneiss	phreatic deposit
DR 038		677597.458	7897188.503	1223	basalt	flow
DR 040		677575.378	7897582.417	1327	trachyte	dome
DR 042		677577.824	7898348.001	1572	andesite (?)	secondary dome
DR 043		677027.546	7898084.500	1269	basanite	bomb
DR 046		667171.181	7880834.337	1155	tephrite	tephra
DR 047		670073.170	7881085.009	1113	basalt / basanite	bomb
DR 048		670704.111	7882318.618	1133	basanite	bomb
DR 049_1		671614.134	7882295.305	1161	basanite	bomb
DR 049_2		671614.134	7882295.305	1161	basanite	bomb
DR 052		672595.591	7882172.282	1171	basanite	flow
DR 053		673074.707	7881659.780	1215	tephrite	bomb
DR 054_1		672806.564	7883564.084	1263	basalt	columns at base of crater
DR 054_2		672806.564	7883564.084	1263	tephrite	bomb
DR 054_3		672806.564	7883564.084	1263	tephrite + basement xenolith	bomb
DR 055		672441.137	7883479.524	1300	tephrite	small flow (ev. secondary)
DR 056		679356.808	7880054.146	1388	tephrite	bomb
DR 058		683914.405	7903836.815	1419	trachyte	not in-situ
DR 061		683220.683	7903812.853	1330	trachyte	block
DR 065		681519.982	7904458.991	1303	basanite	bomb
DR 066_1		681535.223	7903169.060	1225	gneiss	xenolith
DR 066_2		681535.223	7903169.060	1225	phonolith	host mat. to DR 066_1
DR 066_3		681535.223	7903169.060	1225	phonolith	flow or plug
DR 068_1	L	681046.105	7906489.406	1265	gneiss	basement clast
DR 068_2	L	681046.105	7906489.406	1265	gneiss	basement clast
DR 068_3		681046.105	7906489.406	1265	tephrite	tephra, host mat. of DR 068_1&
DR 068_4		681046.105	7906489.406	1265	Augite crystals	from overlying explosion layer
DR 071		681348.005	7907144.636	1244	Augite crystals	from same layer as DR 068_4
DR 072		681244.555	7906910.136	1194	trachyte	dome

DR 074		685968.321	7876534.192	1461	basanite	bomb
DR 075		686751.065	7872869.713	1422	basanite	bomb
DR 076_1		687354.801	7868228.066	1299	phonolite	clast, not juvenile
DR 076_2		687354.801	7868228.066	1299	basanite	bomb, host mat. of DR 076_3 &
DR 076_3	L	687354.801	7868228.066	1299	pegmatite	xenolith
DR 076_4		687354.801	7868228.066	1299	mica crystals (Bi & Ms)	extracted from DR 076_3
DR 076_5		687354.801	7868228.066	1299	gneiss	xenolith
DR 077		686856.381	7871769.544	1350	tephrite	small flow
DR 078		687124.794	7876361.405	1418	basanite / phonolite	flow
DR 085_1		675018.139	7907744.142	1070	granodiorite	xenolith
DR 085_2		675018.139	7907744.142	1070	basanite	flow, host mat. of DR 085_2
DR 087_1		674953.663	7907628.376	1075	basanite + basement xenolith	blocks and bombs
DR 087_2		674953.663	7907628.376	1075	Pyroxene crystals	from finer fraction of scoria
DR 088		672784.211	7906486.287	983	phonolite	flow
DR 090		678702.337	7902227.400	1340	tephrite (?)	bomb
DR 091		678976.746	7902094.277	1448	trachyte	top of dome
DR 092		678780.747	7901203.489	1447	trachyte	dome
DR 093		680004.011	7902133.556	1170	tephrite	flow
DR 096_1		682474.211	7887579.129	1285	trachyte	clast, middle unit
DR 096_2		682474.211	7887579.129	1285	gneiss	block, upper unit
DR 096_3		682474.211	7887579.129	1285	trachyte	not in-situ, assumed lower unit
DR 097		682330.763	7887693.020	1352	trachyte	dome
DR 099_1		682946.051	7886553.515	1648	trachyte	top of dome, fine grained
DR 099_2		682946.051	7886553.515	1648	trachyte	top of dome, coarse grained
DR 100		682654.742	7888243.189	1303	tephrite	bomb
DR 101_1		681588.225	7888281.207	1325	basanite	bomb
DR 101_2		681588.225	7888281.207	1325	granite	xenolith
DR 101_3		681588.225	7888281.207	1325	basalt / basanite	host mat. to DR 101_3
DR 101_4		681588.225	7888281.207	1325	trachyte	clast
DR 101_5		681588.225	7888281.207	1325	basanite + basement xenolith	clast
DR 101_6		681588.225	7888281.207	1325	gneiss	xenolith from tephra layer
DR 102		681797.895	7889595.610	1404	basanite	not in-situ
DR 104		682377.619	7888984.235	1415	trachyte	dome
DR 106_1		680767.533	7902653.717	1221	basanite + basement xenolith	bomb / block
DR 106_2		680767.533	7902653.717	1221	basanite + basement xenolith	bomb / block
DR 109		680616.057	7905193.431	1233	Pyroxene crystals	similar to DR 087_2
DR 110_1		680787.193	7904963.443	1218	Pyroxene crystals	similar to DR 087_2
DR 110_2		680787.193	7904963.443	1218	tephrite	bomb, host mat. of DR 110_2
DR 116		682516.512	7897129.347	1289	trachyte	dome
DR 118		682786.026	7892700.586	1387	trachyte	dome
DR 119		682405.158	7892465.906	1397	trachyte	dome
DR 120_1		682976.669	7893783.942	1278	trachyte	dome, weathered
DR 120_2		682976.669	7893783.942	1278	trachyte	dome
DR 121		728196.544	7842397.134	1824	basalt	flow
DR 128_1		706433.131	7800869.891	1520	hardground	lower unit
DR 128_2		706433.131	7800869.891	1520	hardground	upper unit
DR 128_3		706433.131	7800869.891	1520	volcanic ash (?)	overlying upper hardground
DR 129_1		706254.997	7800822.470	1546	basalt + Ol-Px cumulate	columnar basalt, weathered
DR 129_2		706254.997	7800822.470	1546	basalt + Ol-Px cumulate	columnar basalt, weathered
DR 129_3		706254.997	7800822.470	1546	basalt + Ol-Px cumulate	columnar basalt, weathered
DR 129_4		706254.997	7800822.470	1546	basalt + Ol-Px cumulate	columnar basalt, weathered
DR 129_5		706254.997	7800822.470	1546	basalt + Ol-Px cumulate	columnar basalt, weathered
DR 133		705669.429	7801123.657	1543	basalt	flow

DR 137	705790.947	7797413.013	1632	basalt	flow, strongly weathered
DR 138_1	705267.175	7797357.310	1666	basanite	bomb, host mat. of DR 138_2
DR 138_2	705267.175	7797357.310	1666	granite	xenolith
DR 140	702803.846	7795691.658	1679	tephrite + basement xenolith	flow
DR 142_1	701675.617	7795917.215	1727	tephrite (?)	rare black tephra in red scoria
DR 142_2	701675.617	7795917.215	1727	basanite	block from secondary flow
DR 142_3	701675.617	7795917.215	1727	granite	xenolith from red scoria
DR 144	700655.884	7801840.124	1544	tephrite	block / bomb
DR 147_1	699285.369	7802467.107	1594	basanite (incl. Qtz xenocrysts)	bomb
DR 147_2	699285.369	7802467.107	1594	basanite + basement xenolith	bomb
DR 148_1	699375.195	7802420.730	1605	gneiss	xenolith from tephra layer
DR 148_2	699375.195	7802420.730	1605	basanite + basement xenolith	bomb
DR 148_3	699375.195	7802420.730	1605	basanite + basement xenolith	bomb
DR 152_1	701480.539	7795184.633	1762	tephrite	flow, host mat. of DR 152_2 & 3
DR 152_2	701480.539	7795184.633	1762	gneiss	xenolith
DR 152_3	701480.539	7795184.633	1762	gneiss	xenolith
DR 153	701531.403	7795107.475	1767	basanite	flow
DR 154	701527.132	7795083.885	1747	basanite	flow
DR 155	701433.898	7795110.419	1763	basanite	flow
DR 158_1	710201.875	7801102.092	1530	tephrite	bomb, host mat. of DR 158_2
DR 158_2	710201.875	7801102.092	1530	gneiss	xenolith
DR 159_1	710323.834	7801045.563	1570	Pyroxene crystals	from fine fraction of tephra,
DR 159_2	710323.834	7801045.563	1570	basanite	bomb, upper sequence
DR 159_3	710323.834	7801045.563	1570	gneiss	xenolith, upper sequence tephra
DR 160_1	710113.444	7801129.433	1563	basanite	bomb, host mat. of DR 160_2
DR 160_2	710113.444	7801129.433	1563	gneiss	xenolith
DR 165	729818.079	7837694.860	1787	rhyolite (?) basement (?)	extremely weathered
DR 166	729478.970	7837787.042	1726	basalt	columnar, weathered
DR 173	712657.432	7817376.715	1852	trachyte	small flow / breccia
DR 174	712176.759	7818638.057	1912	basalt	flow
DR 176	712596.941	7819396.332	1960	trachyte	flow (?)
DR 179_1	713073.689	7819918.708	2041	basanite	breccia
DR 179_2	713073.689	7819918.708	2041	trachyte	breccia
DR 181	707993.734	7805216.051	1599	basanite	block / bomb
DR 182_1	708281.143	7804933.318	1636	pegmatite	phreatic deposit
DR 182_2	708281.143	7804933.318	1636	gneiss	phreatic deposit
DR 183_3	708281.143	7804933.318	1636	basanite	tephra overlying DR 182_1 & 2
DR 186_1	698596.624	7801300.447	1529	basanite	flow, host mat. of DR186_2
DR 186_2	698596.624	7801300.447	1529	gneiss	xenolith
DR 188	697823.984	7799344.187	1586	basanite	bomb
DR 192	700340.596	7796367.370	1741	gneiss	xenoliths in tephra
DR 193	697550.338	7803706.143	1587	basanite	bomb
DR 194	698204.112	7809151.719	1642	basalt	flow
DR 195	700714.595	7810732.233	1769	basalt	flow
DR 196_1	701155.418	7812049.417	1786	gneiss	xenoliths in tephra
DR 196_2	701155.418	7812049.417	1786	basanite	block / bomb, host mat. of DR
DR 197	701004.058	7812257.260	1857	granite	xenoliths in tephra
DR 203	705938.736	7800786.073	1546	basanite + basement xenolith	breccia
DR 206_1	705634.010	7801468.454	1579	volcanic ash (?)	overlying lateritisized flow
DR 206_2	705634.010	7801468.454	1579	basalt	flow
DR 207	705725.388	7801537.023	1582	basalt	flow
DR 209	705920.762	7801722.055	1554	basalt (?)	flow
DR 211	705714.322	7800878.290	1578	gneiss	xenolith in tephra

DR 218	L	701433.898	7795110.419	1763	gneiss	basement underlying flow
DR 340_1		696506.955	7806252.234	1492	phreatic explosion deposit	upper unit
DR 340_2		696506.955	7806252.234	1492	phreatic explosion deposit	lower unit
DR 351		703359.064	7804866.026	1732	phonolite	plug
DR 357		708351.071	7799689.036	1496	basalt	flow
DR 361_1	L / G	705411.760	7799936.124	1560	phreatic explosion deposit	below hardground
DR 361_2	L / G	705411.760	7799936.124	1560	phreatic explosion deposit	below hardground
DR 361_3	L / G	705411.760	7799936.124	1560	phreatic explosion deposit	above hardground
DR 370_1	L / G	696696.705	7799868.335	1600	phreatic explosion deposit	lower unit
DR 370_2	L / G	696696.705	7799868.335	1600	phreatic explosion deposit	upper unit
DR 426		706365.582	7797310.776	1577	basalt / basanite	bomb
DR 431		705475.834	7798783.849	1585	basalt	flow
DR 469	L / G	707923.309	7799742.806	1461	phreatic explosion deposit	upper unit
DR 471_1	L / G	707406.628	7800073.318	1539	phreatic explosion deposit	lower unit
DR 471_2	L / G	707406.628	7800073.318	1539	phreatic explosion deposit	upper unit
DR 472		704491.107	7797051.410	1791	basalt	clast
DR 483_1	L / G	701150.993	7811730.484	1800	phreatic explosion deposit	lower unit
DR 483_2	L / G	701150.993	7811730.484	1800	phreatic explosion deposit	upper unit
DR 488	L / G	704844.939	7801725.366	1552	phreatic explosion deposit	lower unit
DR 490		692623.195	7805593.032	1370	basalt	flow
DR 493		697120.864	7806152.398	1622	basanite	block / bomb
DR 509		701018.820	7795430.581	1764	basanite	block / bomb
DR 511		698677.076	7802454.677	1563	basanite	scoria
DR 512		698803.972	7803025.667	1615	basanite	bomb
DR 515		699645.497	7803981.648	1596	tephrite	flow
DR 516		698465.191	7804479.899	1639	basanite	block / bomb
DR 517_1		697039.870	7806593.958	1560	basalt	flow, weathered (wollsack)
DR 517_2		697039.870	7806593.958	1560	basalt	not in-situ
DR 522		696604.541	7805323.335	1554	basanite	bomb
DR 524		697629.614	7803676.591	1595	basanite	bomb
DR 525		695965.198	7801901.513	1520	basanite	flow
DR 527		696375.142	7801371.044	1534	basanite	block / bomb
DR 528		695984.683	7797248.924	1706	tephrite	bomb
DR 531		697651.403	7798796.968	1698	basanite	bomb
DR 532		698580.034	7797931.768	1591	basanite	flow
DR 533_1		700160.962	7804354.477	1536	gneiss	xenolith from flow
DR 533_2		700160.962	7804354.477	1536	gneiss	xenolith from flow
DR 535		701563.686	7795279.300	1705	gneiss	xenolith from scoria
DR 606		678000.446	7898747.059	1433	andesite (?)	flow
DR 607		677970.293	7899444.734	1301	limburgite	small flow
DR 635	G	707406.628	7800073.318	1539	laterite	underlying DR 471_1
DR 637	G	705411.760	7799936.124	1560	laterite	underlying DR 361_1
DR 638_1	G	704844.939	7801725.366	1552	laterite	underlying DR 488
DR 638_2	G	704844.939	7801725.366	1552	phreatic explosion deposit	overlying DR 488
DR 641_1	G	696696.705	7799868.335	1600	tephra	overlying DR 370_1
DR 641_2	G	696696.705	7799868.335	1600	tephra	underlying DR 370_2
DR 641_3	G	696696.705	7799868.335	1600	tephra	overlying DR 370_2
DR 642_1		696506.955	7806252.234	1492	laterite	underlying DR 340_2
DR 642_2		696506.955	7806252.234	1492	tephra	overlying DR 340_2
DR 642_3	G	696506.955	7806252.234	1492	paleosoil	underlying DR 340_1
DR 642_4	G	696506.955	7806252.234	1492	tephra	overlying DR 340_1

APPENDIX D

Major and trace elements (XRF)

"It is a capital mistake to theorize before one has data."

Sir Arthur Conan Doyle (1859 - 1930), Author, creator of Sherlock Holmes

Table D.1 *Major elements measured by X-Ray Fluorescence (XRF) at the Institute for Mineralogy and Petrology, ETH Zürich, Switzerland between 29/05/2009 and 31/05/2009. Abundances corrected for loss on ignition (LOI).*

Sample	SiO_2 wt.%	TiO_2 wt.%	Al_2O_3 wt.%	Fe_2O_3 wt.%	MnO wt.%	MgO wt.%	CaO wt.%	Na_2O wt.%	K_2O wt.%	P_2O_5 wt.%	Cr_2O_3 wt.%	NiO wt.%	LOI wt.%	Total
DR 121	41.292	2.678	9.758	12.022	0.191	14.671	13.202	2.007	1.454	0.661	0.115	0.047	1.363	99.461
DR 133	52.035	1.799	17.279	9.674	0.188	2.808	5.905	4.583	3.351	1.098	0.001	0.001	0.006	98.727
DR 138-1	42.875	2.857	14.263	14.071	0.204	8.032	10.550	3.687	1.838	0.834	0.028	0.013	-0.037	99.216
DR 155	48.960	2.260	14.063	11.312	0.162	8.080	9.472	3.386	1.880	0.502	0.039	0.020	-0.350	99.785
DR 158-1	44.991	2.337	13.722	12.512	0.194	9.443	11.621	2.628	1.689	0.747	0.056	0.021	0.200	100.158
DR 159-2	43.355	2.412	12.775	12.805	0.192	11.127	11.755	2.351	1.179	0.766	0.080	0.035	0.739	99.572
DR 186-1	43.293	2.964	14.069	13.327	0.191	9.294	11.259	3.287	1.716	0.658	0.039	0.019	-0.509	99.607
DR 188	43.561	2.452	13.599	13.176	0.183	9.478	11.550	2.227	1.053	0.626	0.049	0.024	1.483	99.460
DR 196-2	43.062	2.468	12.650	12.675	0.189	10.197	12.570	3.188	1.281	1.068	0.063	0.023	0.020	99.451
DR 203	45.150	2.552	14.290	12.826	0.188	8.049	10.859	2.993	1.547	0.803	0.032	0.016	-0.070	99.233
DR 357	44.664	2.291	13.651	12.260	0.196	9.527	11.364	2.498	1.624	0.739	0.059	0.022	0.115	99.010
DR 426	41.781	2.810	13.784	14.006	0.199	9.668	12.010	3.009	1.490	0.881	0.042	0.017	-0.247	99.451
DR 490	43.896	2.782	14.084	13.335	0.188	8.944	11.001	2.983	1.664	0.618	0.039	0.018	-0.162	99.388
DR 493	47.988	2.422	16.099	11.454	0.196	4.972	8.493	4.074	2.248	0.978	0.010	0.007	-0.012	98.930
DR 509	47.509	2.366	13.780	11.635	0.166	8.657	10.161	3.179	1.668	0.507	0.042	0.020	0.019	99.708
DR 512	42.800	2.966	13.633	13.252	0.190	9.980	11.663	3.156	1.564	0.665	0.047	0.021	-0.281	99.655
DR 515	43.270	2.904	13.724	13.028	0.188	9.756	11.529	3.263	1.631	0.648	0.046	0.020	-0.304	99.702
DR 516	45.965	2.425	14.198	12.628	0.182	8.597	10.560	3.311	1.487	0.693	0.040	0.019	-0.379	99.723
DR 517-1	48.510	2.385	16.338	11.416	0.193	4.724	8.220	3.569	2.308	0.958	0.009	0.006	0.357	98.993
DR 525	47.222	2.405	15.144	12.540	0.185	7.335	9.375	3.490	1.582	0.663	0.024	0.014	-0.361	99.618
DR 528	47.424	2.084	14.374	12.096	0.187	7.897	10.216	3.265	1.607	0.734	0.039	0.019	-0.162	99.780
DR 531	44.283	2.384	13.679	13.020	0.189	9.922	11.240	2.742	1.318	0.742	0.051	0.024	0.162	99.755
DR 532	44.748	2.276	13.750	12.747	0.185	9.990	11.175	3.062	1.348	0.702	0.055	0.026	-0.464	99.600

Table D.2 *Trace elements measured by X-Ray Fluorescence (XRF) at the Institute for Mineralogy and Petrology, ETH Zürich, Switzerland between 29/05/2009 and 31/05/2009. Abundances corrected for loss on ignition (LOI).*

Sample	**Rb** ppm	**Ba** ppm	**Sr** ppm	**Nb** ppm	**Zr** ppm	**Hf** ppm	**Y** ppm	**Ga** ppm	**Zn** ppm	**Cu** ppm	**Ni** ppm	**Co** ppm	**Cr** ppm	**V** ppm	**Sc** ppm	**La** ppm	**Ce** ppm	**Nd** ppm	**Th** ppm	**U** ppm
DR 121	62.4	1088.6	963.1	89.7	243.4	5.0	33.9	15.8	91.0	86.6	374.5	62.9	794.5	299.3	28.7	45.5	134.3	48.7	4.4	12.5
DR 133	70.1	1605.3	1429.5	90.7	363.8	8.4	46.8	21.9	113.7	16.0	7.0	19.4	4.8	83.4	3.4	67.1	172.9	61.5	6.1	17.8
DR 138-1	27.1	857.3	1145.9	81.3	235.7	4.8	41.2	20.2	98.5	58.9	103.8	49.6	189.5	247.1	24.4	45.9	141.8	51.3	3.5	13.4
DR 155	55.2	596.4	750.5	48.1	192.1	4.4	33.7	20.3	87.3	61.1	160.0	46.9	265.0	214.5	19.4	22.0	92.8	35.2	7.1	12.5
DR 158-1	32.3	752.0	870.4	65.3	206.6	4.4	38.3	19.3	96.2	62.2	161.6	51.7	381.8	281.5	27.0	35.6	110.2	40.9	3.7	12.0
DR 159-2	23.8	679.8	1187.7	62.6	180.4	4.4	37.6	16.0	90.5	73.2	277.6	54.3	553.6	265.5	26.0	41.5	116.2	42.9	1.6	11.4
DR 186-1	27.7	708.7	953.9	66.6	225.1	5.5	38.9	19.4	94.5	60.8	151.7	50.3	267.7	277.2	23.6	24.6	107.7	40.1	2.8	11.1
DR 196-2	29.1	878.5	1158.7	71.9	218.4	4.5	39.1	18.3	94.5	57.6	183.8	58.1	430.2	284.2	27.1	53.5	134.6	48.8	3.9	13.4
DR 203	18.2	828.5	984.2	61.5	209.1	5.4	40.7	19.8	99.1	76.2	122.4	48.4	215.9	257.2	24.7	37.1	121.1	44.4	4.4	12.3
DR 357	32.4	834.9	851.2	65.1	202.7	4.8	38.3	19.2	93.7	63.0	170.8	51.0	404.5	268.2	26.4	34.2	102.4	38.2	2.1	10.9
DR 426	30.6	665.2	848.9	70.6	211.4	3.9	38.2	19.6	89.9	63.9	129.8	55.1	289.9	296.6	26.1	34.3	101.3	37.9	2.1	9.9
DR 490	18.6	687.0	935.1	58.1	169.6	5.1	37.0	17.4	91.6	64.5	140.2	51.2	264.6	272.6	27.8	18.4	101.3	38.0	2.6	11.2
DR 493	42.0	1002.1	1193.8	81.5	269.7	5.6	43.0	19.5	102.9	42.4	54.4	31.9	65.9	174.6	13.5	53.0	141.6	51.2	2.4	13.9
DR 509	41.8	595.6	779.8	48.9	192.1	4.1	34.0	18.7	86.8	67.8	153.7	45.2	285.3	229.1	25.4	35.4	84.4	32.4	4.1	11.4
DR 512	37.9	716.9	934.8	70.0	227.3	5.2	38.7	17.9	93.5	67.2	162.2	56.3	319.5	285.2	26.3	34.1	118.7	43.7	2.0	12.2
DR 515	32.0	734.3	928.1	67.8	227.1	5.1	37.6	18.4	93.2	68.7	155.8	55.6	313.2	280.9	26.5	30.1	114.4	42.2	0.2	12.7
DR 516	21.2	687.5	906.9	58.7	204.0	4.2	37.4	19.5	99.4	58.0	147.8	48.9	270.1	239.1	24.7	30.2	101.3	37.9	1.3	11.4
DR 188	21.0	630.8	926.6	53.9	161.9	4.1	34.7	18.1	94.4	63.6	188.3	54.1	342.4	249.2	30.8	29.3	83.1	32.0	1.9	11.6
DR 517-1	42.8	1059.7	1196.9	84.1	279.6	6.4	57.3	20.7	104.5	41.2	49.2	28.6	59.4	172.2	13.1	59.1	143.7	51.8	5.4	15.5
DR 525	24.7	734.0	879.2	56.5	219.0	4.7	37.5	21.5	107.0	52.4	108.0	44.3	162.8	210.3	19.1	32.1	110.2	40.9	1.9	10.4
DR 528	22.3	803.7	946.7	63.6	211.2	5.4	37.8	17.9	98.0	68.6	148.6	49.1	266.7	233.2	22.0	37.2	124.6	45.6	4.3	11.6
DR 531	17.2	660.5	887.2	60.7	181.2	4.1	35.5	19.1	96.8	72.6	192.3	55.8	352.6	250.3	25.6	32.6	106.6	39.7	1.9	11.3
DR 532	19.1	648.0	805.7	59.9	183.4	4.5	35.3	19.5	94.4	78.7	202.2	52.8	374.5	245.5	25.0	25.5	89.5	34.1	3.0	10.4

APPENDIX E

Bernese Low Argon Blank Line Assembly (BLA-BLA) Machine Interface and Data Acquisition System (M.I.D.A.S.)

Daniel Rufer & Julien Allaz

Institute of Geological Sciences, University of Bern, Switzerland

"Not everything that counts can be counted, and not everything that can be counted counts."

Albert Einstein (1879 - 1955), Physicist

BERNESE LOW ARGON BLANK LINE ASSEMBLY (BLA-BLA) - MACHINE INTERFACE AND DATA ACQUISITION SYSTEM (M.I.D.A.S.)

Due to abiding technical problems of the MAP 215-50 noble gas mass-spectrometer in the Bern lab, extensive replacements of parts became inevitable and were carried out in conjunction with the move of the mass spectrometer to a new facility in summer 2006. Not all components could be replaced with identical systems, though, and as a consequence, the old controlling software became incompatible. A migration from the old 8086 DOS based platform to a 32bit platform (Windows NT) was required (particularly by the NI PCI-6602 / BNC-2121 counter/timer and connector block assembly).
After analyzing and reverse engineering the old, "home-made" and undocumented code it was decided that porting to a new system was infeasible due to various irresolvable timing issues and other programming problems.
Therefore, Daniel Rufer and Julien Allaz planned, designed and implemented the new *Machine Interface and Data Acquisition System* (M.I.D.A.S.) between autumn 2006 and late spring 2007. Testing and debugging occurred in the latest phases of implementation and up to summer 2007. The current build of the software (Version 0.8 build 21) is stable and operational.
Due to further technical problems in other components of the mass-spectrometer and the resulting shift of the thesis' priorities to luminescence dating, some non-essential features are not yet implemented and no manual has been written. The latter is a minor problem, as the source code is well documented and the software is almost self-explanatory for users familiar with the predecessor.

M.I.D.A.S. is written in Visual Basic 6.0 to facilitate later interaction and provides control interfaces between the graphical user interface and the spectrometer as well as controlling measurement procedures and data acquisition.
The system uses an IEEE-488 General Purpose Interface Bus (GPIB) to interface with the spectrometer and a Solartron SI-7071 Computing Multimeter, the latter providing data acquisition for the faraday cups (FC). The electron multiplier tubes (EMT) connect via a BNC-2121 connector block to a NI PCI-6602 counter/timer using GPIB.
Spectrometer controlling entails fine and coarse range magnet control via hall-probe feedback, accelerator high voltage control and FC / EMT selection via beam deflection and EMT protection. SI-7071 controlling allows for the full range of interaction available using control strings.
M.I.D.A.S. provides two selectable dead-time correction algorithms and a fully automatic peak-centering routine capable of identifying and filtering erroneous signal spikes,

discerning multiple or asymmetrical peaks and automatically using adaptive scanning speeds in order to minimize the time required for successful peak-centering.
Measurements are taken based on so called *optionsets*, ASCII-files that contain the general measurement parameters plus a separate set of instructions for each mass to be measured. The stipulated backward compatibility to existing optionset files from the predecessor software is observed and M.I.D.A.S. further allows easy editing of optionsets over the graphical user interface. Data output is in form of ASCII files, as it has to be identical to the old data output files. This is dictated by the way the data is later externally processed.

Due to its length of over 25'000 lines, the source code cannot be given here, as this would require almost 500 pages. It is instead included in the electronic version of this thesis.

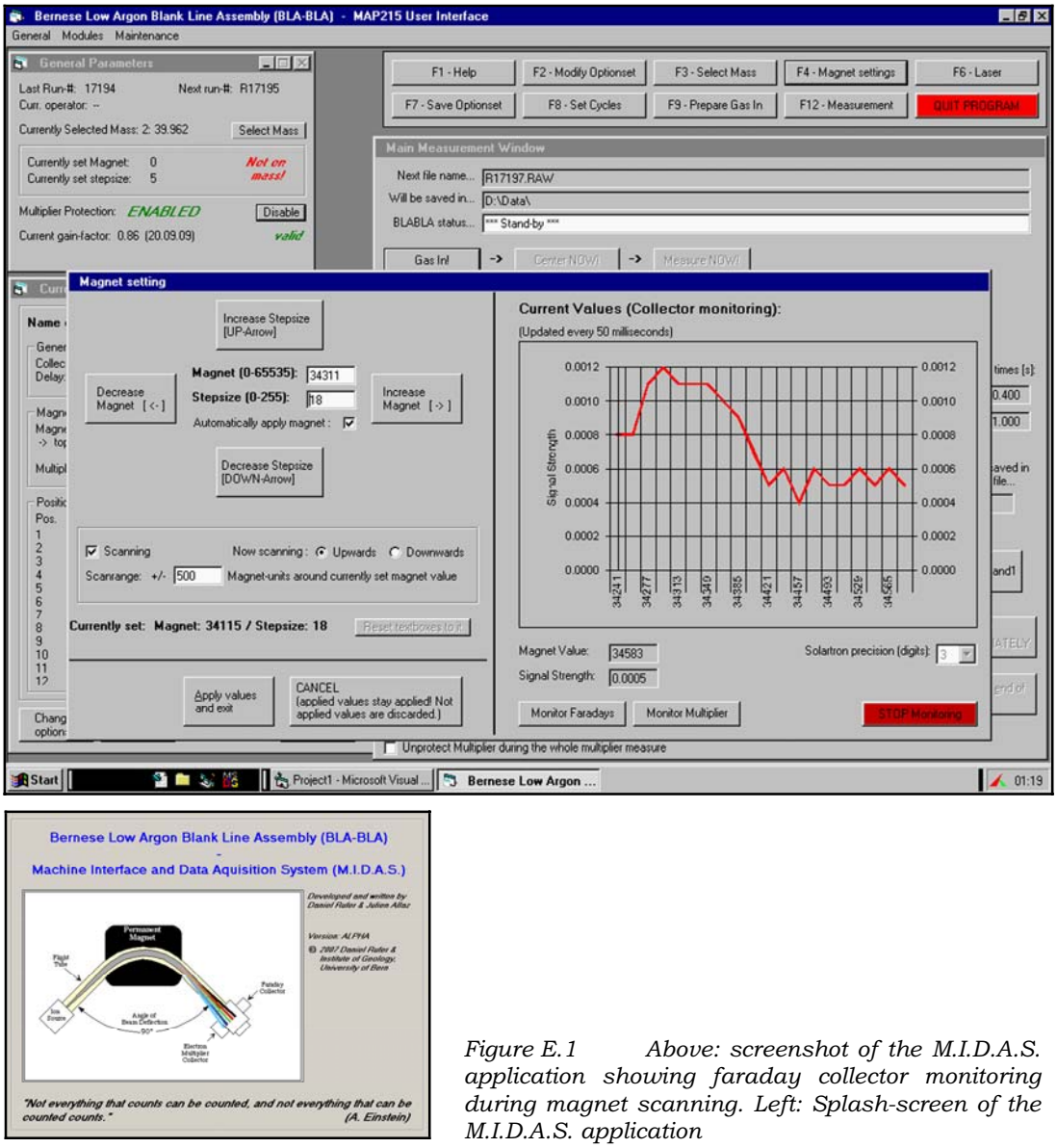

Figure E.1 Above: screenshot of the M.I.D.A.S. application showing faraday collector monitoring during magnet scanning. Left: Splash-screen of the M.I.D.A.S. application

DECLARATION

Erklärung

gemäss Art. 28 Abs. 2 RSL 05

Name/Vorname: *Rufer Daniel*
Matrikelnummer: *98-118-987*
Studiengang: *Doktorat Phil-nat. (Erdwissenschaften)*

Bachelor ☐ Master ☐ Dissertation ☒

Titel der Arbeit: *Characterization and age determination of Quaternary volcanism in the southern Ankaratra region (central Madagascar) through novel approaches in luminescence dating.*

Leiter der Arbeit: *PD Dr. G. Schreurs, PD Dr. A. Berger, PD Dr. E. Gnos, PD Dr. F. Preusser*

Ich erkläre hiermit, dass ich diese Arbeit selbstständig verfasst und keine anderen als die angegebenen Quellen benutzt habe. Alle Stellen, die wörtlich oder sinngemäss aus Quellen entnommen wurden, habe ich als solche gekennzeichnet. Mir ist bekannt, dass andernfalls der Senat gemäss Artikel 36 Absatz 1 Buchstabe o des Gesetzes vom 5. September 1996 über die Universität zum Entzug des auf Grund dieser Arbeit verliehenen Titels berechtigt ist.

Bern, 29. September 2009

CURRICULUM VITAE

Daniel Rufer

Date of birth 31. July 1976
Nationality Swiss

University education

2005 – 2009 Dissertation at the Institute of Geological Sciences, University of Bern, Switzerland

PhD thesis: *Characterization and age determination of Quaternary volcanism in the southern Ankaratra region (central Madagascar) through novel approaches in luminescence dating*

Supervisor: PD Dr. Guido Schreurs

1998 – 2005 Studies in Earth Sciences at the Institute of Geological Sciences, University of Bern, Switzerland

Degree: Master of Science in Earth Sciences
Master thesis: *Mapping and geochmistry of Nisyros volcano (Greece)*
Supervisor: Prof. Dr. Igor M. Villa

Geological mapping campaign on Nisyros Island, Greece

Primary and secondary education

1992 – 1997 Realgymnasium Bern-Kirchenfeld, Bern, Switzerland

Degree: Matura Typus C (Natural Sciences)

1990 – 1992 Untergymnasium Eisengasse, Bolligen, Bern, Switzerland

1983 – 1990 Primar- and Sekundarschule, Ittigen, Bern, Switzerland